THE EVOLUTIONARY FOREST OF PANCREATIC CANCER

by

Katelyn Marie Mullen

A Dissertation

Presented to the Faculty of the Louis V. Gerstner, Jr.
Graduate School of Biomedical Sciences,
Memorial Sloan Kettering Cancer Center

in Partial Fulfillment of the Requirements for the Degree of
Doctor of Philosophy

New York, NY

September 2023

_____ _____
Christine Iacobuzio-Donahue, MD PhD Date
Dissertation Mentor

DEDICATION

I dedicate my dissertation to every patient who had the misfortune of succumbing to this terrible disease. I hope that this body of work, in some way, enables the development of more effective treatment strategies for future PDAC patients so that they may have better quality of life to share with loved ones. To the patients who consented to research protocols that enabled me to conduct this work, I thank you. Your trust in science is paramount to the research process.

And to my husband, whose unwavering patience and support sustained me these past five years. Thank you for always having dinner on the table and for teaching me how to code. Your contributions cannot be overstated.

ABSTRACT

The evolutionary features of pancreatic ductal adenocarcinoma (PDAC) have not been systematically studied to date. Here, we assembled a cohort of 90 PDAC patients to investigate the genomic landscape and clonal composition across the full spectrum of clinical disease contexts. The timing of driver mutations, including truncal and subtruncal events, did not differ significantly across clinical contexts. However, higher truncal densities were significantly associated with worse overall survival after adjusting for stage at diagnosis, age and smoking history, representing a potential prognostic biomarker. While we observed clonal mixing in most patients, distinct clones were also identified in different samples from the same patient, highlighting intratumoral heterogeneity. Treatment status and disease stage were associated with the clonal composition of PDAC with treated and late-stage patients having increased odds of being polyclonal. Oligometastatic patients had fewer drivers and loss of heterozygosity (LOH) events compared to those with widespread metastatic disease, suggesting more genomically stable tumors that may impact management. In sum, our findings reveal novel insights into subclonal evolution in PDAC beyond established genetic paradigms.

BIOGRAPHICAL SKETCH

Katelyn Mullen was raised in North Attleboro, Massachusetts. There, she attended the North Attleboro Public School system throughout elementary, middle, and high school. In her junior year of high school, she realized her passion for biology while taking AP Biology under the instruction of Mr. Ted Duluk. In the Fall of 2012, she enrolled in the Commonwealth Honors College at the University of Massachusetts Amherst as a Biology major. During the spring semester of her freshman year, she joined the laboratory of Dr. Benjamin Normark as an undergraduate researcher where she was introduced to molecular systematics. During her three and a half years in the lab, Katelyn received several academic accolades including the Biology Junior Fellowship, the Outstanding Research Award, the Corning Incorporated Foundation Presidential Scholarship in Science and Technology, and the inaugural Biology Undergraduate Travel Award, which enabled her to travel to Sicily to present her senior thesis at the International Symposium on Scale Insect Studies.

After graduating *summa cum laude*, Katelyn spent two years conducting research at Harvard University in the laboratory of Dr. Matthew Shair where she focused on identifying predictive biomarkers for potential small molecule therapeutic agents against acute myeloid leukemia. This experience solidified her interest in translational cancer research, propelling her to matriculate into the Gerstner Sloan Kettering Graduate School of Biomedical Sciences (GSK) at Memorial Sloan Kettering Cancer Center (MSKCC) to pursue her PhD in Cancer Biology in July 2018. At the end of her first year, she joined the laboratory of Dr. Christine Iacobuzio-Donahue in the Human Oncology and Pathogenesis Program. There, she studied genetic intratumoral heterogeneity and tumor evolution in pancreatic cancer, which presented the ultimate fusion of her prior research experiences

and interests. During this time, Katelyn was supported by the MSKCC Geoffrey Beene Fellowship and the NIH Ruth L. Kirschstein National Research Service Award. In addition to her thesis research, Katelyn also worked as a curator for OncoKB, MSK's Precision Oncology Knowledge Base, where she curated biologic and oncogenic effects of mutations found in cancer. Outside of the laboratory, Katelyn was also actively involved in the GSK/MSKCC community, acting as Secretary and Co-Chair of the GSK Student Council from 2019-2021, as well as a student representative on the MSKCC Diversity in Science Council from 2020-2022.

ACKNOWLEDGEMENTS

First and foremost, I would like to thank several of my high school teachers, Ted Duluk, Tara Bennett, Alex Russo, and Scott Holster. Mr. Duluk and Ms. Bennett, thank you for igniting my passion for biology. Mr. Russo and Mr. Holster, thank you for teaching me how to write effectively. Your constructive criticism was invaluable and has served me well in numerous aspects of my life.

Next, I would like to thank my undergraduate PI, Dr. Benjamin Normark, and the entire Normark laboratory. Ben, thank you for taking me under your wing when I was a freshman. You nurtured my growth as a scientist by providing me with opportunities to learn basic molecular biology techniques, train other students, craft an independent research project, and present my work at an international symposium. Additionally, I would like to recognize your ethos around student contributions and being one of the few PIs at UMass who paid their undergraduate research assistants. You enabled me to graduate debt free, and for that I will forever be grateful.

There are numerous individuals who contributed to my success at MSKCC. First, I would like to acknowledge the GSK graduate school Deans and Assistant Deans, Ken Marians (former Dean), Michael Overholtzer (current Dean), Linda Burnley (former Associate Dean), and Tom Magaldi (current Associate Dean), as well as graduate school support staff, David McDonagh, Julie Masen and Raphaelle Chassagne for their unwavering support over the years. You have cultivated such an extraordinary community at GSK, and I am honored to have been a part of it. I would also like to thank the GSK student body for enriching my graduate school experience on multiple levels. Doing most of my PhD during the COVID-19 pandemic was challenging to say the least, so thank you for keeping me sane with all the beers, park hangs, encouragement, and laughs.

With regards to professional development, I would like to thank multiple members of the Office of Scientific Education and Training, including Thalyana Stathis, Ushma Neil, and Inna Bakman-Sanchez. Thalyana organized a wide range of career and networking events that helped me explore what life after a PhD could look like. Furthermore, Ushma Neil and Inna Bakman-Sanchez enabled me to get out of lab and have fun with other trainees through initiatives like the MSK Fun Fund.

Next, I would like to thank my PI, Dr. Christine Iacobuzio-Donahue, and all the Iacobuzio lab members. Chris took a huge gamble on me when I decided to take on a predominantly computational project in her lab with little to no coding experience. I would also like to thank computational biologist Jungeui Hong for running alignment and mutation calling pipelines on my data multiple times as the lab optimized genomic analysis workflows. Next, I would like to thank research technician Amanda Zucker for being an amazing colleague and dear friend. Beyond assisting me with cutting and staining hundreds of tissue sections, Amanda and I saw many Broadway shows together, shared an enormous number of desserts, frolicked in lavender fields, and commiserated over graduate school; I do not know where I would be without her. Furthermore, I want to thank research technician Elias Ramzey-Karnoub for always being there to listen, bounce ideas off of, and celebrate. Elias's generosity and game for anything attitude made lab and life so much more fun; it has been an immense privilege to be in his orbit. I would also like to acknowledge Jerry Melchor for being the best lab dad I could have asked for. Thanks for checking in, sharing your city hacks, and helping me navigate life, Jerry. Lastly, this project would not have been possible without additional help from former and current lab members including Michael Kinnaman, Alvin Makohon-Moore, Marc Attiyeh, Akimasa Hayashi,

Hitomi Sakamoto, Zachary Kohutek, Rajya Kappagantula, Caitlin Mcintyre, and Nicholas Lecomte.

Furthermore, I would like to acknowledge all the core facilities at the Sloan Kettering Institute that helped me with my project. The Integrated Genomics Operation sequenced hundreds of samples on my behalf, and Dr. Nicolas Socci of the Bioinformatics Core was instrumental in helping me navigate the world of high-performance computing. Additionally, Marinela Capanu and Joanne Chou of the Biostatistics Core ensured that every analysis was supported by the appropriate statistical tests and that conclusions were properly drawn given the outlined limitations.

I would also like to thank my collaborators from Benjamin Raphael's lab at Princeton whose contributions were essential to the completion of this project. Dr. Matthew Myers, thank you for your patience and your expertise with running and optimizing HATCHet; without your assistance, the quality of my copy number data would have been mediocre at best. Similarly, I would like to thank Dr. Brian Arnold for his support with HATCHet and DeCiFer analyses. We learned a great deal about these programs together, Brian; thank you for helping me troubleshoot and interpret my results with such care.

Lastly, I would like to thank my friends and family for their encouragement and understanding during this challenging chapter. husband, In particular, I would like to thank my husband, Sean McGrath, for his unconditional love and support throughout this journey. Thank you for uprooting your life and moving to NYC with me, for putting up with all my complaining, and for planning countless fun Saturdates. I could not have done this without you.

Table of Contents

LIST OF FIGURES

LIST OF TABLES

LIST OF ABBREVIATIONS

BAF	B-allele frequency
BAM	Binary Alignment Map
BWA	Burrows-Wheeler Aligner
CCF	Cancer Cell Fraction
COSMIC	Catalogue of Somatic Mutations in Cancer
CNA	Copy Number Alteration
DCF	Descendent Cell Fraction
DNA	Deoxyribonucleic Acid
EGA	European Genome-phenome Archive
ERK	Extracellular signal-regulated kinase
FOLFIRINOX	5-fluorouracil, leucovorin, irinotecan, and oxaliplatin
FFPE	Formalin-Fixed, Paraffin Embedded
GATK	Genome Analysis Toolkit
GISTIC	Genomic Identification of Significant Targets in Cancer
gITH	genetic intratumoral heterogeneity
ICGC	International Cancer Genome Consortium
H&E	Hematoxylin and Eosin
HATCHet	Holistic Allele-specific Tumor Copy-number Heterogeneity
IMPACT	Integrated Mutational Profiling of Actionable Cancer Targets
INDEL	Insertions and deletions
KRAS	Kirsten rat sarcoma virus
LOH	Loss of heterozygosity
OpenCRAVAT	Open Custom Ranked Analysis of Variants Toolkit
OncoKB	Oncology Knowledge Base
OS	Overall Survival
PanIN	Pancreatic Intraepithelial Neoplasia
PDAC	Pancreatic Ductal Adenocarcinoma
REVEL	Rare Exome Variant Ensemble Learner
TCGA	The Cancer Genome Atlas
SNV	Single Nucleotide Variant
SV	Structural Variant
VAF	Variant Allele Frequency
WES	Whole Exome Sequencing
WGD	Whole Genome Duplication
WGS	Whole Genome Sequencing
WT	Wild-Type

CHAPTER ONE: INTRODUCTION

Pancreatic ductal adenocarcinoma

Pancreatic ductal adenocarcinoma (PDAC) is the most common neoplasm of the pancreas, accounting for >90% of all pancreatic malignancies[1]. This tumor type poses a significant health problem globally, with 495,773 (262,865 male and 232,908 female) new cases diagnosed in 2020 and an associated 466,003 (246,840 male and 219,163 female) deaths in the same year[2]. While the incidence rate for pancreatic cancer has increased by about 1% per year since 2000, the death rate has increased only slightly by 0.2% per year[3]. Furthermore, the incidence rate increases with age, with the average age at diagnosis being 70 years[2]. According to GLOBOCAN 2020 estimates, pancreatic cancer ranks as the twelfth most common malignancy (2.6% of all cancers) and the seventh leading cause of cancer mortality (4.7% of all cancers)[4]. If outcomes do not improve, the disease is projected to surpass breast cancer as the third leading cause of cancer death by 2025 in the European Union and become the second leading cause of cancer-related death in the United States by 2030[5,6]. Despite significant advances in understanding the biology of PDAC and numerous clinical trials, the prognosis for patients with pancreatic cancer remains poor with a 5-year relative survival of 11% for all stages and only 3% for metastatic disease[3].

Treatment

Therapeutic options in PDAC are lacking. Surgical resection in early stage (Stage I/II) patients offers the only opportunity for cure. However, only 10-20% of patients with PDAC have resectable disease[1]. The primary surgical treatment for PDAC is a pancreaticoduodenectomy (Whipple procedure), which involves the removal of the head of the pancreas, most of the duodenum, the gallbladder and a portion of the bile duct[7]. For

tumors of the pancreatic tail, a distal pancreatectomy with splenectomy is performed[8]. A total pancreatectomy is rarely required except for tumors that are either centrally located or expand the entire length of the organ[9]. Overall, pancreatic cancer surgery has acceptably low mortality rates of <5% thanks to centralization of patient care to high-volume centers[10,11] and improved perioperative management[12]. However, of those who undergo resection followed by adjuvant therapy, ~80% will relapse and ultimately die of their disease[8].

For Stage III/IV patients with good performance status, chemotherapy is the first-line treatment option. Gemcitabine has been the standard chemotherapy drug for many years, but combination therapies with nab-paclitaxel and FOLFIRINOX have recently shown better survival outcomes in patients with advanced PDAC[13]. Conversely, patients with a poor performance status generally receive either gemcitabine alone or in combination with erlotinib or capecitabine integrated with palliative care[13]. For select patients with locally advanced disease, radiation-based therapy is either administered as a single modality or in combination with chemotherapy[14]. Approximately 10% of PDACs contain mutations in DNA damage repair genes such as BRCA2 and PALB2[15]. Consequently, these tumors exhibit large numbers of structural variants (SVs), exceeding 200 per genome[16]. For patients with this scale of genomic instability, platinum salts (e.g. cisplatin and oxaliplatin) and PARP inhibitors are becoming important therapeutic strategies[17]. Although mismatch repair deficiency only occurs in <1% of PDACs[18], it confers favorable responses to immune checkpoint inhibitors, likely owing to a higher neoantigen burden. Overall, improvements in patient outcomes have been modest and incremental compared to the prior treatment standard, single agent gemcitabine.

Novel and innovative treatment approaches are urgently needed to improve clinical outcomes in patients with PDAC. One promising area of research is the development of mRNA vaccines against pancreatic cancer. These vaccines work by delivering mRNA molecules that encode tumor-associated antigens, which stimulate an immune response against the cancer[19]. In a recent Phase 1 trial, Balachandran et al. tested an mRNA vaccine encoding neoantigens in PDAC patients. They found the vaccine was safe and generated functional T cell responses against multiple neoantigens in patients[20]. In a follow-up study, they analyzed neoantigen quality in long-term survivors versus short-term survivors[21]. Survivors had T cells targeting neoantigens with higher MHC binding affinity. However, over time, clones targeting these high-quality neoantigens were selectively lost. This reveals a process of immunoediting, where cancer cells expressing high affinity neoantigens are eliminated, leading to outgrowth of cells with lower quality neoantigens no longer targeted by T cells. These findings provide insights into PDAC immune escape and have implications for mRNA vaccine design and T cell monitoring approaches. Optimizing neoantigen selection and combatting T cell exhaustion may be key to improving mRNA vaccine efficacy in PDAC.

PDAC genetics

PDAC is characterized by a high prevalence of mutations in KRAS, TP53, CDKN2A, and SMAD4. Oncogenic KRAS mutations occur in over 90% of PDACs and are considered a key early event in pancreatic tumorigenesis[15,16,22]. Multiple oncogenic KRAS alleles have been identified, including G12D, G12V, and G12R, as well as numerous other hotspot codon 12 and 61 mutant alleles at a lower prevalence[15,16,22–24]. Somatic TP53 mutations are also detected in up to 85% of PDACs[25] with as many as 66% of TP53 mutations being

missense mutations that affect the DNA binding domain[22].Inactivation of the CDKN2A tumor suppressor, which regulates p16INK4A and p19ARF, is found in >90% of PDACs through mutation, deletion, or promoter methylation[26]. Finally, inactivation of SMAD4 occurs in approximately 55% of PDACs either by homozygous deletion (30%) or by an intragenic mutation coupled with loss of the second copy (25%)[27].

Furthermore, PDAC also harbors extensive copy number alterations (CNAs). In a TCGA study of 150 pancreatic cancers, arm-level CNAs were identified in over a third of PDAC tumors using both SNP microarrays and whole-exome sequencing (WES)[15]. Amplifications of 1q (33%) and deletions of several chromosomal regions such as 6p (41%), 6q (51%), 8p (28%), 9p (48%), 17p (64%), 17q (31%), 18p (32%), and 18q (71%) were consistent with previous studies[16,28,29]. GISTIC analysis of focal amplifications and deletions in the high-purity group of tumors revealed recurrent events containing known oncogenic drivers including amplifications of GATA6, ERBB2, KRAS, AKT2, and MYC, as well as deletions of CDKN2A, SMAD4, ARID1A, and PTEN.

In addition to these common single nucleotide variants (SNVs) and CNAs, PDAC genomes exhibit complex structural variations such as deletions, inversions, interchromosomal translocations and tandem duplications [16]. Analysis of whole-genome sequencing data from 100 PDACs by Waddell et al. revealed that pancreatic cancers contained an average of 119 SVs per tumor (range 15–558) and the majority of structural variants were intra-chromosomal. The authors defined four subgroups of PDAC based on the frequency and distribution of structural rearrangements found within a sample, including stable, locally rearranged, scattered and unstable. The stable subtype (20% of all samples) contained ≤ 50 structural variation events and often exhibited widespread

aneuploidy, which suggested defects in cell cycle/mitosis. In the locally rearranged subtype (30% of all samples), the genome exhibited a significant focal event on either one or two chromosomes. Roughly one third of locally rearranged genomes contained regions of copy number gain that harbor known oncogenes, KRAS, SOX9, and GATA6, as well as in therapeutic targets such as ERBB2, MET, CDK6, PIK3CA, and PIK3R3 at low prevalence. These data suggest that there is a significant diversity of mechanisms involved in PDAC progression. The remaining local rearrangements involved complex genomic events such as breakage–fusion–bridge or chromothripsis[30,31]. In the scattered subtype (36% of all samples), tumors exhibited a moderate range of non-random chromosomal damage and <200 structural variation events. Lastly, the unstable subtype (14% of all samples) exhibited a large number of structural variation events (>200; maximum of 558), indicative of defects in DNA maintenance. Upon further analysis, the authors found that unstable tumors were associated with a high BRCA mutation signature and deleterious mutations in BRCA pathway genes. While mutations in other genes involved in DNA maintenance such as ATM, FANCM, XRCC4, and XRCC6 were also detected in tumors with an unstable genome, these events had not been causally linked to these genomic events at the time of the authors' analysis.

Genetic intratumoral heterogeneity

PDAC exhibits multiple types of genetic Intratumoral Heterogeneity (gITH). In solid tumors, gITH can be categorized into three types[32]; Type 1 gITH refers to genomic differences between any two cells within the primary tumor; Type 2 gITH refers to genomic differences between any two cells within a metastasis; and Type 3 gITH refers to genomic differences between two different metastasis-initiating cells within the primary

tumor. An additional distinction to be made is whether gITH corresponds to any mutation (silent and non-silent) or to deleterious driver gene alterations specifically. From a clinical perspective, gITH is associated with cancer progression and contributes to therapeutic resistance[33].

In a multiregion study of treatment-naïve Stage IV PDAC, identical driver mutations were identified in every metastatic lesion for each patient studied with respect to pathogenic SNVs, focal CNAs, and SVs[34]. The only Type 3 gITH identified corresponded to passenger (silent and non-deleterious) mutations, which when quantified yielded higher (i.e., more related) Jaccard relatedness indices compared to those of normal tissue. These findings suggest that at least one clonal sweep occurred in all the PDACs examined, resulting in a genetically homogeneous tumor prior to metastatic dissemination. Furthermore, these results have encouraging clinical implications for the success of future potential targeted therapies against clonal drivers in advanced-stage PDAC, suggesting that they could provide an initial clinical benefit. This rationale is believed to underlie exceptional responses to cisplatin or PARP inhibitors in patients with germline or somatic BRCA2 mutations[17].

By contrast, in a separate study of patients that were originally diagnosed with Stage I/II resectable PDAC who recurred after adjuvant therapy, all primary tumors exhibited evidence of Type 1 gITH with respect to driver genes[35]. These primary tumors were further categorized according to their phylogenetic relationship to the recurrent disease. “Outgroup” primaries were distantly related to the recurrent disease, suggesting that recurrence was the product of the expansion of a single residual clone (monophyletic). Conversely, “ingroup” primaries were as related to the recurrent disease as any other

sample in the patient, suggesting that recurrence arose from clonally diverse (polyphyletic) residual disease. Irrespective of phylogenetic category, recurrent disease was enriched for functionally deleterious SNVs and CNAs that activate MAPK/ERK and PI3K/AKT signaling. Notably, droplet digital PCR confirmed the presence of these SNVs in the primary tumor. Cumulatively, these findings demonstrate that gITH for deleterious driver gene alterations exists in Stage I/II PDAC upon which treatment imposes a genetic bottleneck. Not only are these results significant because they support investigation into the role for MAPK and PI3K inhibitors in the adjuvant setting, but when considered in tandem with other multiregion studies[34], they demonstrate that clinically relevant gITH is stage and context dependent.

PDAC from an evolutionary perspective

Stages of PDAC evolution

PDAC is a highly aggressive cancer that arises from the exocrine cells of the pancreas and its evolution can be characterized into three general stages. These stages are tumor initiation via the acquisition of a driver gene mutation, clonal expansion of the cell carrying the initiating mutation, and dissemination of the neoplastic population into foreign microenvironments[32]. While the occurrence of the initiating driver gene mutation is necessary for PDAC progression, this event alone is insufficient; it is not until the initiating mutation becomes fixed in the epithelial cell population that PDAC can develop. The subsequent clonal expansion stage corresponds to the development of PDAC precursor lesions called pancreatic intraepithelial neoplasia (PanINs)[36], during which high frequency (*KRAS, CDKN2A, TP53, SMAD4)* and low frequency (*KMT2C, ARID1A* and *SF3B1)* somatic mutations[16] accumulate. These mutations commonly accumulate in a stepwise

manner[37], but in rare cases multiple alterations can be acquired simultaneously in the aftermath of a catastrophic genome-wide event such as chromothripsis[38]. Once cells break through the basement membrane into the surrounding stroma, various selective pressures shape them into subclonal populations with varying degrees of fitness.

Timeline of PDAC evolution

The timeline of PDAC evolution spans multiple decades. Quantitative analyses of the timing of the genetic evolution of PDAC suggest that at least a decade passes between the occurrence of the initiating mutation and the birth of the non-metastatic founder cell[39]. The same model also predicts that at least five more years are required for the acquisition of metastatic ability, after which most patients die a few years later. Therefore, the time from tumor initiation to death of the patient has been estimated to take >20 years, providing a large window of opportunity for early detection of PDAC while it is still in its early, curable stage.

Evolutionary trajectories in PDAC

There is a range of evolutionary trajectories in cancer, both within and across tumor types. At one end of the spectrum, tumors follow a classical Darwinian growth pattern, displaying extensive gITH that is characterized by heterogeneous subclonal driver mutations and CNAs[40]. Clear cell renal cell carcinoma (ccRCC) typifies this end of the spectrum and clinically is characterized by having a more indolent growth pattern, oligometastatic disease and relatively long-term survival[41]. At the other end of the spectrum, PDAC patients typically have multiple clonal (truncal) driver gene alterations consisting of both somatic coding mutations and CNAs, and their subsequent evolutionary trajectories are relatively monoclonal[40]. From a clinical perspective, these patients usually suffer from

rapid progression and dissemination across multiple metastatic sites, succumbing to their disease early. However, a minority of advanced stage PDAC patients exhibit an indolent disease course and relatively long-term survival[42], similar to patients with ccRCC[40]. Deep genomic profiling of one such unusual patient revealed a truncal *CTNNA2* deletion as the sole genetic event.

How and why these different evolutionary growth patterns emerge remains unclear. Moreover, it is unknown if the clinical timepoint at which samples are collected represents the full scope of evolutionary trajectories that can occur within a particular disease. For patients with ccRCC, surgery plays a major role in disease management[41]. This clinical paradigm has supported evolutionary studies in this tumor type because both the primary tumor and matched synchronous metastases can be sampled as a byproduct of delivering routine care. Conversely, surgical management plays a more limited role in patients diagnosed with PDAC. Not only is surgical resection difficult because the pancreas lies deep within the abdomen adjacent to vital veins and arteries, but PDAC is commonly asymptomatic until it progresses to more advanced stages. Consequently, most patients present with unresectable disease that is either locally advanced at diagnosis or has metastasized to distant organs[8]. As a result, multiregion studies of PDAC have been performed on samples that have been obtained primarily through post-mortem collection[34,35,43]. It is unknown whether there are underappreciated biases from these tissue sampling practices related to the extent and prevalence of gITH both between and within tumor types. Furthermore, multiple factors including the pathogenicity of driver event(s), disease latency, cell of origin and tumor microenvironment, as well as exogenous and endogenous mutational processes, may also contribute[44].

Evolutionarily informed therapies

From a therapeutic perspective, targeting the evolutionary mechanisms of PDAC has emerged as a promising strategy to improve patient outcomes. One example of an evolutionary-based therapy is inhibition of the KRAS pathway, which has been a longstanding challenge due to the lack of druggable targets[45]. However, recent advances have led to the development of novel KRAS inhibitors, such as AMG510 (sotorasib) and MRTX849 (adagrasib), which have shown promising results in preclinical and early-phase clinical trials[46,47]. AMG510 and MRTX849 are covalent inhibitors that lock KRAS G12C in an inactivated GDP-bound state, thus decreasing functional KRAS and ultimately leading to cell cycle arrest and apoptosis in KRAS-mutant tumors. Unlike other tumor types including non-small-cell lung cancer and colorectal cancer, KRAS G12C is a rare mutation that only occurs in 1-2% of pancreatic cancers patients, thus limiting its utility in this clinical context. Excitingly, a non-covalent inhibitor of KRAS G12D, MRTX1133, has recently demonstrated potent inhibition of KRAS G12D-dependent signaling and tumor regression in xenograft models[48]. While phase I/II clinical trials have only recently launched in early 2023, MRTX1133 could have a far greater impact on PDAC patients as KRAS G12D is present in approximately 34% of cases[49]. Targeting early events like KRAS that drive tumorigenesis is widely considered to be an optimal therapeutic strategy because most if not all the tumor cells will harbor the alteration of interest. However, subclonal mutations may also be useful targets in combination therapies if they play a functional role in subclones influencing tumor progression.

Scope of thesis

gITH has been associated with cancer progression and is thought to be a major contributor to treatment resistance. However, the extent to which different genetic drivers that arise during carcinogenesis specifically influence subsequent evolutionary trajectories and clinical course remains unknown. Ultimately, a deeper understanding of evolutionary trajectories within and across multiple tumor types, as well as before and after treatment may distinguish patients with more indolent disease biology or oligometastatic progression from those with more rapid dissemination and clinical courses. Such insights have the potential to facilitate clinical trial stratification and disease management. The aim of this project is to determine the extent to which diversity and evolutionary timing of driver gene mutations impacts clinical disease course in a single cancer type, PDAC. While there are known driver genes in PDAC, the extent to which the quantity, quality, or chronology of these drivers impacts tumor evolution remains unclear.

CHAPTER TWO: MATERIALS AND METHODS

Tissue sample collection and processing

Tumor and matched normal tissues were collected through the Gastrointestinal Cancer Rapid Medical Donation Program at the Johns Hopkins Hospital and the Medical Donation Program at Memorial Sloan Kettering Cancer Center. Pre-mortem informed consent was obtained from all subjects. Following their demise, a research autopsy was conducted and samples from any primary tumor (if not already resected), local recurrence, or metastasis were harvested. All samples were split into two equal halves for snap freezing in liquid nitrogen and formalin fixing respectively, such that the fresh frozen sample is a mirror image of the formalin-fixed, paraffin embedded (FFPE) sample. H&E sections were prepared from either frozen or FFPE tissues and reviewed by a gastrointestinal pathologist (A.H. and C.A.I.-D.) and tumor rich regions were identified for DNA purification. Either serial 20 μm sections were cut and the area of interest scraped from the slide using a blade or alternatively a core was directly punched from the tissue block.

DNA sequencing

Genomic DNA was extracted using the DNeasy Blood & Tissue Kit (Qiagen) following the manufacturer's protocol. DNA quantification, library preparation, and sequencing were performed in the Integrated Genomics Operation and preliminary bioinformatics analysis was performed by the Bioinformatics Core at Memorial Sloan Kettering Cancer Center (New York, NY). Briefly, an Illumina HiSeq 2000, HiSeq 2500, HiSeq 4000 or NovaSeq 6000 platform was used. The majority of samples (n=545) underwent whole exome sequencing (WES) at 250X coverage, 34 samples underwent WES at 150X coverage, and

77 samples underwent whole genome sequencing (WGS) at 60X coverage. The resulting sequencing reads were analyzed in silico to assess quality and overall coverage, and alignment to the human reference genome hg19 was performed with BWA v0.7.17[50]. Read deduplication, base quality recalibration, and multiple sequence realignment were performed using the Picard Suite and GATK v.3.1[51]. Somatic single-nucleotide variants and insertion–deletion mutations were detected using Mutect2 (v4.1.2.0) and HaplotypeCaller v.2.4[52]. To validate the mutations found from WES and WGS datasets, one of two different targeted sequencing approaches were used. The majority of samples (n = 347) were sequenced with one of multiple versions of the MSK IMPACT panel (IMPACT 410, n = 68; IMPACT 468, n = 105; IMPACT 505, n = 174), with a mean coverage of 500-1000×. Another 285 samples were sequenced using a custom targeted panel described elsewhere [Hong et al. in preparation]. BAM files and associated metadata have been uploaded to the European Genome-phenome Archive (EGA; http://www.ebi.acu.uk/ega) under the accession number EGAS00001007379[53].

Filtering and annotation of variants

For each patient, somatic variants were filtered using the following criteria: patient-matched normal coverage ≥ 10 reads, variant count in patient-matched normal < 2 reads, patient-matched normal variant frequency < 0.02, tumor coverage ≥ 20 reads, and tumor variant allele frequency (VAF) ≥ 0.05 in at least one tumor sample. Variants were further filtered to include those present in coding regions only. Mutations located in blacklisted regions defined by ENCODE and RepeatMasker (https://github.com/mskcc/ngs-filters/blob/master/data/source.txt) were ignored. In FFPE samples, if a mutation exhibited

VAF < 0.1 and was identified as a C→T substitution, it was considered an FFPE artifact and thus, excluded from subsequent analyses.

Table 1. OpenCRAVAT module versions.

Annotator	Local version	Local data version
CHASMplus	1.3.0	v1.0.0
ClinVar	2023.02.01	2023.02.01
COSMIC	94.0.0	v94
OncoKB	1.1.3	09.06.22
REVEL	2022.11.29	v4.3a

Filtered variants were then annotated by OpenCRAVAT v2.2.7[54] to identify likely functional driver mutations. When available, criteria for determining whether a mutation should be considered a driver by a given module were informed by recommendations made for interpreting results from the module in the OpenCRAVAT store. For CHASMplus[55], the adjusted p-value needed to be < 0.05. For COSMIC[56], variants needed to be present at least four times in the database to be considered a driver. For ClinVar[57], the Clinical Significance value needed to be ”Pathogenic”, ”Pathogenic/Likely pathogenic”, ”Likely pathogenic”, ”Pathogenic, drug response, other”, or ”drug response” and the Review Status needed to be ”criteria provided, multiple submitters, no conflicts” or ”reviewed by expert panel”. For OncoKB[58], a mutation needed to be labeled as either ”Oncogenic” or ”Likely Oncogenic”. For REVEL, the Score needed to be > 0.7[59,60]. These modules were selected based on a survey of commonly used variant annotators in the scientific literature. Module versions are detailed in Table 1. A final driver score for each mutation was calculated by tallying how many annotators classified the mutation as a driver event (max score = 5).

Mutations with a score of 2 or higher were considered driver mutations and those with a score of 1 or lower were not.

Copy number analysis and WGD prediction

Whole genome duplication (WGD) and allele-specific copy number alterations were inferred for WES and WGS datasets using HATCHet v1.2.0[61,62]. Only autosomes were used for copy number analysis and phasing was performed with SHAPEIT v2.r90[63]. Upon manual review of computed read-depth ratios, B-allele frequencies, and clusters, parameters for clustering refinement were reviewed for consensus by four of the authors (K.M.M., B.J.A., M.A.M., B.J.R). Copy number calls of sufficient quality could not be obtained for 20 patients, as indicated in Supplemental Table 2.

Evolutionary analysis of driver mutations

To identify clusters of SNVs which occur in the same phylogenetic branch of tumor evolution, we used DeCiFer v2.1.3[64]. HATCHet output was used as the copy number input for this analysis. Therefore, only the subset of 70 patients with HATCHet results underwent analysis with DeCiFer. To ensure timely run completion, we required a minimum VAF of 0.05 for WES datasets and 0.1 for WGS datasets. To generate custom state trees, a maximum copy number of 6 was used for each patient. When the total copy number profile of a given mutation was > 6 or read depths were not > 1 across all samples, mutations could not be analyzed by DeCiFer. Furthermore, the timing of driver mutations identified exclusively in targeted sequencing datasets could not be analyzed with DeCiFer because HATCHet could not be performed on these datasets. Truncal and subtruncal densities were

calculated by dividing the number of truncal or subtruncal SNVs at sites with > 10X depth by the number of genomic positions using the same depth threshold.

De novo mutational signature analysis

De novo mutational signatures including Single Base Substitution (SBS), Double Base Substitution (DBS) and Insertion and Deletion (ID) were evaluated in comparison with COSMIC Mutational signatures version 3 (https://cancer.sanger.ac.uk/signatures/) using the R package Palimpsest[65]. Only somatic variants that met the filtering criteria outlined in the Filtering and annotation of variants section above, as well as those located within 5' or 3' UTR regions, were included in this analysis. Additionally, FFPE tumor samples were excluded as they induce massively unique signatures that are not relevant with cancer progression. Significant de novo mutational signatures were extracted using the Non-negative Matrix Factorization (NMF) algorithm[66]. The maximum number of NMF runs and de novo signatures were set to 30 and 20, respectively. Finally, we assigned the most representative de novo signature of the SBS, DBS and ID types among all those extracted to each variant based on probability scores generated by Palimpsest.

Data Visualizations

The oncoprint was created with CoMut[67]. Anatomic and other cartoons were created using BioRender (https://biorender.com/)

CHAPTER THREE: THE EVOLUTIONARY FOREST OF PDAC

Introduction

The genetic basis of pancreatic ductal adenocarcinoma has been well documented throughout the era of next-generation sequencing. Through the International Cancer Genome Consortium[16,24,29], The Cancer Genome Atlas[15], PCAWG[68,69], and others[22,23], whole-genome (WGS) and whole-exome sequencing (WES) has been performed on hundreds of samples to reveal the complex mutational landscape of primary tumors. These studies have revealed both common and infrequent drivers associated with PDAC and clarified the genetic basis of responsiveness to different standard-of-care therapies[15,16]. Notably, most samples used in these studies were obtained from surgical resections. This is rational given the amount of material needed for sequencing and that surgical resection is the most common mode of obtaining PDAC tissue for research purposes. However, patients with resectable disease comprise only 12% of newly diagnosed PDAC cases (seer.cancer.gov). Furthermore, of those who undergo resection followed by adjuvant therapy, more than 80% relapse and ultimately die of their disease[70–72]. These statistics highlight the need to better understand the more common clinical contexts of PDAC, including patients with locally advanced or metastatic disease.

Nonetheless, collecting tumor tissue from patients with stage III or IV disease has proven to be challenging. Unlike early-stage patients, late-stage patients do not undergo surgical resection as part of their disease management; therefore, samples are typically collected using either a small tumor core biopsy or fine-needle aspiration. Frequently, these specimens are mixed with a high proportion of stromal tissue, yielding low-purity tumors that make comprehensive genomic assessment difficult, if not impossible[73]. Owing to these

technical challenges, PDAC has been underrepresented in recent studies of metastatic cancer genomes across tumor types[74,75]. Conversely, the MSK-MET pan-cancer cohort contains nearly 1800 PDAC samples, the largest study of metastatic PDAC to date[76]. While this cohort is sizable, genomic characterization is limited due to the use of a targeted sequencing approach. Furthermore, only a single metastatic sample was studied for most patients. Single-sample analyses can underestimate intratumoral heterogeneity because variants identified as clonal in one sample may be subclonal or even absent in another, giving rise to the "illusion of clonality"[77].

To circumvent some of these obstacles, sampling can be conducted postmortem via research autopsies to enable more extensive sampling than otherwise possible in a living patient[78]. Although it remains unclear how many samples are required to conclusively determine the composition and clonality of drivers present in a patient's tumor, a multiregion study of clear cell renal cell carcinoma suggests that for larger tumors, 4-8 samples are sufficient to capture the majority of events[41]. Thus far, a handful of multiregion studies have been published addressing specific clinical contexts of PDAC, including treatment-naive stage IV patients[34], patients with recurrent disease after resection and adjuvant therapy[79], and treated late-stage patients [Hong et al. in preparation]. Additionally, the genetic correlates of transcriptional phenotypes in metastatic patients have been explored[43,80]. Cumulatively, these cohorts contained relatively few patients[43] and focused on transcriptional and genomic features during metastatic progression[80], thus limiting the statistical power for a broader investigation of the evolutionary histories of PDAC. Consequently, we believe that a comprehensive analysis of PDAC, including all stages of diagnosis and major treatment paradigms, is lacking. To this end, we clarify the extent to

which genetic features of PDAC are stage-and/or context-dependent using a multiregion sampling approach, permitting us to define the genetics and evolutionary histories of PDAC on a scale that has not yet been attempted.

Results

Overview of cohort

We screened 364 research autopsies to identify PDAC patients for inclusion in this study. Inclusion and exclusion criteria for patients and samples are detailed in Figure 2. WES or WGS sequencing data from 53 patients have been previously reported in multiple studies[34,43,79]. Thirty-seven patients were newly sequenced for the purposes of this study, including 14 research autopsies and 23 multiregion sampled surgical resections. Collectively, our cohort included 270 primary tumor samples, 295 metastatic samples, and one normal tissue sample from each of the 90 patients. The median number of tumor samples per patient was five, three of which were derived from spatially distinct regions within the primary tumor, and the other two from distinct metastatic sites (Figure 1A). All samples derived from surgically resected patients were treatment-naive and came from distinct regions of the primary tumor at least 0.5 cm apart. The cohort contained a broad spatial representation of metastases encompassing 12 distinct metastatic sites (Figure 1B). Fourteen patients were oligometastatic, which we defined as having no more than five metastatic lesions cumulatively from diagnosis to death, as detected by the latest scan results and comprehensive sampling at autopsy[81,82]. All stages of diagnosis were represented with 36 (40%), 24 (27%), and 30 (33%) patients initially presenting with stage I/II, III, and IV disease, respectively. The overall survival of the patients was consistent with the expected outcomes based on the clinical stage at diagnosis[83] (Figure 1C). Male

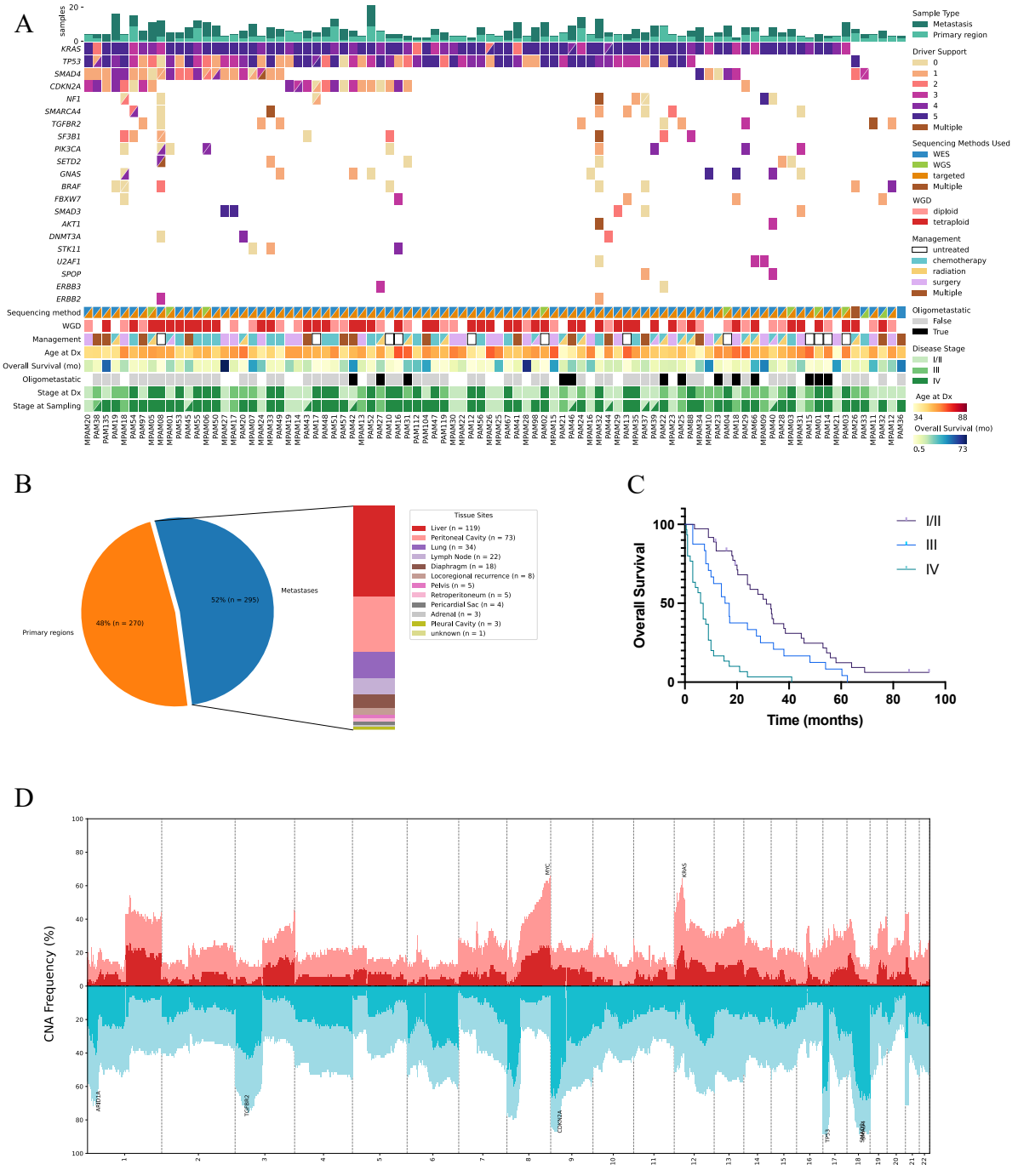

Figure 1. Overview of cohort.

(A) Overview of somatic alterations detected in tumor samples of 90 PDAC cases. Mutations were annotated by OpenCRAVAT (Methods). A complete list of genes harboring likely functional drivers is in Supplemental Table 3. Multiple indicates three or more mutations, treatment modalities, or sequencing methods. Split mutation patches containing Multiple indicate that a patient contained multiple mutations in a gene, one of which had a Support Level of 3 or higher. (B) Overview of different tumor sites sampled. (C) Survival statistics of cohort with respect to stage at diagnosis. (D) Frequency of CNAs in the multiregion PDAC cohort. Copy number gains and losses are indicated in red and blue respectively. Clonal CNAs are shown in darker and subclonal CNAs in lighter shades of their respective colors. Genomic regions containing known driver mutations are annotated.

A

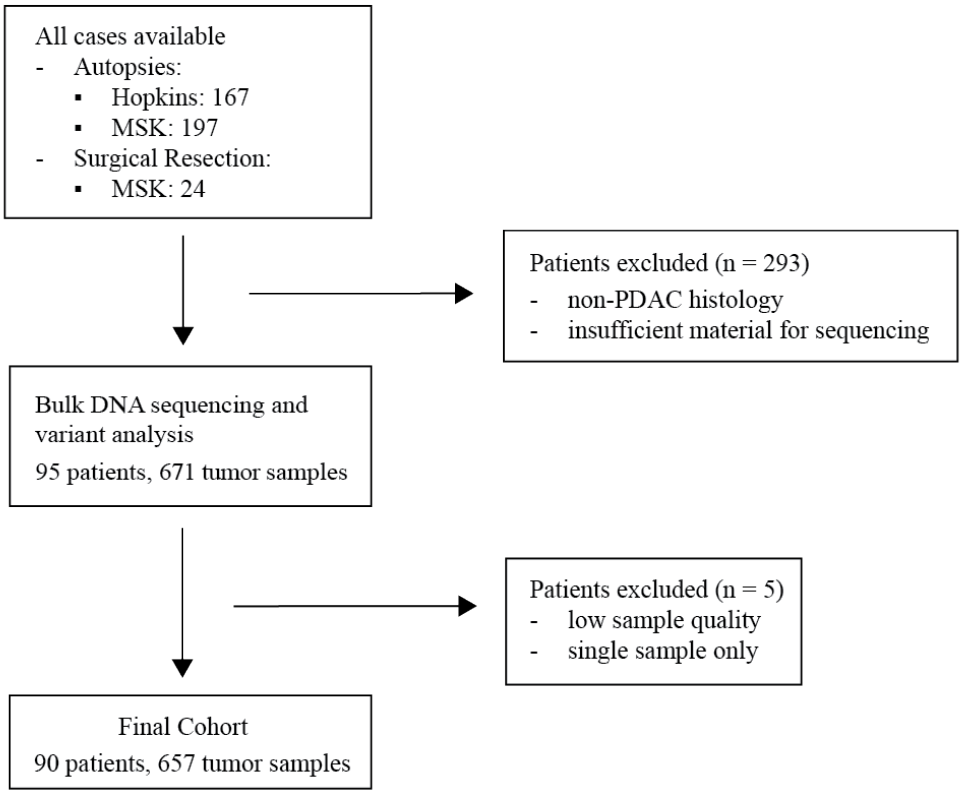

Figure 2. Cohort inclusion and exclusion criteria.

and female patients were nearly equally represented, with the average age at diagnosis for females being 66±13 years and 63±12 years for males, respectively. Forty-one patients (46% of cohort) reported a former or current history of smoking, and 24 patients (27% of cohort) had a history of Type 2 Diabetes Mellitus, both of which are common risk factors for PDAC[84,85]. Additional detailed clinical annotations for each patient are provided in Supplemental Table 1.

Annotation of driver events in PDAC

When selecting a sequencing assay, there is a trade-off between depth and breadth; a high depth is required to accurately recover clone frequency, whereas genome-wide detection of passenger mutations helps identify distinct clones[86]. To maximize our ability to both assess the clonal architecture of patients' tumors and identify likely functional driver mutations with high fidelity, we sequenced samples using at least two different methods (Figure 1A, Supplemental Table 2, Methods) when sufficient tissue was available. To build upon previous PDAC studies that highlighted all non-silent variants for a subset of genes, here, we report which SNVs and INDELs are predicted to be likely functional drivers. Using a multi-tool annotation approach (Methods), we identified 231 unique driver mutations across 121 genes (Supplemental Table 3), where the most frequently observed PDAC drivers (i.e., KRAS, TP53) generally yielded the highest support values (Figure 1A). Fourteen percent of drivers were identified exclusively in the targeted sequencing dataset, including major drivers such as KRAS, TP53, CDKN2A, and SMAD4, highlighting the importance of using orthogonal methods to detect driver mutations, especially in lower-purity samples. The median number of driver mutations identified per patient was three (range 1-15), in line with other recent reports[87]. Of the five patients with

eight or more driver mutations, four harbored somatic mutations in mismatch repair genes, including MSH6 and MSH2, of which 50% concurrently demonstrated loss of heterozygosity (LOH). An additional patient harbored a somatic mutation in ATM, indicating a defect in homologous recombination. The median number of driver mutations identified per sample was three (range 1-7), indicating a degree of driver gene heterogeneity within the cohort.

To address whether the genomic landscape of end-stage PDAC differs from that of early stage PDAC, we compared our findings to other published datasets that contain a predominance of resectable PDAC[16,88]. Common driver genes, including KRAS, TP53, and SMAD4, among others, were mutated at similar frequencies across TCGA, ICGC, and our multiregion cohort (Figure 3A). KRAS mutations were identified in 84/90 (93%) patients, in line with previous reports[15,29], although we identified a broader spectrum of mutant alleles, including E31K, G13P, and G12L (Figure 3C). We did not observe meaningful differences in survival with respect to different KRAS alleles (Figure 3D). KRAS WT patients harbored driver mutations in TP53, SMAD4, BRAF, BRCA2, and RBM10. An additional 19 known driver genes were common between our cohort and TCGA (n=14) or the ICGC (n=5), whereas 92 genes were found to harbor driver mutations unique to our cohort, including U2AF1 and SMAD2 (Figure 3B).

Nine patients in our cohort contained longitudinal data, with one sample collected at surgical resection and the rest collected after disease recurrence at autopsy. Seven patients acquired additional driver mutations following treatment, including alterations in PIK3CA, PDGFRB, HLA-B, and MSH2. While we did not have longitudinal data for most patients, we compared drivers identified in patients with early- and late-stage disease with

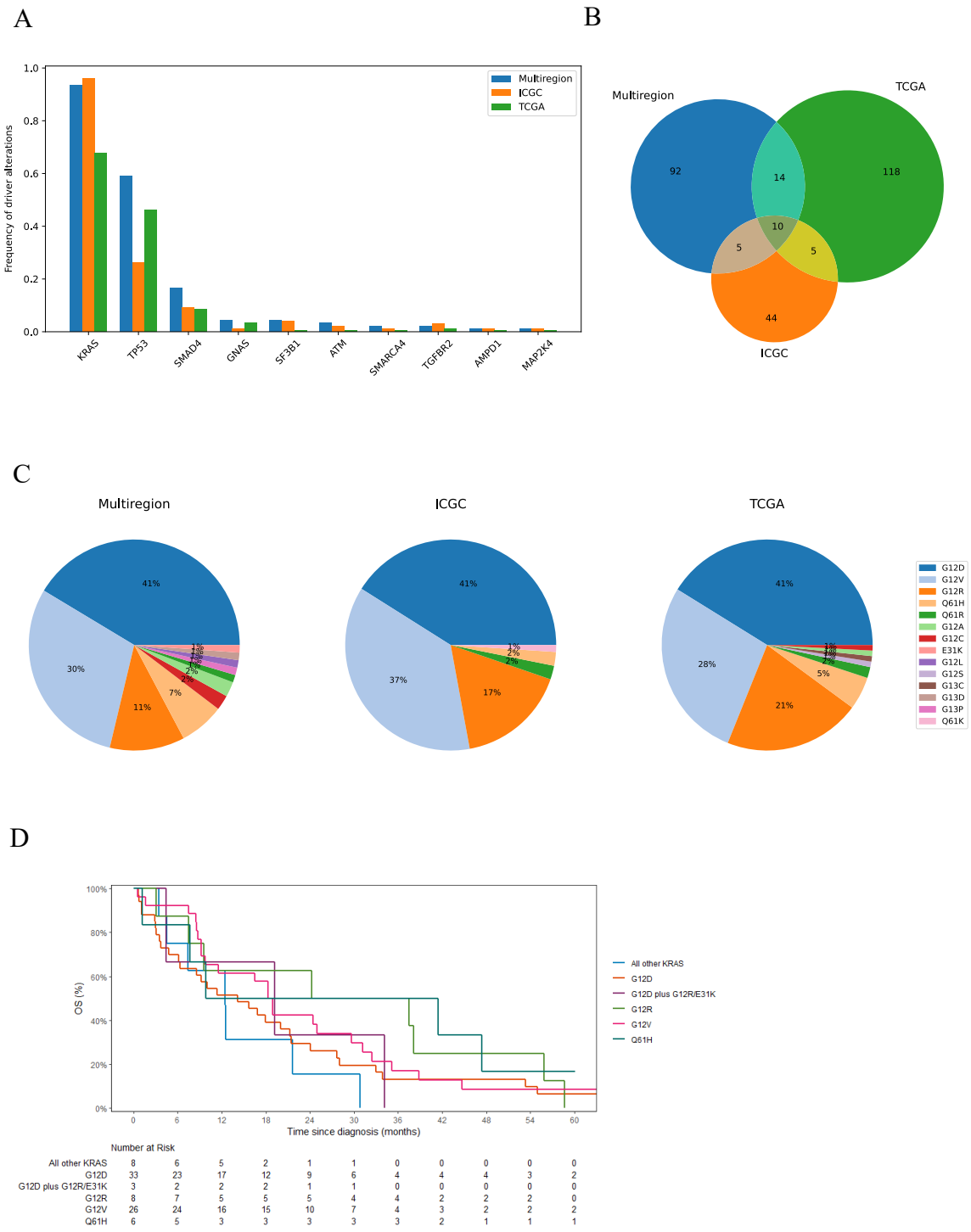

Figure 3. Driver mutations in large PDAC cohorts.

(A) Mutational frequency of common driver genes in multiregion cohort and two large scale PDAC studies, the ICGC and TCGA. Mutational frequencies represent only mutations identified as likely drivers, not all mutations identified in the indicated genes. (B) Number of unique driver genes identified per cohort. (C) Prevalence of KRAS alleles in multiregion cohort, the ICGC, and TCGA. (D) Survival of patients in multiregion cohort with respect to the most common KRAS alleles.

respect to different therapeutic interventions to determine the extent to which drivers were stage-and/or treatment-dependent. The majority of drivers identified were only observed in a single patient; however, SMAD3 and NF1 were the only recurrent driver genes exclusively found in treatment-naive patients who underwent surgical resection as part of their clinical management. Furthermore, we did not identify a significant difference in driver counts between treated and treatment-naive patients (Wilcoxon rank-sum test, P = 0.55).

Given the range of driver mutations identified, we also explored whether there was any relationship between the quantity or quality of drivers with respect to tissue type. To account for correlations within samples and between patients, we used a generalized linear mixed model with random intercept and unconstructed covariance structure to model the number of distinct driver mutations with respect to sample type (Primary vs Metastasis). In a univariate analysis, we observed a significant increase in the expected mean driver mutation count in metastatic samples compared to primary samples (Figure 4A, beta=0.178, 95% CI: 0.027-0.32, P = 0.02). Given this observation, we further investigated whether there was any relationship between the driver count and different metastatic routes (lymphatic, hematogenous, and directly seeded). Using the model outlined above, we found no significant association between the route of metastasis and number of driver genes (Figure 4B, P = 0.60). Although multiple driver genes were identified across distinct metastatic sites or routes, some were only observed in the context of specific sites or routes. However, these mutations were rare events, and we did not find any significant associations between gene enrichment of different core signaling pathways and routes of metastasis (Table 2). Cumulatively, these data suggest that the expansion of a subclone, potentially

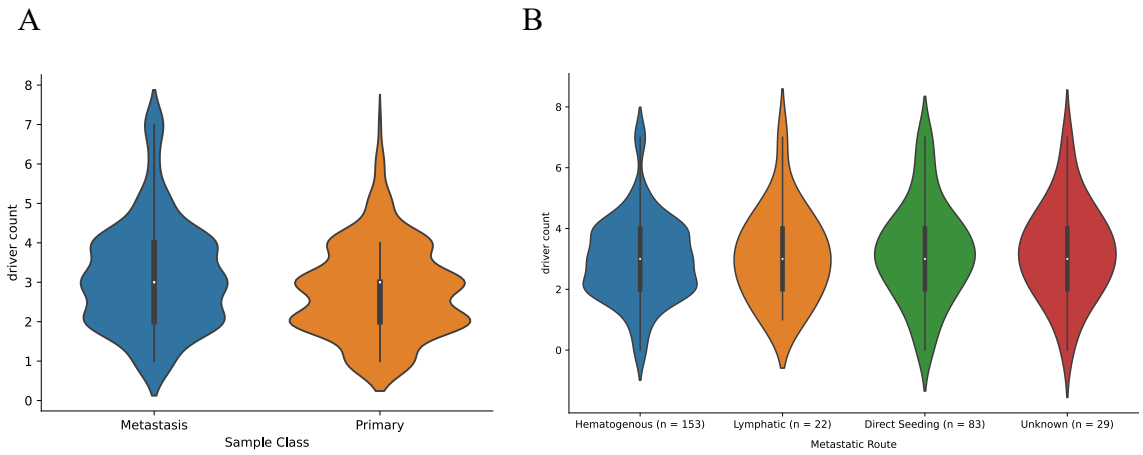

Figure 4. Driver counts with respect to metastasis.

(A) Driver mutation counts with respect to sample type. (B) Driver mutation counts of different metastases with respect to different routes to metastasis. Unknown encompasses sites whose metastatic route is uncertain (e.g., diaphragm, pleural cavity, pericardial sac, adrenal gland). Metastatic sites and their corresponding routes to metastasis are located in Supplemental Table 2.

Table 2. Prevalence of driver genes grouped by functional pathways with respect to route of metastasis.

Pathway	Direct seeding	Hematogenous	Lymphatic	Unknown	Total
RAS_RTK					
Yes	86 (32.2%)	160 (35.2%)	24 (35.3%)	30 (31.9%)	300 (34.9%)
Cell cycle					
Yes	64 (23.9%)	140 (30.8%)	16 (23.5%)	25 (26.6%)	245 (27.7%)
TGFβ					
Yes	43 (16.1%)	30 (6.6%)	5 (7.4%)	8 (8.5%)	86 (9.7%)
Chromatin Modification					
Yes	5 (1.8%)	5 (1.1%)	1(1.5%)	1 (1.1%)	12 (1.3%)
DDR					
Yes	5 (1.8%)	16 (3.5%)	4 (5.8%)	4 (4.2%)	29 (3.2%)
RNA processing					
Yes	1 (0.3%)	7 (1.5%)	0 (0%)	1 (1.0%)	9 (1.0%)

containing one or more additional driver alterations, precedes its dissemination and growth in secondary sites. However, the lack of association between any specific gene or pathway and a particular metastatic route suggests that alternative genetic, epigenetic, or post-translational mechanisms promote organ-specific colonization, as previously reported[89,90].

Somatic copy number alterations

Previous genomic analyses of PDAC have revealed numerous somatic copy number alterations (CNAs) affecting key oncogenes and tumor suppressor genes, including KRAS, TP53, SMAD4, and CDKN2A, among others[15,16,22,29]. To this end, we used HATCHet (Methods) to infer both allele-and clone-specific CNAs and their relative proportions across multiple samples from a subset of 70 patients for which these metrics could be reliably derived[61,62]. Our analysis revealed a notably high frequency of both clonal and subclonal gains in KRAS and MYC compared to the rest of the genome (Figure 1D, Supplemental Table 4). Moreover, these regions were distinguished by a relatively high proportion of subclonal gains. Similarly, other genes on chromosome 8 demonstrated the highest frequencies of subclonal gains in the cohort, including C8orf31, AK3P2, LY6E, ZNF16, NRBP2, BAI1, MROH4P, and ARC. The prevalence of LOH of 8p, TP53, CDKN2A, SMAD4, and SMAD2 was also remarkably high compared with that observed at other loci; however, these events were disproportionately clonal. Additionally, homozygous deletions in the latter genes were identified in 3-9% of patients, the majority of which were subclonal and co-occurred with LOH events in the same gene. Of the four KRAS WT patients, we were able to obtain CNA calls for (MPAM11, MPAM12, PAM26, and PAM32), two exhibited gains in KRAS (PAM26 and PAM32). All four patients

demonstrated LOH of SMAD4 and CDKN2A, whereas PAM26 and PAM32 also exhibited LOH of TP53.

Overall, both clonal (Wilcoxon rank-sum test, P = 2e-11) and subclonal (Wilcoxon rank-sum test, P = 0.0001) LOH events were significantly more common than gains in our cohort (Figure 5A). LOH was detected in all patients, however PAM25 was the sole patient without any copy number gains. Furthermore, both subclonal gains (Wilcoxon rank-sum test, P = 4.7e-14) and LOH events (Wilcoxon rank-sum test, P = 7.3e-12) were significantly more common than clonal copy number events (Figure 5A), suggesting that the majority of CNA events occurred relatively later in tumor evolution, as reported previously24, and that they may play a crucial role in driving intratumoral heterogeneity and tumor progression.

Whole-genome duplication (WGD) was identified in nearly two-thirds (45/70) of patients (Figure 1A). This exceeds previously reported rates of WGD in metastatic PDAC[68,74], likely due to more comprehensive sampling per patient. No significant association was found between the number of driver mutations and tetraploid status (odds ratio [OR]:1.11, 95% CI:0.88-1.51, P = 0.4). We observed that tetraploid patients had a significantly higher number of clonal (Wilcoxon rank-sum test, P = 0.013) and subclonal (Wilcoxon rank-sum test, P = 2.99e-6) LOH events (i.e., fractional allelic loss) than diploid patients, likely due to increased genomic instability (Figure 5B). Neither the proportion of clonal nor subclonal gain events differed significantly with respect to WGD status (Figure 5B). Furthermore, we found that WGD did not occur more frequently in treated than in treatment-naïve patients (Fisher's exact test, P = 0.23).

A

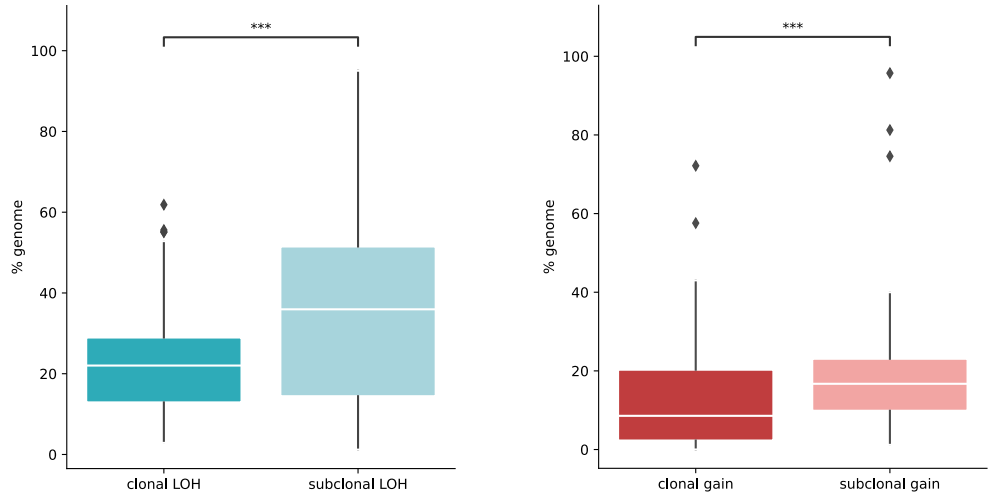

B

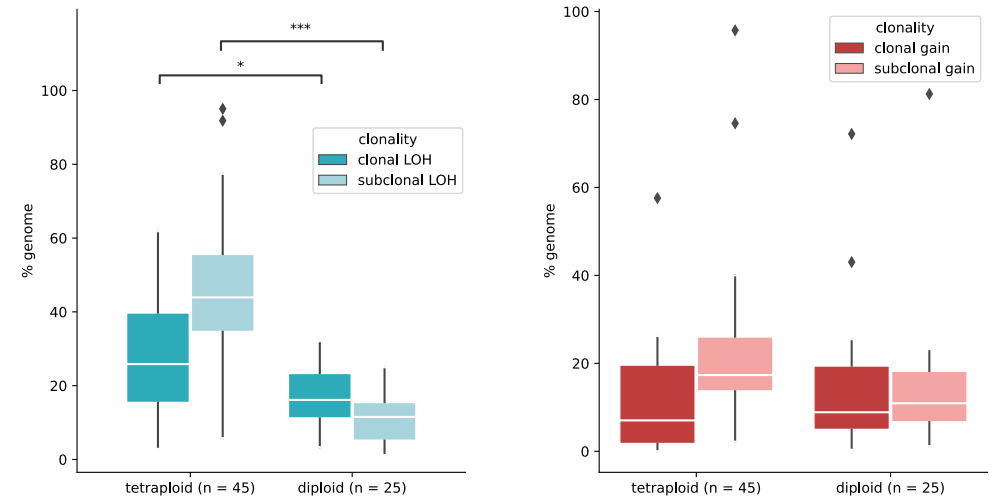

Figure 5. Quantification of CNA events.

(A) Fractional allelic loss and gains identified in multiregion cohort. Clonal CNAs are shown in darker and subclonal CNAs in lighter shade of color. (B) Fractional allelic loss and gains with respect to WGD status.

Timing of somatic events

A previous study of patients with late-stage PDAC demonstrated limited intratumoral heterogeneity of driver mutations in the absence of therapeutic pressure[34], indicating that they were acquired prior to the formation of metastatic subclones. To determine the evolutionary timing of driver alterations across the spectrum of PDAC clinical contexts, we analyzed the subset of our cohort (n = 70) for which we obtained CNA calls using DeCiFer (Methods). SNVs were classified as truncal if they were inferred to occur before the most recent common ancestor and subtruncal otherwise[91]. Of the 63% of putative drivers for which a truncal status could be determined (Methods), 79% were classified as truncal and the other 21% were subtruncal (Figure 6A). To compare our results to traditional CCF methods, we ran DeCiFer in CCF mode to determine whether truncal mutations were consistently clonal. Overall, we found that most truncal driver mutations were considered clonal based on CCF calculations. Notably, we identified two KRAS mutations and one TP53 mutation that were all found to be truncal yet had variant allele frequencies that were consistent with subclonality. Upon further investigation, we found that subclonal deletions and gains likely contributed to these truncal mutations having subclonal mutation frequencies, leading to erroneous conclusions regarding the evolutionary timing of somatic mutations from CCF estimates alone.

Notably, KRAS driver mutations were not universally determined to be truncal events. Of the two patients harboring subtruncal KRAS mutations, one had alternative truncal driver events in AKT1 and GNAS (PAM40). The second patient, PAM46, underwent surgical resection followed by adjuvant chemoradiation before passing away from locally recurrent disease. Both the original surgical resection and all samples of recurrent disease harbored a G12R mutation, which was determined to be truncal.

Conversely, a subtruncal G12D mutation was identified in two of the eight samples of the locoregional recurrence. Two additional patients, MPAM26 and PAM44, also harbored multiple KRAS mutations. Similar to PAM46, PAM44 also experienced locoregional recurrence after surgical resection. Unlike PAM46, PAM44 harbored a G12D mutation in every sample of recurrent disease and only harbored a G12R mutation in the original surgically resected sample. Additional mutational analysis revealed that the original resection was an independent primary tumor; thus, the timing of this event could not be inferred[79]. Both KRAS G12D and E31K mutations identified in MPAM26 were inferred to be truncal; however, they were found on different alleles. Cumulatively, these patients demonstrated convergent evolution toward increased KRAS signaling in the context of patients diagnosed with early-stage disease followed by surgical resection. Additional functional studies investigating the differences in downstream signaling and the efficacy of pan-KRAS inhibitors in this context are warranted.

Given the spectrum of clinical management represented in our dataset, we aimed to determine whether the timing of driver mutations differed across these contexts. We found no differences in the number of truncal or subtruncal drivers between treatment-naïve patients with early- versus late-stage disease, patients with treatment-naive versus treated late-stage disease, or patients pre- versus post-surgical resection (Figure 6B). Furthermore, patients with WGD did not have a significantly different number of truncal or subtruncal driver mutations compared to diploid patients. The median number of truncal drivers per patient was 2. Using this cutoff, we did not observe any difference in OS between those with more vs less than 2 truncal drivers (Log rank test, P = 0.2, Figure 6C). Although we found that a one-unit increase in the number of truncal drivers increased all-cause mortality

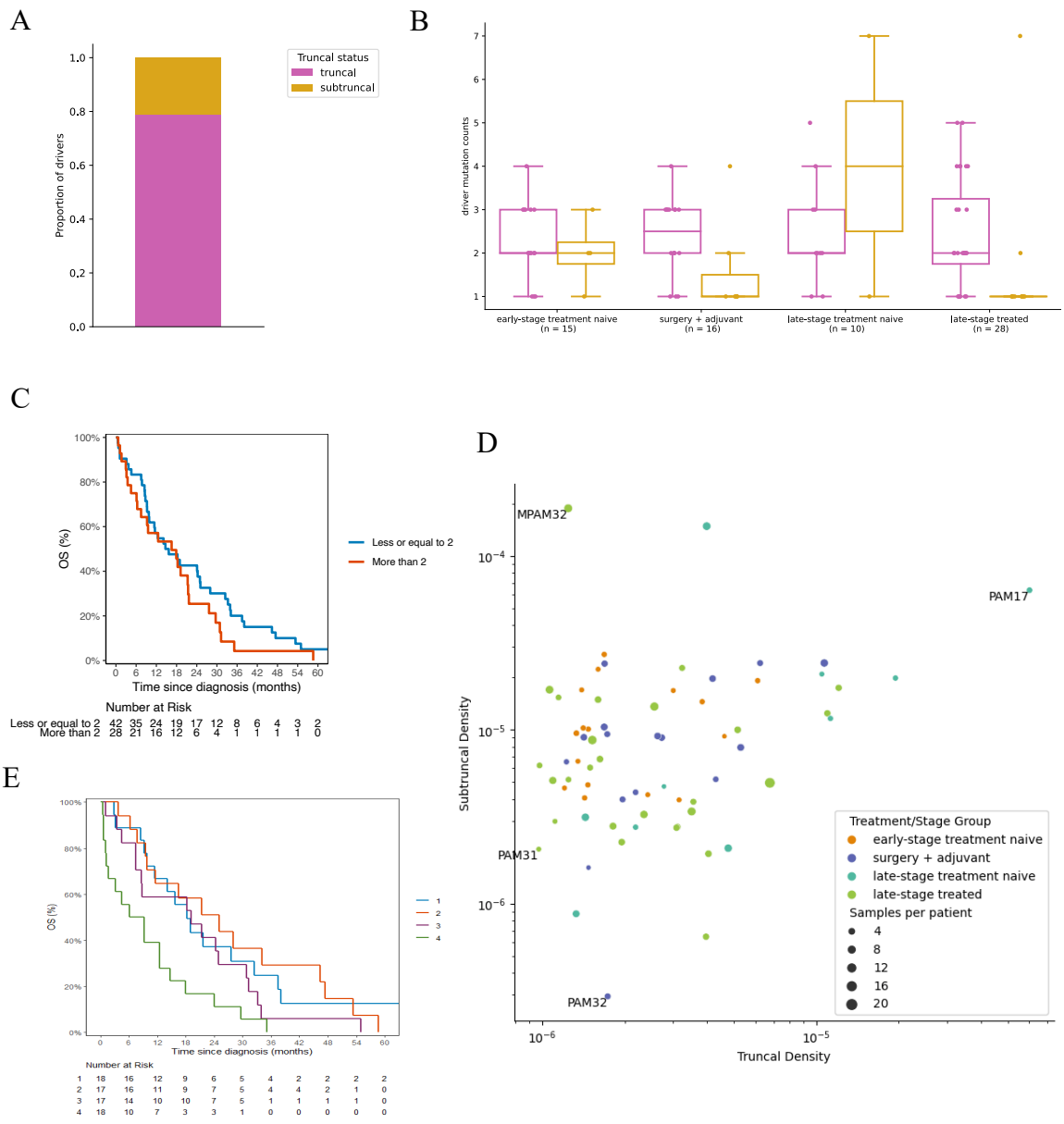

Figure 6. Timing of somatic events.

(A) Proportion of truncal vs subtruncal drivers in multiregion cohort. (B) Number of truncal and subtruncal drivers with respect to different clinical contexts. Samples from early-stage treatment naive patients were collected pre-surgical resection. (C) Overall survival with respect to number of truncal driver mutations. (D) Truncal and subtruncal densities per patient. Data points are scaled by the number of samples per patient and colored by treatment and stage information. The top and bottom 1% of outliers are annotated. (E) Overall survival with respect to truncal density. Patients were categorized into quartiles based on their truncal densities.

by 20% (HR:1.20, 95% CI:0.95-1.53), this association did not reach statistical significance (P = 0.14). Given how few subtruncal drivers were identified, we could not predict whether truncal alterations in specific genes were associated with an increased or decreased likelihood of subsequent subtruncal alterations[92].

In light of these observations, we expanded our scope to assess the timing of all SNV/INDEL events. To do this, we calculated truncal and subtruncal densities for each patient (Methods). Across the cohort, we observed that subtruncal densities were significantly larger than truncal densities (Wilcoxon rank-sum test, P = 2.17e-09). No relationship was observed between subtruncal density and the number of samples per patient (Figure 6D). The majority of patient outliers harbored mutations in genes associated with DNA damage response, including MSH2, MSH3, ATM and POLQ. When comparing early- versus late-stage treatment-naive patients, we found that late-stage patients had larger truncal densities compared to early-stage patients (Wilcoxon rank-sum test, P = 0.02); however, no significant differences were observed with respect to subtruncal densities between these two groups (Wilcoxon rank-sum test, P = 0.74). There were no significant differences in the truncal or subtruncal densities between patients pre- versus post-surgical resection. While there were no significant differences between the subtruncal densities of late-stage treatment-naive versus late-stage treated groups (Wilcoxon rank-sum test, P = 0.53), treatment-naive patients had significantly larger truncal densities (Wilcoxon rank-sum test, P = 0.03). Moreover, we did not observe a relationship between truncal density and the number of truncal drivers identified per patient.

Given these findings, we determined the relationship between truncal and subtruncal density and survival. We found a significant association between truncal

densities (per 1 unit increase in log-scale) and overall survival (OS) (HR:1.67, 95% CI:1.16-2.42, P =0.006). Upon categorizing truncal densities into quartiles and adjusting for stage at diagnosis, age at diagnosis, and smoking history, we continued to observe worse survival for patients with higher truncal densities (Q4) compared to the reference group (Q1) with the lowest truncal densities [HR:2.91, 95% CI:1.42-5.99, P =0.004] (Figure 6E). Conversely, we did not observe any association between subtruncal density and OS (HR:1.07, 95% CI:0.81-1.42, P = 0.64). Cumulatively, these data suggest that the extent of accumulation of coding somatic alterations prior to the MRCA is a prognostic marker for PDAC.

Smoking is a common risk factor for PDAC, contributing to the development of up to 25% of cases[93,94]. Therefore, we investigated the relationship between smoking and the mutational landscape of patients' tumors. We did not observe a significant association between smoking status and truncal density (Fisher's exact test, P = 0.2). We did not observe a significant association between smoking status and truncal density (Fisher's exact test, P = 0.2) thus we investigated the relationship between smoking and the mutational signatures prevalent within each sample. De novo extraction of mutational signatures from 134,772 somatic alterations identified seven double base substitutions signatures, two indel signatures and six SBS (single base substitution) signatures. SBSs accounted for 92.3% of all somatic mutations identified, thus we focused solely on this subset for evaluating the relationship of smoking related mutational signatures to PDAC evolutionary features. SBS de novo signature 4, representing 21.0% of all SBSs, was found to be most similar to COSMIC signature SBS29, whose etiology is tobacco-related[95], though it also showed similarity to COSMIC SBS4 (Figure 7 and Methods). To account for correlations within

A

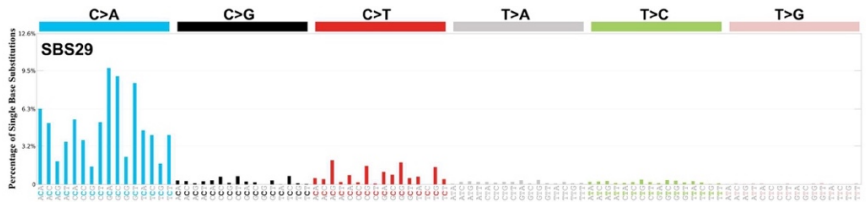

B

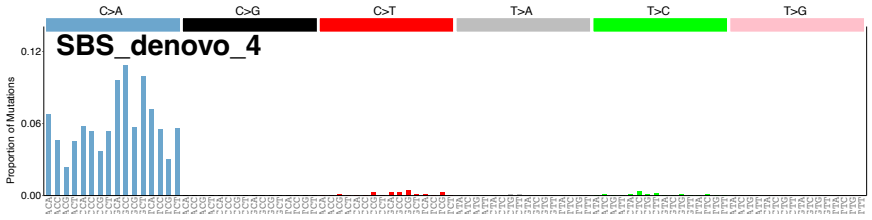

C

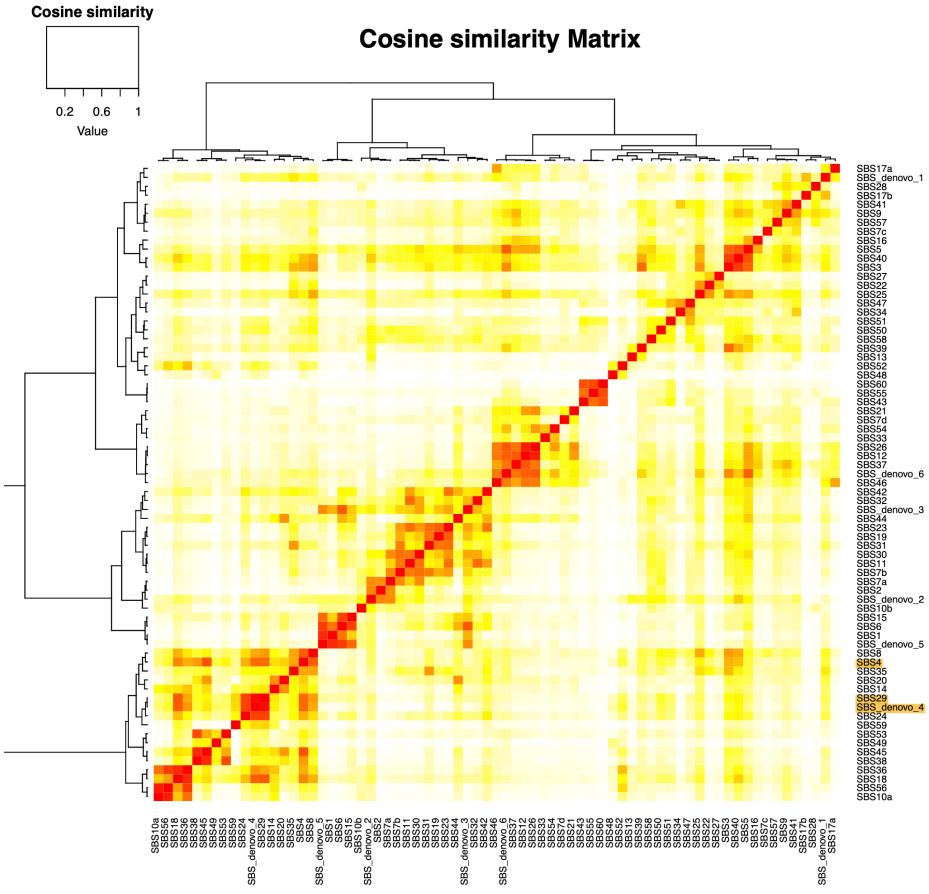

Figure 7. De novo mutational signature analysis reveals tobacco-related signature in multiregion cohort.

(A) Mutational signature SBS29 (COSMIC Version 3) has been identified in cancer samples from individuals with a tobacco chewing habit. (B) Mutational signature of de novo SBS signature 4. (C) Cosign similarity of each de novo SBS signature compared to COSMIC V3 signatures. Mutational signature SBS_denovo_4 is very similar to that of SBS29.

samples, we used a GLMM with random intercept and unconstructed covariance structure to model the number of SBS de novo signature 4 mutations with respect to smoking history status. In a univariate analysis, we did not observe any relationship between smoking history and the number of mutations attributed to the de novo SBS4 signature (P = 0.72). Similar to previous reports[92], some patients with smoking histories (current or former) contained samples that did not harbor any smoking related mutations. Conversely, several never-smokers harbored mutations attributed to SBS de novo signature 4. These findings suggest that despite substantial tobacco exposure in some patients, PDAC initiation may be independent of smoking-mediated mutagenesis.

Quantification of subclones and clinical correlates

To date, the clonal composition of PDAC remains poorly understood. To this end, we used HATCHet[61,62] to infer clonal populations and their relative proportions jointly across multiple samples from the same patient. The number of subclones identified per patient ranged from one to five with 34% of patients being classified as monoclonal (Figure 8A). Patients with polyclonal disease demonstrated varying degrees of clonal mixing, with some patients exclusively comprising polyclonal samples (26%) and others harboring a mix of monoclonal and polyclonal samples (39%).

We identified a single polyclonal patient who did not exhibit any clonal mixing with two clones identified across five monoclonal samples (Figure 8A, B). Notably, all samples collected from the right liver and the abdominal wall metastasis were composed of one clone and the metastasis from the left liver (MPAM01PT5) was comprised exclusively of a different clone (Figure 9). While all five of the driver mutations identified in MPAM01 were truncal and present in every sample, we observed mirrored-subclonal

A

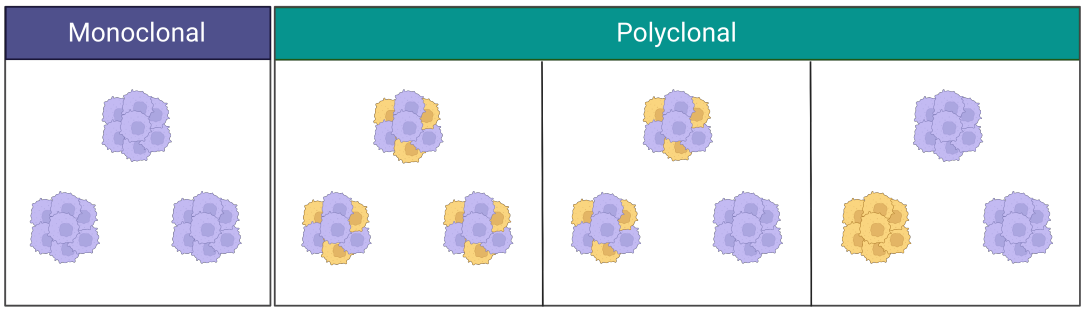

B

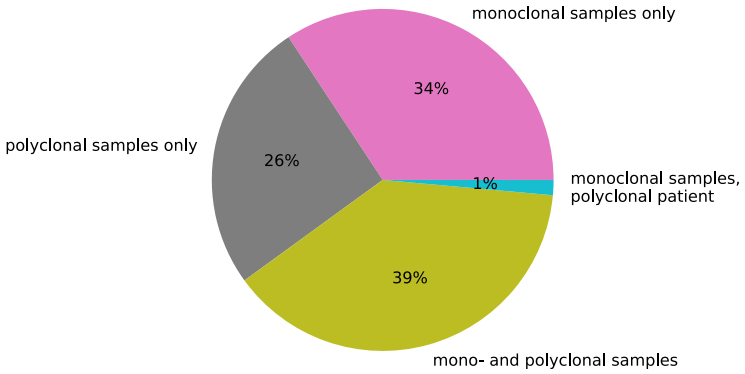

Figure 8. Clonal composition of PDAC tumors.

(A) Schematic of possible clonal compositions of patients. Polyclonal patients can be comprised of monoclonal or polyclonal samples. (B) Quantification of scenarios outlined in (A).

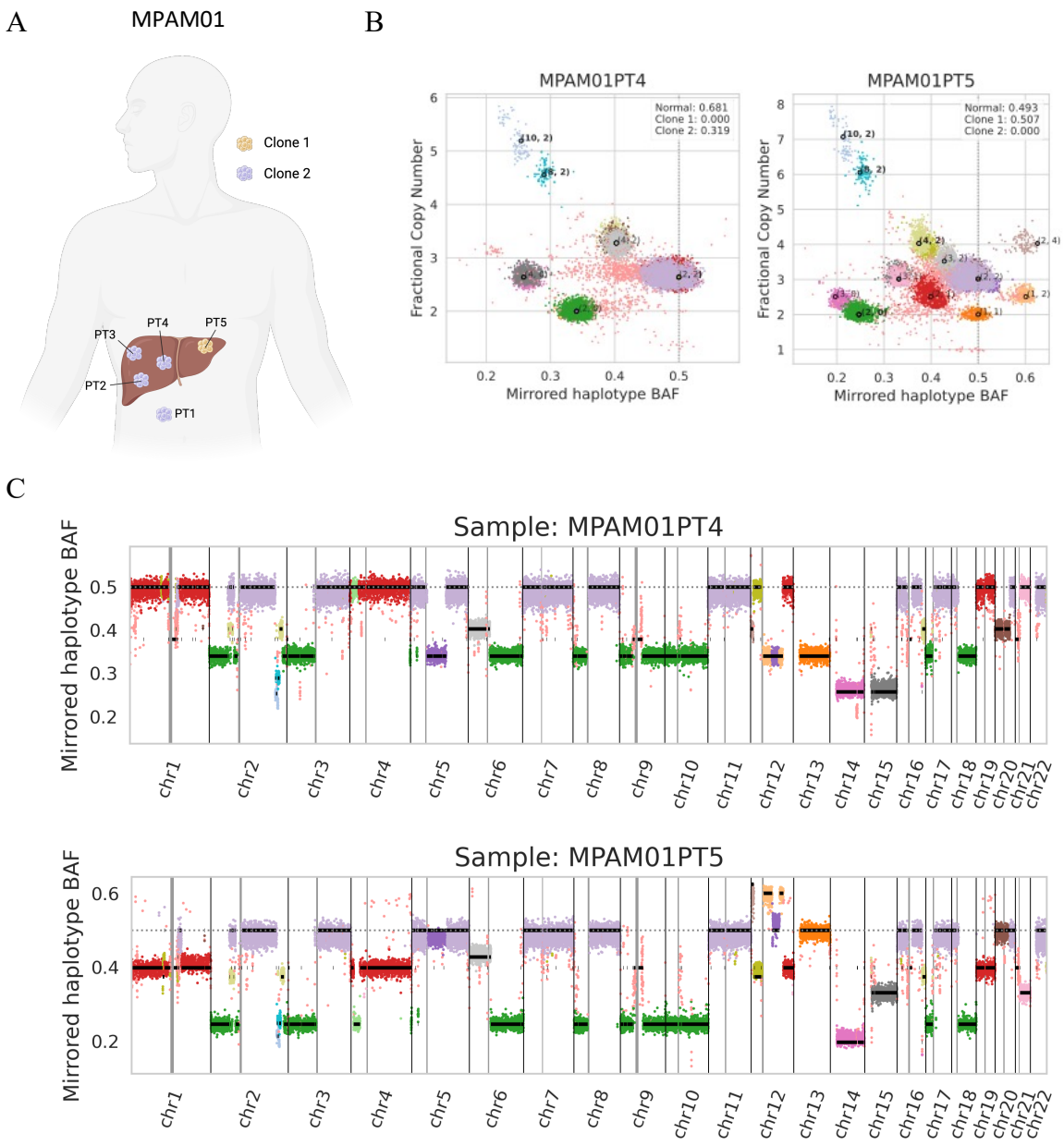

Figure 9. Polyclonal patients can comprise monoclonal samples with distinct copy number profiles.

(A) Distribution of metastatic disease in patient MPAM01. All lesions are monoclonal. (B) Inferred copy-number states for clone 1 and clone 2 in samples PT4 and PT5, respectively. Each point is a genomic bin whose position corresponds to its inferred mirrored haplotype BAF (mhBAF, x-axis) and fractional copy number (y-axis). Each bin is colored by its inferred copy-number state. Points labeled (A, B) are the expected position of the corresponding haplotype-specific copy-number state with A copies of the major haplotype and B copies of the minor haplotype. Bolded copy-number states are clonal events that are present in all tumor clones. (C) mhBAF values across the genome. Black lines indicate the expected mhBAF of the assigned copy-number state (analogous to labeled points in panel B).

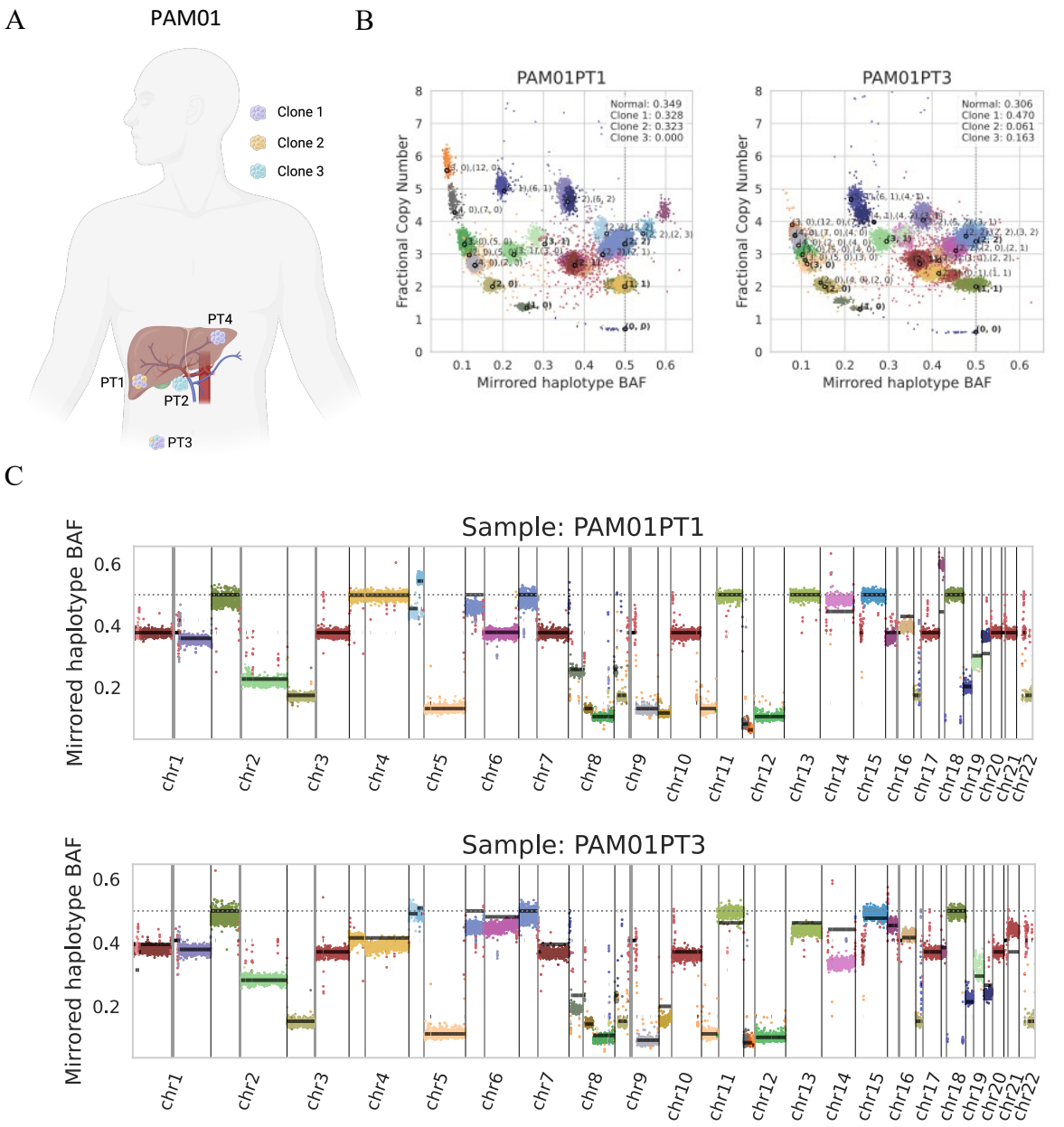

Figure 10. Polyclonal patients can comprise both mono- and polyclonal lesions.

(A) Distribution of metastatic disease in patient PAM01. Some lesions are monoclonal (PT2, PT4) and others are polyclonal (PT1, PT3). (B) Inferred copy-number states for samples PT1 and PT3, respectively. Each point is a genomic bin whose position corresponds to its inferred mirrored haplotype BAF (mhBAF, x-axis) and fractional copy number (y-axis). Each bin is colored by its inferred copy-number state. Points labeled (A, B) are the expected position of the corresponding haplotype-specific copy-number state with A copies of the major haplotype and B copies of the minor haplotype. Bolded copy-number states are clonal events that are present in all tumor clones. When multiple copy number states are annotated, they correspond to the values inferred for each clone present in the sample. (C) mhBAF values across the genome. Black lines indicate the expected mhBAF of the assigned copy-number state (analogous to labeled points in panel B).

CNAs, or differential gains or losses of the maternal and paternal chromosomes in distinct tumor clones[62]. We found that clone 1 had a copy state (1,2) or (2,4) across regions of chromosome 12 totaling 46.3 Mb, excluding KRAS (Figure 9B, C). Within these same regions, clone 2 demonstrated LOH and amplifications of the opposite allele with copy-states (2,0) and (4,2). Numerous additional subclonal CNA events were also observed on chromosomes 1, 4, 5, 13, 15, 19, 20 and 21.

Similarly, PAM01 demonstrated an abundance of subclonal CNAs spanning across all chromosomes and totaling 1.7Gb (Figure 10B, C). These events varied in size, ranging from relatively focal events (8q, olive green) to entire chromosomes (chromosome 4, goldenrod) (Figure 10C). The copy number state of KRAS differed in each of the three identified clones; however, all clones exhibited LOH of the B-allele (clone 1: 3,0; clone 2: 12,0; clone 3: 5,0). Notably, mirrored subclonal CNAs were observed on different chromosomes compared to MPAM01, including 5p and 18p. Overall, 51% (36/70) of patients harbored mirrored-subclonal CNAs and the average frequency of any genomic bin harboring such an event was 5.4%. This phenomenon was observed on every chromosome, with chromosomes 3, 7 and 21 being the most commonly altered across patients. Notable genes exhibiting the highest frequencies of mirrored subclonal CNAs included TGFBR2, MLH1, and SETD2, all of which localize to chromosome 3p[96].

With respect to treatment, we found that treated patients had increased odds of being polyclonal compared to treatment-naive patients in a multivariable adjusted analysis (OR: 4.54, 95% CI:1.33-17.3, P = 0.019) (Table 3). No significant association was found between the number of driver genes and polyclonal status (OR:1.08, 95% CI:0.86-1.45, P = 0.6). Among treatment-naive patients, we found that those with early-stage disease were

Table 3. Factors associated with polyclonal status.

Characteristic	N	OR[1]	95% CI[1]	p-value	OR[1]	95% CI[1]	p-value
Number of distinct driver mutation	70	1.08	0.86, 1.45	0.6			
AGE_AT_DIAGNOSIS	70	0.94	0.89, 0.98	0.011	0.95	0.90, 1.00	0.075
Smoking History	70						
Never/Unknown		—	—				
Yes		1.28	0.48, 3.54	0.6			
type2.diabetes	70						
No/Unknown		—	—				
Yes		0.63	0.21, 1.90	0.4			
PRIMARY_REGIONS_PER_PATIENT	70	1.02	0.80, 1.31	>0.9			
Stage at diagnosis	70						
Stage I-II		—	—		—	—	
Stage III		0.75	0.20, 2.75	0.7	0.54	0.12, 2.34	0.4
Stage IV		3.45	1.06, 12.7	0.047	4.07	1.08, 18.1	0.047
TREATED	70						
Not treated		—	—		—	—	
Treated		4.45	1.58, 13.3	0.006	4.54	1.33, 17.3	0.019
GENDER	70						
F		—	—				
M		1.29	0.48, 3.52	0.6			
race	70						
All Other		—	—				
Caucasian non-Hispanic White		2.29	0.69, 7.73	0.2			

[1]OR = Odds Ratio, CI = Confidence Interval

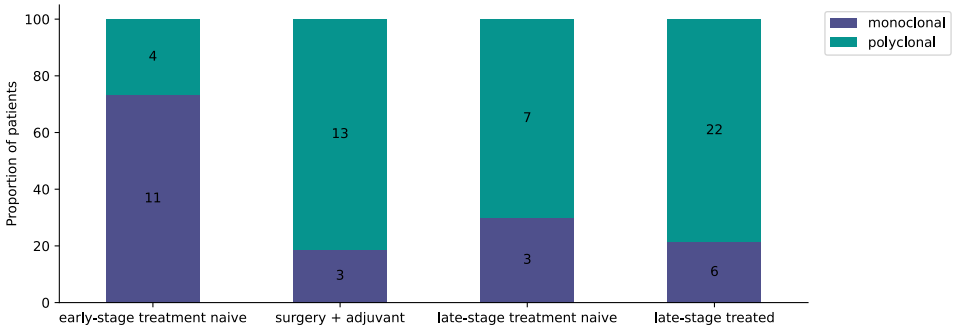

Figure 11. Prevalence of polyclonality with respect to disease stage and treatment.

(A) Proportions of patients with mono- vs polyclonal disease with respect to different clinical contexts. Samples from early-stage treatment naive patients were collected pre-surgical resection.

more often monoclonal compared to those with late-stage disease (Fisher's exact test; P = 0.049; Figure 11). Furthermore, we found that treatment-naive samples collected from patients who underwent surgical resection were more often monoclonal compared to samples collected from patients with late-stage disease who subsequently received adjuvant therapy and ultimately relapsed (Figure 11, Fisher's exact test, P = 0.004). Amongst patients with late-stage disease, we did not find a significant difference in the proportion of patients with mono-vs polyclonal disease (Fisher's exact test, P = 0.7). After correcting for age at diagnosis and treatment status, we observed that patients with stage IV disease had increased odds of being polyclonal compared to patients with stage I/II disease (Figure 11A, OR: 4.07, 95% CI: 1.08-18.1, P = 0.047). Cumulatively, our findings indicate that the clonal composition of PDAC is significantly associated with both advanced stage at diagnosis and treatment status.

Expanding upon these observations, we considered the diversity of metastatic sites represented in our cohort and investigated the prevalence of polyclonality with respect to different tissues. While we found that metastases were frequently polyclonal with respect to different sites and routes of metastatic dissemination (Supplemental Table 2, Figure 12A, B), none of these observations reached statistical significance. However, the number of metastatic samples sequenced was significantly higher in polyclonal patients compared with monoclonal patients (Wilcoxon rank-sum test, P = 0.00096; Figure 12C). Additionally, we observed a higher proportion of polyclonal disease in tetraploid patients (33/45) compared to diploid patients (13/25), however this did not reach statistical significance (Figure 12D, Fisher's exact test, P = 0.11).

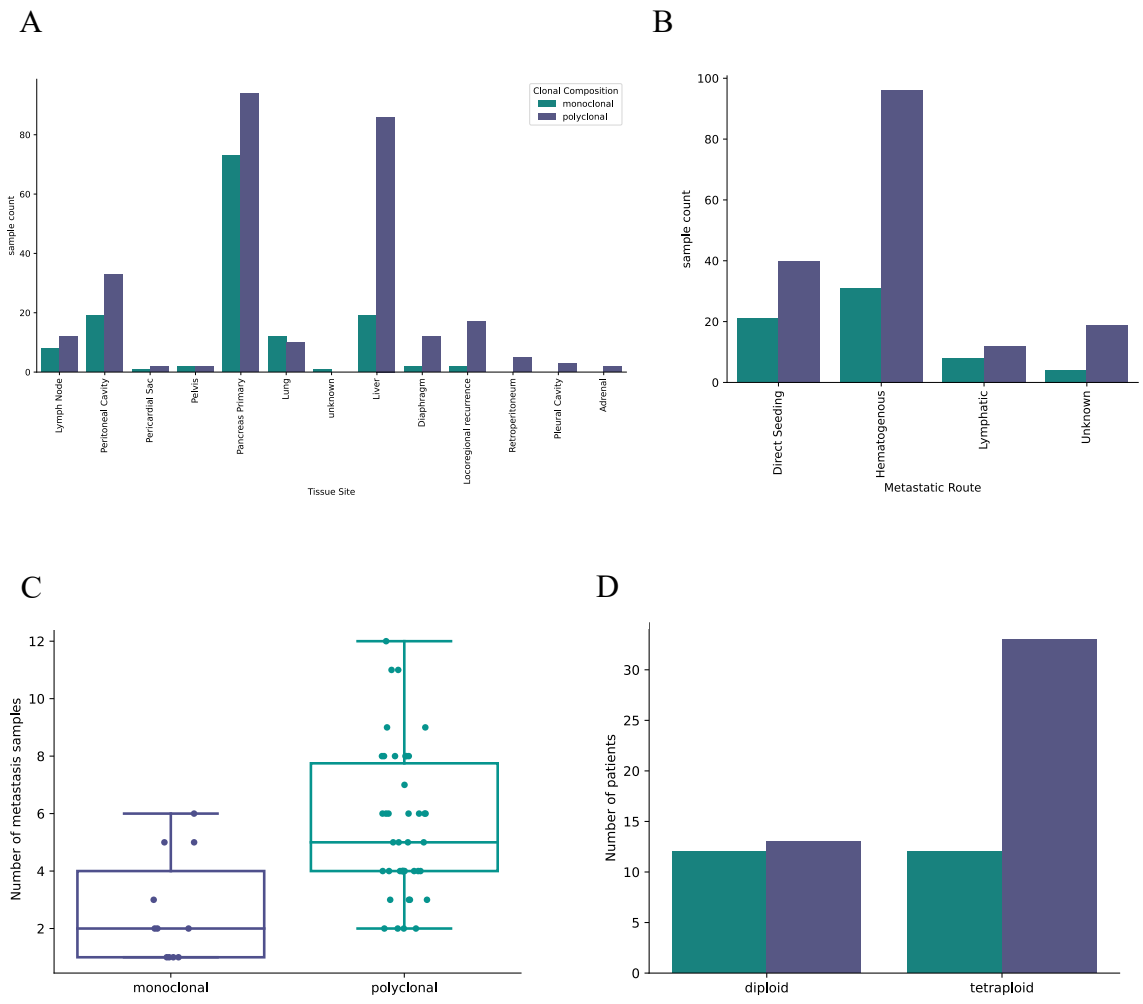

Figure 12. Polyclonality with respect to metastasis.

Clonal composition with respect to different tissue sites (A) and routes to metastasis (B). (C) Number of metastatic samples sequenced in patients with mono- vs polyclonal disease. (D) Clonal composition with respect to WGD status.

Features of oligometastatic patients

While chemotherapy is the standard of care for patients with metastatic disease, clinical management strategies remain poorly defined for patients with oligometastatic disease[97,98]. To this end, we determined the extent to which oligometastatic patients harbored genetic differences compared to patients with widespread metastatic disease. We found that oligometastatic patients have a median of one fewer drivers compared to patients with metastatic disease, but this did not reach statistical significance (Wilcoxon rank-sum test, $P = 0.081$) (Figure 13A). No significant associations between gene enrichment of various core signaling pathways and oligometastatic status were found. Furthermore, we found no differences in the number of truncal or subtruncal drivers or densities between patients with oligometastatic versus metastatic disease.

With respect to CNAs, oligometastatic patients contained significantly fewer LOH events compared to metastatic patients (Wilcoxon rank-sum test, $P = 0.02$), though no differences were observed with respect to gains (Figure 13B). Notably, LOH in both TP53 and SMAD4 was significantly less common in oligometastatic patients (Fisher's exact test, $P = 0.49$), however no difference was observed in other common tumor suppressor genes. While MYC gains were less prevalent in oligometastatic patients, this did not reach statistical significance (Fisher's exact test, $P = 0.16$). Extending upon these findings, we found that patients with oligometastatic disease were more often monoclonal compared to patients with widespread metastatic disease (Fisher's exact test, $P < 0.001$, Figure 13C). Cumulatively, these data suggest that patients with oligometastatic disease have more genomically stable tumors, which in turn may restrain metastatic efficiency[99].

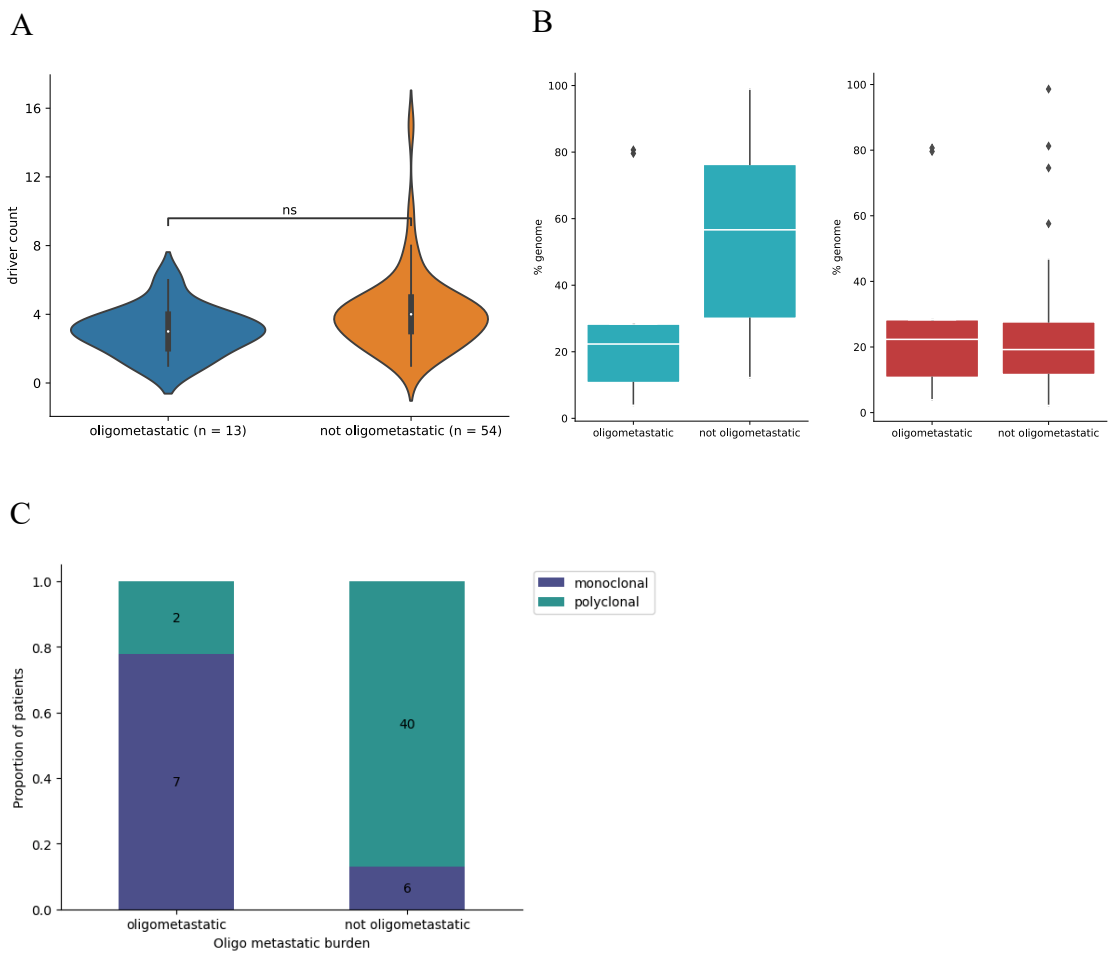

Figure 13. Genetic features of oligometastatic disease.

(A) Driver mutation counts, (B) fractional allelic loss and gains, and (C) proportion of monoclonal vs polyclonal disease in patients with and without oligometastatic disease.

CHAPTER FOUR: DISCUSSION

Summary

This study both corroborates and enriches existing knowledge of the PDAC genome[15,16,34]. Collectively, our multiregion sampling approach[78] and broad spectrum of disease presentations enabled us to quantify the diversity of evolutionary features in this tumor type and correlate them with clinical attributes. Comparing our findings to previously published datasets, we observed recurrent alterations in the genomic landscape of PDAC across different disease stages, supporting the notion that key genetic events occur early in the course of the disease. Our analysis identified 122 driver genes, with 92 being unique to our cohort, suggesting a diverse array of mechanisms contributing to tumorigenesis and disease progression in PDAC. However, further investigation is needed to validate and understand the functional significance of these novel driver events. While our driver analysis focused on SNV/INDEL-level alterations, we acknowledge that our ability to assess drivers at the CNA level was limited due to the quality of copy number calls obtained for the cohort. Future studies should aim to incorporate both SNV/INDEL and CNA alterations, as well as germline mutations, to provide a more comprehensive understanding of the genetic landscape of PDAC. Patient consent was not obtained for germline analyses in this cohort.

We identified subtruncal KRAS drivers in two patients, indicating that alternative pathways can drive tumorigenesis in PDAC. This finding suggests that targeting multiple pathways may be necessary for developing effective treatment strategies, especially considering ongoing clinical trials of KRAS inhibitors[46,47]. A recent study demonstrated that dual inhibition of ERBB and KRAS signaling may be synergistic and help overcome

acquired resistance to MRTX1133, a non-covalent inhibitor of KRAS G12D[100]. Furthermore, the authors determined that combining MRTX1133 with downstream inhibitors against MEK or ERK did not provide meaningful synergy, suggesting that drugs targeting this pathway will not likely provide additional benefit. Additionally, combination therapy of commonly used chemotherapeutics 5-FU or Gemcitabine with MRTX1133 did not produce synergistic results. However, these results were solely derived from preclinical studies, thus necessitating additional human trials to validate these findings. Furthermore, investigation into the functional significance of subtruncal KRAS drivers and their impact on treatment response is warranted.

A notable insight from this study was derived from our introduction of the concept of truncal density. This metric quantifies the accumulation of somatic alterations in the lineage leading to the infiltrating carcinoma and found to be an independent prognostic variable, regardless of disease stage, patient age, or smoking history. Truncal density can be influenced by various endogenous factors such as age-related clock-like mutagenesis[101], chronic genotoxic stress induced by ROS[102], inflammation and increased cellular turnover[103], as well as exogenous factors such as carcinogens from tobacco smoke[104]. Conversely, there are mechanisms that could potentially decrease truncal density over an individual's lifetime, including inherent efficiency of DNA repair[105,106], immunoediting[21], or genetic drift[107]. Notably, smoking history was neither related to truncal density nor was it correlated with the presence of a tobacco-related mutational signature. This does not imply that smoking is not a risk factor for PDAC, only that its contribution to PDAC incidence may extend beyond accumulation of mutations. This finding aligns with recent research on smoking and lung carcinogenesis[92], presenting significant implications for both

early detection and prevention of PDAC. Furthermore, truncal density did not demonstrate any relationship with the number or type of driver mutations. This observation could reflect a more generalized feature of the PDAC lineage, such as the extent of epigenetic memory following the resolution of inflammation or other injuries[108].

We confirmed that the majority of driver mutations were truncal, and subtruncal drivers were relatively uncommon[109], irrespective of disease stage and treatment. This observation lends optimism to the potential application of targeted therapies against prevalent driver genes in this disease, including KRAS[47,48], as previously mentioned. We also found that patients with oligometastatic disease had a median of one fewer driver mutations than those with widespread metastasis. This observation might be indicative of differences in the number of clonal expansions between these two groups where one such expansion in the widespread metastasis group may have encompassed an additional driver mutation. These clonal expansions likely occurred prior to diagnosis given that nearly half of oligometastatic patients did not experience disease progression between diagnosis and death. Moreover, these expansions may have occurred in association with microenvironmental cues or cell intrinsic features that provided a survival advantage. Validation of this theory may guide surgical management in the setting of oligometastatic disease, which remains a controversial topic.

Subclonal LOH and gains were significantly more common than clonal copy number events, suggesting that the majority of CNAs occurred relatively later in tumor evolution, as reported previously[110], and that they may play a crucial role in driving intratumoral heterogeneity and tumor progression. Subclonal CNAs, ranging in size from focal events to entire chromosomes, defined distinct populations in polyclonal patients.

Notably, some of these events had different numbers of copies of both parental haplotypes in different tumor clones, which we refer to as mirrored subclonal CNAs[62]. While mirrored subclonal CNAs were identified genome-wide, their biological significance remains unknown. Chromosome 3p had the highest rate of mirrored subclonal CNAs, which may indicate that genes in this region are particularly impacted by convergent evolution[41].

Finally, our findings underscore the necessity of analyzing evolutionary features within the context of different tumor types and clinical scenarios. The evolutionary histories exhibited in our study display profound differences compared to other solid tumors, where subtruncal drivers are more prevalent[86] and current investigations are examining their role in shaping clinical management strategies[111]. Elucidating these patterns in large-scale datasets has the potential to unravel unique, disease-specific therapeutic approaches, fostering an era of more personalized and effective cancer treatment strategies.

Future directions

One of the most impactful ways to study the evolutionary dynamics of cancer is through longitudinal studies[41,112–115]. By periodically sampling tumor tissue from the same patient, temporal changes can be captured, thus enabling real-time tracking of clonal evolution, emergence of resistance mechanisms, and identification of potential therapeutic windows[116]. Moving forward, we plan to conduct evolutionary studies on longitudinal samples collected pre- and post-treatment from the Tracking Of Pancreatic Cancer RegressiOn and ResisTance (TOPCOAT) program. TOPCOAT was initiated by the David M. Rubenstein Center for Pancreatic Cancer Research in March 2020 for the purpose of prospectively identifying information on the biology of pancreas cancer. This program has

an accrual goal of 160 patients across four hospital services, of which 150 have already been consented. This concerted effort will generate the largest tissue bank of longitudinal PDAC data to date, enabling researchers to dive deeper into the intricacies of PDAC evolution, identify new therapeutic targets, and refine treatment strategies for patients.

In addition to genomic data, TOPCOAT biospecimens will enable researchers to collect data about the transcriptome, metabolome, and tumor microenvironment, which together will help provide a more holistic picture of how genetic changes translate to functional outcomes. Zhang et al.'s work on the International Cancer Genome Consortium Data Portal underscores the importance and potential of such multiomics integrations, enabling researchers to find correlations between gene mutations, expression patterns, and patient outcomes[117]. This integrated approach will lead to a better understanding of tumor heterogeneity, disease prognosis, and potential therapeutic targets.

While generating high-quality datasets is incredibly important, methods development cannot be overlooked. A truncal status could be determined for only 63% of putative driver mutations in our cohort, a result of several technical limitations. Thirty-four driver mutations were identified exclusively in targeted sequencing datasets, precluding them from analysis with HATCHet on account of insufficient genomic bins for identifying heterozygous germline SNPs. Another 58 driver mutations were excluded because they either did not harbor reads in all samples within the patient or the reads present in each sample did not reach the minimum read depth threshold (mean number of tumor reads per site per sample). Furthermore, another 17 driver mutations were excluded because they were unable to be assigned well to a cluster and were placed in an outlier file. Finally, 69 driver mutations had a total copy number greater than 6, which precluded their analysis

with DeCiFer on account of the program not being able to finish with high total copy number states.

To address these issues, methods optimization can be performed at the bench and computationally. First, higher purity tumors could be collected at the outset with the assistance of techniques like laser capture microdissection (LCM)[118]. However, the equipment required for LCM is a costly investment, often exceeding a million dollars[119]. Associated consumables, including nuclease-free membrane slides and collection tubes, also come at a premium, costing significantly more than standard items. Additionally, exposure of tissue of interest to fixatives and staining agents can compromise their suitability for subsequent analyses. Therefore, ample time in training and problem-solving is essential to achieve reliable outcomes using this technique. From a computational perspective, further development of copy number and clustering tools like HATCHet and DeCiFer is imperative to extracting high quality information from subpar samples. These tools were originally designed for multiregion, high-depth WGS datasets, which are few and far between in practice due to cost limitations. Therefore, it is imperative that these tools be adapted to analyze a wider range of sequencing inputs such that existing data can be examined more effectively.

Numerous studies have used phylogenetic trees derived from somatic mutations across various anatomical sites to deduce a cancer cell's migratory history within a patient. In most cases, these inferences relied on a combination of two flawed assumptions that do not generally hold in cancer sequencing data. The first is sample homogeneity, which incorrectly assumes genetic uniformity across cells within a sequenced sample. The second is that migration history follows directly from the topology and branch lengths of a

phylogenetic tree. This is problematic because a tree does not encode the anatomical sites of ancestral clones. While somatic mutations can be used as markers for cellular lineage, they do not directly model the history of cellular migrations between anatomical sites. To infer migration histories in PDAC, future analyses could be performed using MACHINA[120], which outputs a directed multigraph to describe the migration of cells between anatomical sites. The topology of this migration graph differs from a standard phylogenetic tree in that it records both the migration *number* and migration *pattern* (for example, monoclonal versus polyclonal, single source versus multisource seeding). While MACHINA has been used to investigate seeding patterns in multiregion PDAC data previously, it was performed on data from only ten patients. Therefore, additional analyses on a larger number of patients spanning the continuum of clinical contexts are necessary to better understand seeding dynamics in PDAC.

More broadly, recognizing cancer as an evolutionary and ecological process is a transformative approach that will offer novel insights into disease progression and treatment strategies[121]. By deciphering the evolutionary trajectories of tumor cells, researchers can predict potential treatment outcomes and drug resistances. Tumors are not homogeneous masses but rather complex systems of multiple cell populations that continuously evolve. These populations compete for resources, adapt to environmental pressures, and exhibit both cooperative and competitive interactions[44,122]. This intratumor heterogeneity is a significant challenge in cancer treatment, as different subpopulations may respond variably to therapies[123]. Moreover, the spatial structure of tumors can further affect the dynamics of drug resistance and tumor progression[124,125].

To refine precision medicine strategies, understanding the interplay between intratumor heterogeneity and the temporal acquisition of driver events is paramount. Collateral sensitivity, the phenomenon in which a population of cells that has evolved resistance to a particular drug becomes simultaneously more sensitive to a different drug, has garnered attention as a potential strategy against multidrug resistance in cancer[126–128]. Game-theoretical models have been applied to understand these interactions and develop strategies that might outmaneuver the evolutionary advantages of the tumor[122,129,130]. In practice, the oncologist would select a treatment based on the disease's state, prompting cancer cells to adapt. This resembles the Stackelberg game[131], where the oncologist leads, and the cancer cells respond to the therapeutic pressures.

To date, a handful of novel clinical strategies informed by evolutionary game theory have been devised to enhance the treatment of cancer. The intermittent dosing method employs sporadic treatment courses, capitalizing on the competition between sensitive tumor cells and resistant clones, thereby potentially extending the efficacy of a therapeutic agent. In a clinical trial involving patients with metastatic castration-resistant prostate cancer, median time to progression extended to at least 27 months, compared to 16.5 months under continuous treatment[131]. In adaptive therapy, drug doses are dynamically adjusted based on the tumor's response. Preclinical studies in mice have shown that this approach can keep the tumor size stable and hinder the swift emergence of resistant clones ovarian and breast cancer[132,133]. Another tactic involves cycling among different drugs or classes of drugs, which could prevent the tumor from becoming too resistant to any single treatment. Theoretically, the goal of an alternating schedule would be to have two distinct clone populations competing, each uniquely sensitive to one of two drugs. By monitoring

the allele frequency of mutations linked to drug sensitivity in these innovative regimens, we can gain insights in real-time.

A significant hurdle with any of these strategies is monitoring the various clones to determine the optimal timing for treatment modifications. While continuously collecting biopsies after each treatment cycle is not feasible, evaluating mutation allele frequencies in circulating tumor DNA is a practical alternative. Notably, such approaches will introduce technical challenges related to quality control of acquisition and analysis of data across multiple clinical sites as well as increased costs[132]. However, considering PDAC's abysmal survival rate coupled with our finding that two-thirds of cases harbored multiple clones, a deeper exploration into the disease's evolutionary dynamics is essential. Strategies grounded in evolutionary game theory may pave the way for transformative therapeutic interventions in this disease type, pending rigorous clinical trials.

BIBLIOGRAPHY

1. Orth, M. *et al.* Pancreatic ductal adenocarcinoma: Biological hallmarks, current status, and future perspectives of combined modality treatment approaches. *Radiation Oncology* **14**, 1–20 (2019).

2. Ilic, I. & Ilic, M. International patterns in incidence and mortality trends of pancreatic cancer in the last three decades: A joinpoint regression analysis. *World J Gastroenterol* **28**, 4698–4715 (2022).

3. American Cancer Society. *Cancer Facts & Figures 2022*. (2022).

4. Sung, H. *et al.* Global Cancer Statistics 2020: GLOBOCAN Estimates of Incidence and Mortality Worldwide for 36 Cancers in 185 Countries. *CA Cancer J Clin* **71**, 209–249 (2021).

5. Ferlay, J., Partensky, C. & Bray, F. More deaths from pancreatic cancer than breast cancer in the EU by 2017. *Acta Oncol (Madr)* **55**, 1158–1160 (2016).

6. Rahib, L. *et al.* Projecting cancer incidence and deaths to 2030: The unexpected burden of thyroid, liver, and pancreas cancers in the united states. *Cancer Res* **74**, 2913–2921 (2014).

7. Hüttner, F. J. *et al.* Pylorus-preserving pancreaticoduodenectomy (pp Whipple) versus pancreaticoduodenectomy (classic Whipple) for surgical treatment of periampullary and pancreatic carcinoma. *Cochrane Database Syst Rev* **2**, CD006053 (2016).

8. Kleeff, J. *et al.* Pancreatic cancer. *Nat Rev Dis Primers* **2**, 1–23 (2016).

9. Hartwig, W. *et al.* Total pancreatectomy for primary pancreatic neoplasms: renaissance of an unpopular operation. *Ann Surg* **261**, 537–46 (2015).

10. Amini, N., Spolverato, G., Kim, Y. & Pawlik, T. M. Trends in Hospital Volume and Failure to Rescue for Pancreatic Surgery. *J Gastrointest Surg* **19**, 1581–92 (2015).

11. de Wilde, R. F. *et al.* Impact of nationwide centralization of pancreaticoduodenectomy on hospital mortality. *Br J Surg* **99**, 404–10 (2012).

12. Hartwig, W. *et al.* Pancreatic cancer surgery in the new millennium: better prediction of outcome. *Ann Surg* **254**, 311–9 (2011).

13. Cheema, A. R. & O'Reilly, E. M. Management of Metastatic Pancreatic Adenocarcinoma. *Surgical Clinics of North America* Preprint at https://doi.org/10.1016/j.suc.2016.07.011 (2016).

14. Rosati, L. M., Kumar, R. & Herman, J. M. Integration of Stereotactic Body Radiation Therapy into the Multidisciplinary Management of Pancreatic Cancer. *Seminars in Radiation Oncology* Preprint at https://doi.org/10.1016/j.semradonc.2017.02.005 (2017).

15. Raphael, B. J. *et al.* Integrated Genomic Characterization of Pancreatic Ductal Adenocarcinoma. *Cancer Cell* **32**, 185-203.e13 (2017).

16. Waddell, N. *et al.* Whole genomes redefine the mutational landscape of pancreatic cancer. *Nature* **518**, 495–501 (2015).

17. Golan, T. *et al.* Maintenance olaparib for germline BRCA-mutated metastatic pancreatic cancer. *New England Journal of Medicine* **381**, 317–327 (2019).

18. Hu, Z. I. *et al.* Evaluating mismatch repair deficiency in pancreatic adenocarcinoma: Challenges and recommendations. *Clinical Cancer Research* **24**, 1326–1336 (2018).

19. Pardi, N., Hogan, M. J., Porter, F. W. & Weissman, D. mRNA vaccines — a new era in vaccinology. *Nat Rev Drug Discov* **17**, 261–279 (2018).

20. Balachandran, V. P. *et al.* Identification of unique neoantigen qualities in long-term survivors of pancreatic cancer. *Nature* **551**, S12–S16 (2017).

21. Łuksza, M. *et al.* Neoantigen quality predicts immunoediting in survivors of pancreatic cancer. *Nature* **606**, 389–395 (2022).

22. Siân Jones, Xiaosong Zhang, D. Williams Parsons, J. C.-H. L. *et al.* Core Signaling Pathways in Human Pancreatic Cancers Revealed by Global Genomic Analyses. *Science (1979)* **1801**, 1801–1806 (2008).

23. Witkiewicz, A. K. *et al.* Whole-exome sequencing of pancreatic cancer defines genetic diversity and therapeutic targets. *Nat Commun* **6**, 1–11 (2015).

24. Notta, F. *et al.* A renewed model of pancreatic cancer evolution based on genomic rearrangement patterns. *Nature* **538**, 378–382 (2016).

25. Yachida, S. *et al.* Clinical significance of the genetic landscape of pancreatic cancer and implications for identification of potential long-term survivors. *Clinical Cancer Research* **18**, 6339–6347 (2012).

26. Schutte, M. *et al.* Abrogation of the Rb/p16 tumor-suppressive pathway in virtually all pancreatic carcinomas. *Cancer Res* **57**, 3126–30 (1997).

27. Hahn, S. A. *et al.* DPC4, a candidate tumor suppressor gene at human chromosome 18q21.1. *Science* **271**, 350–3 (1996).

28. Iacobuzio-Donahue, C. A. *et al.* Large-Scale Allelotype of Pancreaticobiliary Carcinoma Provides Quantitative Estimates of Genome-Wide Allelic Loss. *Cancer Res* **64**, 871–875 (2004).

29. Bailey, P. *et al.* Genomic analyses identify molecular subtypes of pancreatic cancer. *Nature* **531**, 47–52 (2016).

30. Stephens, P. J. *et al.* Massive genomic rearrangement acquired in a single catastrophic event during cancer development. *Cell* **144**, 27–40 (2011).

31. Korbel, J. O. & Campbell, P. J. Criteria for inference of chromothripsis in cancer genomes. *Cell* **152**, 1226–36 (2013).

32. Makohon-Moore, A. & Iacobuzio-Donahue, C. A. Pancreatic cancer biology and genetics from an evolutionary perspective. *Nat Rev Cancer* **16**, 553–565 (2016).

33. Greaves, M. Darwinian medicine: a case for cancer. *Nat Rev Cancer* **7**, 213–21 (2007).

34. Makohon-Moore, A. P. *et al.* Limited heterogeneity of known driver gene mutations among the metastases of individual patients with pancreatic cancer. *Nat Genet* **49**, 358–366 (2017).

35. Sakamoto, H. *et al.* The Evolutionary Origins of Recurrent Pancreatic Cancer. *Cancer Discov* **10**, 792–805 (2020).

36. Aram F. Hezel, Alec C. Kimmelman, Ben Z. Stanger, Nabeel Bardeesy, and R. A. D. Genetics and biology of pancreatic ductal adenocarcinoma. *Genes Dev* **20**, 1218–1249 (2006).

37. Hruban, R. H., Goggins, M., Parsons, J. & Kern, S. E. Progression model for pancreatic cancer. *Clinical Cancer Research* **6**, 2969–2972 (2000).

38. Notta, F. *et al.* A renewed model of pancreatic cancer evolution based on genomic rearrangement patterns. *Nature* **538**, 378–382 (2016).

39. Yachida, S. *et al.* Distant metastasis occurs late during the genetic evolution of pancreatic cancer. *Nature* **467**, 1114–1117 (2010).

40. Iacobuzio-Donahue, C. A., Litchfield, K. & Swanton, C. Intratumor heterogeneity reflects clinical disease course. *Nat Cancer* **1**, 3–6 (2020).

41. Turajlic, S. *et al.* Deterministic Evolutionary Trajectories Influence Primary Tumor Growth: TRACERx Renal. *Cell* **173**, 595-610.e11 (2018).

42. Kohutek, Z. A. *et al.* An unusual genomic variant of pancreatic ductal adenocarcinoma with an indolent clinical course. *Cold Spring Harb Mol Case Stud* **3**, 1–11 (2017).

43. Hayashi, A. *et al.* A unifying paradigm for transcriptional heterogeneity and squamous features in pancreatic ductal adenocarcinoma. *Nat Cancer* **1**, 59–74 (2020).

44. Maley, C. C. *et al.* Classifying the evolutionary and ecological features of neoplasms. *Nat Rev Cancer* **17**, 605–619 (2017).

45. Huang, L., Guo, Z., Wang, F. & Fu, L. KRAS mutation: from undruggable to druggable in cancer. *Signal Transduct Target Ther* **6**, 386 (2021).

46. Strickler, J. H. *et al.* Sotorasib in KRAS p.G12C-Mutated Advanced Pancreatic Cancer. *N Engl J Med* **388**, 33–43 (2023).

47. Bekaii-Saab, T. S. *et al.* KRYSTAL-1: Updated activity and safety of adagrasib (MRTX849) in patients (Pts) with unresectable or metastatic pancreatic cancer (PDAC) and other gastrointestinal (GI) tumors harboring a KRAS G12C mutation. *Journal of Clinical Oncology* **40**, 519–519 (2022).

48. Hallin, J. *et al.* Anti-tumor efficacy of a potent and selective non-covalent KRASG12D inhibitor. *Nat Med* **28**, 2171–2182 (2022).

49. Li, S., Balmain, A. & Counter, C. M. A model for RAS mutation patterns in cancers: finding the sweet spot. *Nat Rev Cancer* **18**, 767–777 (2018).

50. Li, H. & Durbin, R. Fast and accurate short read alignment with Burrows-Wheeler transform. *Bioinformatics* **25**, 1754–60 (2009).

51. DePristo, M. A. *et al.* A framework for variation discovery and genotyping using next-generation DNA sequencing data. *Nat Genet* **43**, 491–8 (2011).

52. Cibulskis, K. *et al.* Sensitive detection of somatic point mutations in impure and heterogeneous cancer samples. *Nat Biotechnol* **31**, 213–219 (2013).

53. Lappalainen, I. *et al.* The European Genome-phenome Archive of human data consented for biomedical research. *Nat Genet* **47**, 692–695 (2015).

54. Pagel, K. A. *et al.* Integrated Informatics Analysis of Cancer-Related Variants. *JCO Clin Cancer Inform* **4**, 310–317 (2020).

55. Tokheim, C. & Karchin, R. CHASMplus Reveals the Scope of Somatic Missense Mutations Driving Human Cancers. *Cell Syst* 9–23 (2019) doi:10.1016/j.cels.2019.05.005.

56. Tate, J. G. *et al.* COSMIC: the Catalogue Of Somatic Mutations In Cancer. *Nucleic Acids Res* **47**, D941–D947 (2019).

57. Landrum, M. J. *et al.* ClinVar: improving access to variant interpretations and supporting evidence. *Nucleic Acids Res* **46**, D1062–D1067 (2018).

58. With, P. *et al.* OncoKB : A Precision Oncology Knowledge Base. *JCO Precis Oncol* 1–16 (2017).

59. Ioannidis, N. M. *et al.* REVEL: An Ensemble Method for Predicting the Pathogenicity of Rare Missense Variants. *The American Journal of Human Genetics* **99**, 877–885 (2016).

60. Tian, Y. *et al.* REVEL and BayesDel outperform other in silico meta-predictors for clinical variant classification. *Sci Rep* **9**, 12752 (2019).

61. Zaccaria, S. & Raphael, B. J. Accurate quantification of copy-number aberrations and whole-genome duplications in multi-sample tumor sequencing data. *Nat Commun* **11**, 4301 (2020).

62. Myers, M. A. *et al.* HATCHet2: clone- and haplotype-specific copy number inference from bulk tumor sequencing data. *bioRxiv* 2023.07.13.548855 (2023) doi:10.1101/2023.07.13.548855.

63. O'Connell, J. *et al.* A General Approach for Haplotype Phasing across the Full Spectrum of Relatedness. *PLoS Genet* **10**, e1004234 (2014).

64. Satas, G., Zaccaria, S., El-Kebir, M. & Raphael, B. J. DeCiFering the elusive cancer cell fraction in tumor heterogeneity and evolution. *Cell Syst* 2021.02.27.429196 (2021) doi:10.1016/j.cels.2021.07.006.

65. Shinde, J. *et al.* Palimpsest: an R package for studying mutational and structural variant signatures along clonal evolution in cancer. *Bioinformatics* **34**, 3380–3381 (2018).

66. Brunet, J.-P., Tamayo, P., Golub, T. R. & Mesirov, J. P. Metagenes and molecular pattern discovery using matrix factorization. *Proceedings of the National Academy of Sciences* **101**, 4164–4169 (2004).

67. Crowdis, J., He, M. X., Reardon, B. & Van Allen, E. M. CoMut: visualizing integrated molecular information with comutation plots. *Bioinformatics* **36**, 4348–4349 (2020).

68. Gerstung, M. *et al.* The evolutionary history of 2,658 cancers. *Nature* **578**, 122–128 (2020).

69. Dentro, S. C. *et al.* Characterizing genetic intra-tumor heterogeneity across 2,658 human cancer genomes. *Cell* **184**, 2239-2254.e39 (2021).

70. Groot, V. P. *et al.* Implications of the Pattern of Disease Recurrence on Survival Following Pancreatectomy for Pancreatic Ductal Adenocarcinoma. *Ann Surg Oncol* **25**, 2475–2483 (2018).

71. Jones, R. P. *et al.* Patterns of Recurrence After Resection of Pancreatic Ductal Adenocarcinoma. *JAMA Surg* **154**, 1038 (2019).

72. Daamen, L. A. *et al.* Preoperative predictors for early and very early disease recurrence in patients undergoing resection of pancreatic ductal adenocarcinoma. *HPB* **24**, 535–546 (2022).

73. Hyman, D. M., Taylor, B. S. & Baselga, J. Implementing Genome-Driven Oncology. *Cell* Preprint at https://doi.org/10.1016/j.cell.2016.12.015 (2017).

74. Priestley, P. *et al.* Pan-cancer whole-genome analyses of metastatic solid tumours. *Nature* **575**, 210–216 (2019).

75. van de Haar, J. *et al.* Limited evolution of the actionable metastatic cancer genome under therapeutic pressure. *Nat Med* (2021) doi:10.1038/s41591-021-01448-w.

76. Nguyen, B. *et al.* Genomic characterization of metastatic patterns from prospective clinical sequencing of 25,000 patients. *Cell* **185**, 563-575.e11 (2022).

77. de Bruin, E. C. *et al.* Spatial and temporal diversity in genomic instability processes defines lung cancer evolution. *Science* **346**, 251–6 (2014).

78. Iacobuzio-Donahue, C. A. *et al.* Cancer biology as revealed by the research autopsy. *Nat Rev Cancer* (2019) doi:10.1038/s41568-019-0199-4.

79. Sakamoto, H. *et al.* The Evolutionary Origins of Recurrent Pancreatic Cancer. *Cancer Discov* **10**, 792–805 (2020).

80. Chan-Seng-Yue, M. *et al.* Transcription phenotypes of pancreatic cancer are driven by genomic events during tumor evolution. *Nat Genet* **52**, 231–240 (2020).

81. Hellman, S. & Weichselbaum, R. R. Oligometastases. *Journal of Clinical Oncology* **13**, 8–10 (1995).

82. Kaneda, H. & Saito, Y. Oligometastases: Defined by prognosis and evaluated by cure. *Cancer Treat Commun* **3**, 1–6 (2015).

83. Wang, H. *et al.* Survival of pancreatic cancer patients is negatively correlated with age at diagnosis: a population-based retrospective study. *Sci Rep* **10**, 7048 (2020).

84. Lynch, S. M. *et al.* Cigarette smoking and pancreatic cancer: a pooled analysis from the pancreatic cancer cohort consortium. *Am J Epidemiol* **170**, 403–13 (2009).

85. Huxley, R., Ansary-Moghaddam, A., Berrington de González, A., Barzi, F. & Woodward, M. Type-II diabetes and pancreatic cancer: a meta-analysis of 36 studies. *Br J Cancer* **92**, 2076–83 (2005).

86. Turajlic, S., Sottoriva, A., Graham, T. & Swanton, C. Resolving genetic heterogeneity in cancer. *Nat Rev Genet* **20**, 404–416 (2019).

87. Martínez-Jiménez, F. *et al.* Pan-cancer whole-genome comparison of primary and metastatic solid tumours. *Nature* (2023) doi:10.1038/s41586-023-06054-z.

88. Bailey, M. H. *et al.* Comprehensive Characterization of Cancer Driver Genes and Mutations. *Cell* (2018) doi:10.1016/j.cell.2018.02.060.

89. McDonald, O. G. *et al.* Epigenomic reprogramming during pancreatic cancer progression links anabolic glucose metabolism to distant metastasis. *Nat Genet* **49**, 367–376 (2017).

90. Reynolds, A. B. *et al.* Regulation of Epithelial Plasticity Determines Metastatic Organotropism in Pancreatic Cancer. *Dev Cell* **45**, (2018).

91. Satas, G., Zaccaria, S., El-Kebir, M. & Raphael, B. J. DeCiFering the elusive cancer cell fraction in tumor heterogeneity and evolution. *Cell Syst* 2021.02.27.429196 (2021) doi:10.1016/j.cels.2021.07.006.

92. Frankell, A. M. *et al.* The evolution of lung cancer and impact of subclonal selection in TRACERx. *Nature* **616**, 525–533 (2023).

93. Fuchs, C. S. *et al.* A prospective study of cigarette smoking and the risk of pancreatic cancer. *Arch Intern Med* **156**, 2255–60 (1996).

94. Momi, N. *et al.* Interplay between smoking-induced genotoxicity and altered signaling in pancreatic carcinogenesis. *Carcinogenesis* **33**, 1617–28 (2012).

95. Alexandrov, L. B. *et al.* The repertoire of mutational signatures in human cancer. *Nature* **578**, 94–101 (2020).

96. Zabarovsky, E. R., Lerman, M. I. & Minna, J. D. Tumor suppressor genes on chromosome 3p involved in the pathogenesis of lung and other cancers. *Oncogene* **21**, 6915–6935 (2002).

97. Ghidini, M. *et al.* Surgery or Locoregional Approaches for Hepatic Oligometastatic Pancreatic Cancer: Myth, Hope, or Reality? *Cancers (Basel)* **11**, (2019).

98. De Simoni, O. *et al.* Oligometastatic Pancreatic Cancer to the Liver in the Era of Neoadjuvant Chemotherapy: Which Role for Conversion Surgery? A Systematic Review and Meta-Analysis. *Cancers (Basel)* **12**, (2020).

99. Zhong, Y. *et al.* Mutant p53 Together with TGFβ Signaling Influence Organ-Specific Hematogenous Colonization Patterns of Pancreatic Cancer. *Clinical Cancer Research* **23**, 1607–1620 (2017).

100. Gulay, K. C. Montecillo. *et al.* Dual inhibition of KRASG12D and pan-ERBB is synergistic in pancreatic ductal adenocarcinoma. *Cancer Res* (2023) doi:10.1158/0008-5472.CAN-23-1313.

101. Alexandrov, L. B. *et al.* Clock-like mutational processes in human somatic cells. *Nat Genet* **47**, 1402–7 (2015).

102. Srinivas, U. S., Tan, B. W. Q., Vellayappan, B. A. & Jeyasekharan, A. D. ROS and the DNA damage response in cancer. *Redox Biol* **25**, 101084 (2019).

103. Greten, F. R. & Grivennikov, S. I. Inflammation and Cancer: Triggers, Mechanisms, and Consequences. *Immunity* **51**, 27–41 (2019).

104. Alexandrov, L. B. *et al.* Mutational signatures associated with tobacco smoking in human cancer. *Science (1979)* **354**, 618–622 (2016).

105. Hoeijmakers, J. H. J. DNA damage, aging, and cancer. *N Engl J Med* **361**, 1475–85 (2009).

106. Roos, W. P., Thomas, A. D. & Kaina, B. DNA damage and the balance between survival and death in cancer biology. *Nat Rev Cancer* **16**, 20–33 (2016).

107. Lipinski, K. A. *et al.* Cancer Evolution and the Limits of Predictability in Precision Cancer Medicine. *Trends Cancer* **2**, 49–63 (2016).

108. Del Poggetto, E. *et al.* Epithelial memory of inflammation limits tissue damage while promoting pancreatic tumorigenesis. *Science* **373**, eabj0486 (2021).

109. Iacobuzio-Donahue, C. A., Litchfield, K. & Swanton, C. Intratumor heterogeneity reflects clinical disease course. *Nat Cancer* **1**, 3–6 (2020).

110. Notta, F. *et al.* A renewed model of pancreatic cancer evolution based on genomic rearrangement patterns. *Nature* **538**, 378–382 (2016).

111. Fittall, M. W. & Van Loo, P. Translating insights into tumor evolution to clinical practice: promises and challenges. *Genome Med* **11**, 20 (2019).

112. Kinnaman, M. D. *et al.* Subclonal somatic copy number alterations emerge and dominate in recurrent osteosarcoma. *bioRxiv* 2023.01.05.522765 (2023) doi:10.1101/2023.01.05.522765.

113. Barthel, F. P. *et al.* Longitudinal molecular trajectories of diffuse glioma in adults. *Nature* 1–9 (2019) doi:10.1038/s41586-019-1775-1.

114. Zhang, S. *et al.* Longitudinal single-cell profiling reveals molecular heterogeneity and tumor-immune evolution in refractory mantle cell lymphoma. *Nat Commun* **12**, 2877 (2021).

115. Nadeu, F. *et al.* Clinical impact of clonal and subclonal TP53, SF3B1, BIRC3, NOTCH1, and ATM mutations in chronic lymphocytic leukemia. *Blood* **127**, 2122–30 (2016).

116. McGranahan, N. & Swanton, C. Clonal Heterogeneity and Tumor Evolution: Past, Present, and the Future. *Cell* **168**, 613–628 (2017).

117. Zhang, J. *et al.* The International Cancer Genome Consortium Data Portal. *Nat Biotechnol* **37**, 367–369 (2019).

118. Espina, V. *et al.* Laser-capture microdissection. *Nat Protoc* **1**, 586–603 (2006).

119. Chung, S. H. & Shen, W. Laser capture microdissection: from its principle to applications in research on neurodegeneration. *Neural Regen Res* **10**, 897–8 (2015).

120. El-Kebir, M., Satas, G. & Raphael, B. J. Inferring parsimonious migration histories for metastatic cancers. *Nat Genet* **50**, 718–726 (2018).

121. Gatenby, R. A., Gillies, R. J. & Brown, J. S. Of cancer and cave fish. *Nat Rev Cancer* **11**, 237–8 (2011).

122. Archetti, M. & Pienta, K. J. Cooperation among cancer cells: applying game theory to cancer. *Nat Rev Cancer* **19**, 110–117 (2019).

123. Hiley, C., de Bruin, E. C., McGranahan, N. & Swanton, C. Deciphering intratumor heterogeneity and temporal acquisition of driver events to refine precision medicine. *Genome Biol* **15**, 453 (2014).

124. Noble, R. *et al.* Spatial structure governs the mode of tumour evolution. *Nat Ecol Evol* (2021) doi:10.1038/s41559-021-01615-9.

125. Strobl, M. A. R. *et al.* Spatial structure impacts adaptive therapy by shaping intra-tumoral competition. *Communications Medicine* **2**, 46 (2022).

126. Ingles Garces, A. H., Porta, N., Graham, T. A. & Banerji, U. Clinical trial designs for evaluating and exploiting cancer evolution. *Cancer Treat Rev* **118**, 102583 (2023).

127. Zhao, B. *et al.* Exploiting Temporal Collateral Sensitivity in Tumor Clonal Evolution. *Cell* **165**, 234–246 (2016).

128. Hall, M. D., Handley, M. D. & Gottesman, M. M. Is resistance useless? Multidrug resistance and collateral sensitivity. *Trends Pharmacol Sci* **30**, 546–556 (2009).

129. Stanková, K., Brown, J. S., Dalton, W. S. & Gatenby, R. A. Optimizing Cancer Treatment Using Game Theory. *JAMA Oncol* **5**, 96 (2019).

130. Wölfl, B. *et al.* The Contribution of Evolutionary Game Theory to Understanding and Treating Cancer. *Dyn Games Appl* **12**, 313–342 (2022).

131. von Stackelberg, H. *Market Structure and Equilibrium*. (Springer Berlin Heidelberg, 2011). doi:10.1007/978-3-642-12586-7.

132. Bailey, C. *et al.* Tracking Cancer Evolution through the Disease Course. *Cancer Discov* **11**, 916–932 (2021).

APPENDIX

Supplemental Table 1. Patient clinical information.

PAM ID	Gender	Chemo	Radiation	Surgery	Stage at Dx	Oligometastatic	Age at Dx	Overall Survival (mo)	Type II Diabetes	Smoking Hx
MPAM01	M	1	0	1	IIB	0	70	30.0	1	Ever-Former
MPAM03	F	1	0	0	IV	0	71	24.0	0	Ever-Current
MPAM05	M	1	1	0	IV	0	73	21.0	0	Ever-Former
MPAM06	F	1	0	0	IV	0	67	9.0	1	Ever-Former
MPAM07	M	1	0	0	III	0	61	54.0	0	Ever-Former
MPAM08	F	0	0	0	IV	0	70	1.0	0	Ever-Former
MPAM09	F	0	0	1	III		66	62.4	0	Never
MPAM10	M	0	0	1	III		60	60.3	0	Ever-Former
MPAM11	M	0	0	1	IIB		71	45.8	0	Never
MPAM12	M	0	0	1	IB		72	33.2	1	Ever-Former
MPAM13	M	0	0	1	III		71	17.2	0	Ever-Former
MPAM14	F	0	0	1	IIB		72	16.0	1	Never
MPAM15	F	0	0	1	IIB		86	54.4	0	Never
MPAM16	F	0	0	1	IIB		79	38.6	1	Ever-Current
MPAM17	M	0	0	1	III		74	15.4	0	Ever-Current
MPAM18	M	0	0	1	III		77	27.5	1	Never
MPAM19	M	0	0	1	IIB		72	31.3	0	Ever-Current
MPAM20	F	0	0	1	IB		53	19.3	1	Never
MPAM21	M	0	0	1	IIA		34	55.9	0	Ever-Current
MPAM22	M	0	0	1	IB		74	19.2	0	Never
MPAM23	M	0	0	1	IB		59	18.4	0	Never

Supplemental Table 1 (continued)

PAM ID	Gender	Chemo	Radiation	Surgery	Stage at Dx	Oligometastatic	Age at Dx	Overall Survival (mo)	Type II Diabetes	Smoking Hx
MPAM24	F	0	0	1	IB		46	38.0	0	Never
MPAM25	M	0	0	1	IB		79	44.7	1	Never
MPAM26	M	0	0	1	IB		86	3.7	1	Never
MPAM27	M	0	0	1	IB		68	93.8	1	Never
MPAM28	M	0	0	1	IIA		68	86.1	1	Never
MPAM29	F	0	0	1	IIA		52	20.3	0	Ever-Current
MPAM30	M	0	0	1	IB		80	11.8	1	Ever-Current
MPAM31	F	0	0	1	IB		77	33.5	0	Ever-Current
MPAM32	F	1	0	0	IV	0	34	9.0	0	Never
PAM01	M	0	0	0	IV	1	59	7.0	1	Ever-Current
PAM02	F	0	0	0	IV	0	69	0.5	0	Ever-Former
PAM03	M	0	0	0	IV	0	79	10.0	1	Never
PAM04	M	0	0	0	IV	0	74	3.0	1	Ever-Former
PAM10	F	0	0	0	IV	0	50	5.0	Unknown	Unknown
PAM104	F	1	1	1	IIB	0	76	53.0		Ever-Former
PAM112	F	1	0	0	IV	0	54	41.0	0	Never
PAM119	M	1	1	0	III	0	64	3.0	1	Ever-Current
PAM12	M	0	0	0	IV	0	49	1.0	Unknown	Unknown
PAM13	F	0	0	0	IV	0	85	2.0	0	Never
PAM135	F	1	1	1	IIA	0	49	69.0	0	Never
PAM14	F	0	0	0	IV	1	78	1.0		Ever-Former
PAM15	F	0	0	0	III	1	84	3.0	1	Ever-Former
PAM16	F	0	0	0	IV	0	88	0.8	0	Never
PAM17	F	0	0	0	IV	0	67	1.0	0	Never

Supplemental Table 1 (continued)

PAM ID	Gender	Chemo	Radiation	Surgery	Stage at Dx	Oligometastatic	Age at Dx	Overall Survival (mo)	Type II Diabetes	Smoking Hx
PAM18	F	0	0	1	IIA	1	83	12.0	0	Never
PAM19	M	1	1	0	III	0	51	8.0	0	Never
PAM20	F	1	1	0	III	0	81	3.0	0	Never
PAM21	M	1	1	0	III	1	36	17.0	0	Never
PAM22	M	1	1	0	III	1	57	17.0	0	Ever-Current
PAM23	M	1	1	0	III	1	77	10.0	1	Ever-Former
PAM24	F	1	1	0	III	0	61	24.0	1	Never
PAM25	M	1	1	0	III	1	64	14.0	Borderline Hyperglycemia	Ever-Former
PAM26	M	1	1	0	III	0	53	14.0		Ever-Current
PAM27	M	1	1	0	III	1	71	29.0	0	Ever-Former
PAM28	F	1	1	0	III	0	65	7.5	0	Never
PAM29	F	1	1	0	III	0	83	9.0	0	Ever-Former
PAM31	F	1	1	0	III	1	85	38.0	0	Never
PAM32	M	1	1	1	IIB	0	50	25.0	0	Never
PAM33	F	1	0	0	III	0	54	11.0	0	Ever-Current
PAM36	F	1	1	1	IIB	0	61	64.0	0	Ever-Former
PAM37	M	1	1	1	IIB	0	66	24.0	1	Never
PAM38	F	1	1	1	III	0	54	8.0	0	Never
PAM39	M	1	0	1	IIA	0	60	11.0	0	Ever-Current
PAM40	F	1	0	1	IIB	0	55	18.0	0	Ever-Former
PAM41	F	1	1	1	IIB	0	60	12.0	0	Ever-Former
PAM42	M	1	1	1	IIA	1	65	58.0	1	Never
PAM43	M	1	1	1	IIB	0	69	24.0	0	Ever-Former

Supplemental Table 1 (continued)

PAM ID	Gender	Chemo	Radiation	Surgery	Stage at Dx	Oligometastatic	Age at Dx	Overall Survival (mo)	Type II Diabetes	Smoking Hx
PAM44	M	1	1	1	IIB	0	74	20.0	0	Ever-Former
PAM45	F	1	1	1	IIB	0	56	33.0	0	Ever-Former
PAM46	M	1	1	1	IIB	1	44	34.0	0	Never
PAM47	F	1	0	0	IV	0	68	4.0	0	Never
PAM48	F	1	0	0	IV	0	64	3.0	0	Never
PAM49	M	1	0	0	IV	0	42	8.0	0	Never
PAM50	F	1	0	0	IV	0	56	11.0	1	Never
PAM51	F	1	0	0	IV	0	76	7.0	0	Never
PAM52	M	1	0	0	IV	0	53	6.0	0	Never
PAM53	M	1	0	0	IV	0	55	15.0	0	Never
PAM54	M	1	0	0	IV	0	63	7.0	0	Never
PAM55	M	1	0	0	IV	0	65	10.0	0	Ever-Former
PAM56	F	1	0	0	IV	0	41	6.0	0	Never
PAM57	M	1	1	1	IIB	0	51	28.0	0	Never
PAM66	M	1	1	0	III	1	67	48.0	0	Never
PAM67	F	1	0	0	IV	0	60	3.0	1	Ever-Former
PAM88	F	1	1	0	IV	0	51	3.0	1	Ever-Former
PAM97	F	1	1	1	IIB	0	69	9.0	0	Never
PAM98	F	1	0	1	IIB	0	74	9.0	0	Never
MPAM33	M	1	0	0	IV	0	57	9.0	0	Never
MPAM34	M	1	1	1	III	0	38	34.0	0	Never
MPAM35	F	1	0	0	IV	0	73	17.0	0	Ever-Former

Abbreviations: Dx, Diagnosis; Hx, History

Supplemental Table 2. Samples per patient summary.

PAM ID	PAM Sample ID	Sample Class	Tissue Site	Metastatic Route	Purity	Ploidy	WGD status	Stage Sample Collected	Clonal Composition
MPAM01	MPAM01N	Normal	Heart					IV	
MPAM01	MPAM01PT1	Metastasis	Peritoneal Cavity	Direct Seeding	0.10	3.52	TETRAPLOID	IV	monoclonal
MPAM01	MPAM01PT2	Metastasis	Liver	Hematogenous	0.37	3.50	TETRAPLOID	IV	monoclonal
MPAM01	MPAM01PT3	Metastasis	Liver	Hematogenous	0.23	3.52	TETRAPLOID	IV	monoclonal
MPAM01	MPAM01PT4	Metastasis	Liver	Hematogenous	0.32	3.52	TETRAPLOID	IV	monoclonal
MPAM01	MPAM01PT5	Metastasis	Liver	Hematogenous	0.51	3.30	TETRAPLOID	IV	monoclonal
MPAM03	MPAM03N	Normal	Skeletal Muscle					IV	
MPAM03	MPAM03PT1	Metastasis	Peritoneal Cavity	Direct Seeding	0.27	2.92	DIPLOID	IV	polyclonal
MPAM03	MPAM03PT2	Primary	Pancreas Primary		0.18	2.85	DIPLOID	IV	polyclonal
MPAM03	MPAM03PT3	Primary	Pancreas Primary		0.22	2.87	DIPLOID	IV	polyclonal
MPAM03	MPAM03PT4	Primary	Pancreas Primary		0.33	2.83	DIPLOID	IV	polyclonal
MPAM03	MPAM03PT5	Metastasis	Peritoneal Cavity	Direct Seeding	0.22	2.86	DIPLOID	IV	polyclonal
MPAM03	MPAM03PT6	Metastasis	Diaphragm	Unknown				IV	
MPAM03	MPAM03PT7	Metastasis	Peritoneal Cavity	Direct Seeding				IV	
MPAM05	MPAM05N	Normal	Skeletal Muscle					IV	
MPAM05	MPAM05PT1	Metastasis	Pleural Cavity	Unknown	0.21	5.15	TETRAPLOID	IV	polyclonal
MPAM05	MPAM05PT10	Metastasis	Liver	Hematogenous	0.15	5.12	TETRAPLOID	IV	polyclonal
MPAM05	MPAM05PT11	Metastasis	Liver	Hematogenous	0.55	5.50	TETRAPLOID	IV	polyclonal
MPAM05	MPAM05PT2	Metastasis	Peritoneal Cavity	Direct Seeding	0.46	5.05	TETRAPLOID	IV	polyclonal
MPAM05	MPAM05PT3	Metastasis	Lung	Hematogenous	0.76	5.54	TETRAPLOID	IV	polyclonal
MPAM05	MPAM05PT4	Metastasis	Lung	Hematogenous	0.12	5.16	TETRAPLOID	IV	monoclonal
MPAM05	MPAM05PT5	Metastasis	Lymph Node	Lymphatic	0.40	5.13	TETRAPLOID	IV	polyclonal
MPAM05	MPAM05PT6	Metastasis	Pericardial Sac	Unknown	0.72	5.47	TETRAPLOID	IV	polyclonal

Supplemental Table 2 (continued)

PAM ID	PAM Sample ID	Sample Class	Tissue Site	Metastatic Route	Purity	Ploidy	WGD status	Stage Sample Collected	Clonal Composition
MPAM05	MPAM05PT7	Metastasis	Diaphragm	Unknown	0.32	5.09	TETRAPLOID	IV	polyclonal
MPAM05	MPAM05PT8	Metastasis	Liver	Hematogenous	1.00	5.46	TETRAPLOID	IV	polyclonal
MPAM05	MPAM05PT9	Metastasis	Liver	Hematogenous	0.98	5.28	TETRAPLOID	IV	polyclonal
MPAM06	MPAM06N	Normal	Skeletal Muscle					IV	
MPAM06	MPAM06PT1	Metastasis	Lung	Hematogenous	0.23	4.19	TETRAPLOID	IV	monoclonal
MPAM06	MPAM06PT10	Metastasis	Retroperitoneum	Direct Seeding	0.38	4.24	TETRAPLOID	IV	polyclonal
MPAM06	MPAM06PT11	Primary	Pancreas Primary					IV	
MPAM06	MPAM06PT2	Metastasis	Lung	Hematogenous	0.28	4.19	TETRAPLOID	IV	monoclonal
MPAM06	MPAM06PT3	Metastasis	Diaphragm	Unknown	0.23	4.19	TETRAPLOID	IV	monoclonal
MPAM06	MPAM06PT4	Metastasis	Liver	Hematogenous	0.64	4.27	TETRAPLOID	IV	polyclonal
MPAM06	MPAM06PT5	Metastasis	Peritoneal Cavity	Direct Seeding	0.13	4.19	TETRAPLOID	IV	monoclonal
MPAM06	MPAM06PT6	Primary	Pancreas Primary					IV	
MPAM06	MPAM06PT7	Primary	Pancreas Primary		0.19	4.19	TETRAPLOID	IV	monoclonal
MPAM06	MPAM06PT8	Metastasis	Liver	Hematogenous	0.47	4.27	TETRAPLOID	IV	polyclonal
MPAM06	MPAM06PT9	Metastasis	Liver	Hematogenous	0.25	4.27	TETRAPLOID	IV	polyclonal
MPAM07	MPAM07N	Normal	Skeletal Muscle					IV	
MPAM07	MPAM07PT1	Primary	Pancreas Primary		0.37	1.68	DIPLOID	IV	monoclonal
MPAM07	MPAM07PT10	Primary	Pancreas Primary		0.57	1.64	DIPLOID	IV	polyclonal
MPAM07	MPAM07PT2	Metastasis	Diaphragm	Unknown	0.65	1.56	DIPLOID	IV	polyclonal
MPAM07	MPAM07PT3	Metastasis	Diaphragm	Unknown	0.65	1.60	DIPLOID	IV	polyclonal
MPAM07	MPAM07PT4	Metastasis	Pleural Cavity	Unknown	0.64	1.61	DIPLOID	IV	polyclonal
MPAM07	MPAM07PT5	Metastasis	Liver	Hematogenous	0.60	1.65	DIPLOID	IV	polyclonal
MPAM07	MPAM07PT6	Metastasis	Liver	Hematogenous	0.80	1.64	DIPLOID	IV	polyclonal

Supplemental Table 2 (continued)

PAM ID	PAM Sample ID	Sample Class	Tissue Site	Metastatic Route	Purity	Ploidy	WGD status	Stage Sample Collected	Clonal Composition
MPAM07	MPAM07PT7	Metastasis	Lymph Node	Lymphatic	0.48	1.58	DIPLOID	IV	polyclonal
MPAM07	MPAM07PT8	Metastasis	Lymph Node	Lymphatic	0.59	1.63	DIPLOID	IV	polyclonal
MPAM07	MPAM07PT9	Primary	Pancreas Primary					IV	
MPAM08	MPAM08N	Normal	Skeletal Muscle					IV	
MPAM08	MPAM08PT1	Metastasis	Liver	Hematogenous	0.46	2.57	DIPLOID	IV	polyclonal
MPAM08	MPAM08PT10	Primary	Pancreas Primary		0.33	2.61	DIPLOID	IV	polyclonal
MPAM08	MPAM08PT11	Metastasis	Peritoneal Cavity	Direct Seeding				IV	
MPAM08	MPAM08PT12	Metastasis	Lymph Node	Lymphatic	0.67	2.57	DIPLOID	IV	polyclonal
MPAM08	MPAM08PT2	Metastasis	Liver	Hematogenous	0.60	2.59	DIPLOID	IV	polyclonal
MPAM08	MPAM08PT3	Metastasis	Peritoneal Cavity	Direct Seeding	0.59	2.57	DIPLOID	IV	polyclonal
MPAM08	MPAM08PT4	Metastasis	Peritoneal Cavity	Direct Seeding	0.63	2.59	DIPLOID	IV	polyclonal
MPAM08	MPAM08PT5	Metastasis	Pericardial Sac	Unknown	1.00	2.71	DIPLOID	IV	polyclonal
MPAM08	MPAM08PT6	Metastasis	Peritoneal Cavity	Direct Seeding				IV	
MPAM08	MPAM08PT7	Metastasis	Peritoneal Cavity	Direct Seeding	0.47	2.54	DIPLOID	IV	polyclonal
MPAM08	MPAM08PT8	Primary	Pancreas Primary		0.34	2.53	DIPLOID	IV	monoclonal
MPAM08	MPAM08PT9	Primary	Pancreas Primary		0.26	2.58	DIPLOID	IV	polyclonal
MPAM09	MPAM09N	Normal	Pancreas					III	
MPAM09	MPAM09PT1	Primary	Pancreas Primary					III	
MPAM09	MPAM09PT2	Primary	Pancreas Primary					III	
MPAM09	MPAM09PT3	Primary	Pancreas Primary					III	
MPAM10	MPAM10N	Normal	Pancreas					III	
MPAM10	MPAM10PT1	Primary	Pancreas Primary					III	
MPAM10	MPAM10PT2	Primary	Pancreas Primary					III	

Supplemental Table 2 (continued)

PAM ID	PAM Sample ID	Sample Class	Tissue Site	Metastatic Route	Purity	Ploidy	WGD status	Stage Sample Collected	Clonal Composition
MPAM10	MPAM10PT3	Primary	Pancreas Primary					III	
MPAM11	MPAM11N	Normal	Pancreas					IIB	
MPAM11	MPAM11PT1	Primary	Pancreas Primary		0.19	1.96	DIPLOID	IIB	monoclonal
MPAM11	MPAM11PT2	Primary	Pancreas Primary		0.40	1.96	DIPLOID	IIB	polyclonal
MPAM11	MPAM11PT3	Primary	Pancreas Primary		0.25	1.92	DIPLOID	IIB	polyclonal
MPAM11	MPAM11PT4	Primary	Pancreas Primary					IIB	
MPAM12	MPAM12N	Normal	Pancreas					IB	
MPAM12	MPAM12PT1	Primary	Pancreas Primary					IB	
MPAM12	MPAM12PT2	Primary	Pancreas Primary		0.13	1.84	DIPLOID	IB	monoclonal
MPAM12	MPAM12PT3	Primary	Pancreas Primary		0.12	1.84	DIPLOID	IB	monoclonal
MPAM13	MPAM13N	Normal	Pancreas					III	
MPAM13	MPAM13PT1	Primary	Pancreas Primary		0.30	1.88	DIPLOID	III	monoclonal
MPAM13	MPAM13PT2	Primary	Pancreas Primary		0.43	1.88	DIPLOID	III	monoclonal
MPAM13	MPAM13PT3	Primary	Pancreas Primary		0.42	1.88	DIPLOID	III	monoclonal
MPAM14	MPAM14N	Normal	Pancreas					IIB	
MPAM14	MPAM14PT1	Primary	Pancreas Primary		0.23	1.94	DIPLOID	IIB	monoclonal
MPAM14	MPAM14PT2	Primary	Pancreas Primary		0.11	1.94	DIPLOID	IIB	monoclonal
MPAM14	MPAM14PT3	Primary	Pancreas Primary		0.36	1.94	DIPLOID	IIB	monoclonal
MPAM14	MPAM14PT4	Primary	Pancreas Primary		0.03	1.94	DIPLOID	IIB	
MPAM14	MPAM14PT5	Primary	Pancreas Primary		0.29	1.94	DIPLOID	IIB	monoclonal
MPAM15	MPAM15N	Normal	Pancreas					IIB	
MPAM15	MPAM15PT1	Primary	Pancreas Primary		0.15	1.96	DIPLOID	IIB	monoclonal
MPAM15	MPAM15PT2	Primary	Pancreas Primary		0.16	1.96	DIPLOID	IIB	monoclonal

Supplemental Table 2 (continued)

PAM ID	PAM Sample ID	Sample Class	Tissue Site	Metastatic Route	Purity	Ploidy	WGD status	Stage Sample Collected	Clonal Composition
MPAM15	MPAM15PT3	Primary	Pancreas Primary					IIB	
MPAM16	MPAM16N	Normal	Pancreas					IIB	
MPAM16	MPAM16PT1	Primary	Pancreas Primary					IIB	
MPAM16	MPAM16PT2	Primary	Pancreas Primary					IIB	
MPAM16	MPAM16PT3	Primary	Pancreas Primary					IIB	
MPAM16	MPAM16PT4	Primary	Pancreas Primary					IIB	
MPAM17	MPAM17N	Normal	Pancreas					III	
MPAM17	MPAM17PT1	Primary	Pancreas Primary		0.34	3.41	TETRAPLOID	III	monoclonal
MPAM17	MPAM17PT2	Primary	Pancreas Primary		0.34	3.41	TETRAPLOID	III	monoclonal
MPAM17	MPAM17PT3	Primary	Pancreas Primary		0.35	3.41	TETRAPLOID	III	monoclonal
MPAM17	MPAM17PT4	Primary	Pancreas Primary					III	
MPAM18	MPAM18N	Normal	Pancreas					III	
MPAM18	MPAM18PT1	Primary	Pancreas Primary					III	
MPAM18	MPAM18PT2	Primary	Pancreas Primary					III	
MPAM18	MPAM18PT3	Primary	Pancreas Primary		0.50	1.82	DIPLOID	III	monoclonal
MPAM18	MPAM18PT4	Primary	Pancreas Primary					III	
MPAM19	MPAM19N	Normal	Pancreas					IIB	
MPAM19	MPAM19PT1	Primary	Pancreas Primary					IIB	
MPAM19	MPAM19PT2	Primary	Pancreas Primary					IIB	
MPAM19	MPAM19PT3	Primary	Pancreas Primary					IIB	
MPAM19	MPAM19PT4	Primary	Pancreas Primary					IIB	
MPAM19	MPAM19PT5	Primary	Pancreas Primary					IIB	
MPAM19	MPAM19PT6	Primary	Pancreas Primary					IIB	

Supplemental Table 2 (continued)

PAM ID	PAM Sample ID	Sample Class	Tissue Site	Metastatic Route	Purity	Ploidy	WGD status	Stage Sample Collected	Clonal Composition
MPAM20	MPAM20N	Normal	Pancreas					IIA	
MPAM20	MPAM20PT1	Primary	Pancreas Primary		0.62	2.03	DIPLOID	IIA	monoclonal
MPAM20	MPAM20PT2	Primary	Pancreas Primary		0.11	2.03	DIPLOID	IIA	monoclonal
MPAM20	MPAM20PT3	Primary	Pancreas Primary		0.38	2.03	DIPLOID	IIA	monoclonal
MPAM20	MPAM20PT4	Primary	Pancreas Primary		0.20	2.03	DIPLOID	IIA	monoclonal
MPAM21	MPAM21N	Normal	Pancreas					IIA	
MPAM21	MPAM21PT1	Primary	Pancreas Primary					IIA	
MPAM21	MPAM21PT2	Primary	Pancreas Primary					IIA	
MPAM21	MPAM21PT3	Primary	Pancreas Primary					IIA	
MPAM22	MPAM22N	Normal	Pancreas					IIA	
MPAM22	MPAM22PT1	Primary	Pancreas Primary					IIA	
MPAM22	MPAM22PT2	Primary	Pancreas Primary					IIA	
MPAM22	MPAM22PT3	Primary	Pancreas Primary					IIA	
MPAM23	MPAM23N	Normal	Pancreas					IIA	
MPAM23	MPAM23PT1	Primary	Pancreas Primary					IIA	
MPAM23	MPAM23PT2	Primary	Pancreas Primary		0.36	3.86	TETRAPLOID	IIA	monoclonal
MPAM23	MPAM23PT3	Primary	Pancreas Primary		0.37	3.86	TETRAPLOID	IIA	monoclonal
MPAM23	MPAM23PT4	Primary	Pancreas Primary					IIA	
MPAM24	MPAM24N	Normal	Pancreas					IIA	
MPAM24	MPAM24PT1	Primary	Pancreas Primary		0.33	3.29	TETRAPLOID	IIA	monoclonal
MPAM24	MPAM24PT2	Primary	Pancreas Primary		0.30	3.29	TETRAPLOID	IIA	monoclonal
MPAM24	MPAM24PT3	Primary	Pancreas Primary		0.22	3.29	TETRAPLOID	IIA	monoclonal
MPAM25	MPAM25N	Normal	Pancreas					IIA	

Supplemental Table 2 (continued)

PAM ID	PAM Sample ID	Sample Class	Tissue Site	Metastatic Route	Purity	Ploidy	WGD status	Stage Sample Collected	Clonal Composition
MPAM25	MPAM25PT1	Primary	Pancreas Primary					IIA	
MPAM25	MPAM25PT2	Primary	Pancreas Primary					IIA	
MPAM25	MPAM25PT3	Primary	Pancreas Primary					IIA	
MPAM26	MPAM26N	Normal	Pancreas					IIA	
MPAM26	MPAM26PT1	Primary	Pancreas Primary		0.48	3.19	TETRAPLOID	IIA	monoclonal
MPAM26	MPAM26PT2	Primary	Pancreas Primary		0.38	3.18	TETRAPLOID	IIA	polyclonal
MPAM26	MPAM26PT3	Primary	Pancreas Primary		0.42	3.20	TETRAPLOID	IIA	polyclonal
MPAM26	MPAM26PT4	Primary	Pancreas Primary		0.49	3.31	TETRAPLOID	IIA	polyclonal
MPAM27	MPAM27N	Normal	Pancreas					IIA	
MPAM27	MPAM27PT1	Primary	Pancreas Primary					IIA	
MPAM27	MPAM27PT2	Primary	Pancreas Primary					IIA	
MPAM27	MPAM27PT3	Primary	Pancreas Primary					IIA	
MPAM28	MPAM28N	Normal	Pancreas					IIA	
MPAM28	MPAM28PT1	Primary	Pancreas Primary					IIA	
MPAM28	MPAM28PT2	Primary	Pancreas Primary		0.29	2.06	DIPLOID	IIA	polyclonal
MPAM28	MPAM28PT3	Primary	Pancreas Primary		0.33	2.04	DIPLOID	IIA	polyclonal
MPAM29	MPAM29N	Normal	Pancreas					IIA	
MPAM29	MPAM29PT1	Primary	Pancreas Primary					IIA	
MPAM29	MPAM29PT2	Primary	Pancreas Primary		0.23	3.31	TETRAPLOID	IIA	polyclonal
MPAM29	MPAM29PT3	Primary	Pancreas Primary		0.45	3.58	TETRAPLOID	IIA	polyclonal
MPAM29	MPAM29PT4	Primary	Pancreas Primary		0.23	3.20	TETRAPLOID	IIA	polyclonal
MPAM30	MPAM30N	Normal	Pancreas					IIA	
MPAM30	MPAM30PT1	Primary	Pancreas Primary		0.43	2.23	DIPLOID	IIA	monoclonal

Supplemental Table 2 (continued)

PAM ID	PAM Sample ID	Sample Class	Tissue Site	Metastatic Route	Purity	Ploidy	WGD status	Stage Sample Collected	Clonal Composition
MPAM30	MPAM30PT2	Primary	Pancreas Primary		0.28	2.23	DIPLOID	IIA	monoclonal
MPAM30	MPAM30PT3	Primary	Pancreas Primary		0.31	2.23	DIPLOID	IIA	monoclonal
MPAM31	MPAM31N	Normal	Pancreas					IIA	
MPAM31	MPAM31PT1	Primary	Pancreas Primary		0.14	3.46	TETRAPLOID	IIA	monoclonal
MPAM31	MPAM31PT2	Primary	Pancreas Primary		0.30	3.46	TETRAPLOID	IIA	monoclonal
MPAM31	MPAM31PT3	Primary	Pancreas Primary		0.24	3.46	TETRAPLOID	IIA	monoclonal
MPAM32	MPAM32N	Normal	Heart					IV	
MPAM32	MPAM32PT1	Metastasis	Peritoneal Cavity	Direct Seeding	0.58	2.65	DIPLOID	IV	polyclonal
MPAM32	MPAM32PT10	Metastasis	Liver	Hematogenous	0.33	2.36	DIPLOID	IV	polyclonal
MPAM32	MPAM32PT11	Metastasis	Lymph Node	Lymphatic	0.42	2.45	DIPLOID	IV	polyclonal
MPAM32	MPAM32PT12	Primary	Pancreas Primary		0.25	2.72	DIPLOID	IV	monoclonal
MPAM32	MPAM32PT13	Primary	Pancreas Primary		0.18	2.72	DIPLOID	IV	monoclonal
MPAM32	MPAM32PT2	Metastasis	Peritoneal Cavity	Direct Seeding	0.84	2.66	DIPLOID	IV	polyclonal
MPAM32	MPAM32PT3	Metastasis	Diaphragm	Unknown	0.35	2.51	DIPLOID	IV	polyclonal
MPAM32	MPAM32PT4	Metastasis	Peritoneal Cavity	Direct Seeding	0.51	2.59	DIPLOID	IV	polyclonal
MPAM32	MPAM32PT5	Metastasis	Diaphragm	Unknown	0.36	2.55	DIPLOID	IV	polyclonal
MPAM32	MPAM32PT6	Metastasis	Peritoneal Cavity	Direct Seeding	0.45	2.73	DIPLOID	IV	polyclonal
MPAM32	MPAM32PT7	Metastasis	Peritoneal Cavity	Direct Seeding	0.75	2.68	DIPLOID	IV	polyclonal
MPAM32	MPAM32PT8	Metastasis	Liver	Hematogenous	0.47	2.50	DIPLOID	IV	polyclonal
MPAM32	MPAM32PT9	Metastasis	Liver	Hematogenous	0.50	2.48	DIPLOID	IV	polyclonal
MPAM33	MPAM33N	Normal	Heart					IV	
MPAM33	MPAM33PT1	Metastasis	Lung	Hematogenous	0.54	3.35	TETRAPLOID	IV	polyclonal
MPAM33	MPAM33PT2	Metastasis	Lung	Hematogenous	0.66	3.27	TETRAPLOID	IV	polyclonal

Supplemental Table 2 (continued)

PAM ID	PAM Sample ID	Sample Class	Tissue Site	Metastatic Route	Purity	Ploidy	WGD status	Stage Sample Collected	Clonal Composition
MPAM33	MPAM33PT3	Metastasis	Lymph Node	Lymphatic	0.43	3.20	TETRAPLOID	IV	polyclonal
MPAM33	MPAM33PT4	Metastasis	Liver	Hematogenous	0.33	2.61	DIPLOID	IV	monoclonal
MPAM33	MPAM33PT5	Metastasis	Liver	Hematogenous	0.74	3.28	TETRAPLOID	IV	polyclonal
MPAM33	MPAM33PT6	Metastasis	Liver	Hematogenous	0.72	3.21	TETRAPLOID	IV	monoclonal
MPAM33	MPAM33PT7	Primary	Pancreas Primary		0.46	2.69	DIPLOID	IV	polyclonal
MPAM33	MPAM33PT8	Primary	Pancreas Primary		0.54	2.96	DIPLOID	IV	polyclonal
MPAM34	MPAM34PT1	Normal	Skeletal Muscle					IV	
MPAM34	MPAM34PT2	Metastasis	Pleural Cavity	Unknown	0.62	1.85	DIPLOID	IV	polyclonal
MPAM34	MPAM34PT3	Metastasis	Lymph Node	Lymphatic	0.37	1.89	DIPLOID	IV	polyclonal
MPAM34	MPAM34PT4	Metastasis	Peritoneal Cavity	Direct Seeding	0.39	1.90	DIPLOID	IV	polyclonal
MPAM34	MPAM34PT5	Metastasis	Diaphragm	Unknown	0.32	1.91	DIPLOID	IV	polyclonal
MPAM34	MPAM34PT6	Metastasis	Lung	Hematogenous	0.48	1.83	DIPLOID	IV	polyclonal
MPAM34	MPAM34PT7	Metastasis	Peritoneal Cavity	Direct Seeding				IV	
MPAM34	MPAM34PT8	Metastasis	Peritoneal Cavity	Direct Seeding	0.48	1.88	DIPLOID	IV	polyclonal
MPAM34	MPAM34PT9	Metastasis	Adrenal	Unknown				IV	
MPAM35	MPAM35PT1	Normal	Skeletal Muscle					IV	
MPAM35	MPAM35PT2	Metastasis	Peritoneal Cavity	Direct Seeding	0.34	2.80	DIPLOID	IV	monoclonal
MPAM35	MPAM35PT3	Primary	Pancreas Primary		0.36	2.80	DIPLOID	IV	monoclonal
MPAM35	MPAM35PT4	Primary	Pancreas Primary		0.10	2.80	DIPLOID	IV	monoclonal
MPAM35	MPAM35PT5	Metastasis	Lymph Node	Lymphatic	0.37	2.80	DIPLOID	IV	monoclonal
MPAM35	MPAM35PT6	Metastasis	Peritoneal Cavity	Direct Seeding	0.28	2.80	DIPLOID	IV	monoclonal
MPAM35	MPAM35PT7	Metastasis	Pelvis	Direct Seeding	0.21	2.80	DIPLOID	IV	monoclonal
MPAM35	MPAM35PT8	Metastasis	Peritoneal Cavity	Direct Seeding	0.28	2.80	DIPLOID	IV	monoclonal

Supplemental Table 2 (continued)

PAM ID	PAM Sample ID	Sample Class	Tissue Site	Metastatic Route	Purity	Ploidy	WGD status	Stage Sample Collected	Clonal Composition
PAM01	PAM01N	Normal	Lung					IV	
PAM01	PAM01PT1	Metastasis	Liver	Hematogenous	0.65	3.16	TETRAPLOID	IV	polyclonal
PAM01	PAM01PT2	Metastasis	Lymph Node	Lymphatic	0.49	3.19	TETRAPLOID	IV	polyclonal
PAM01	PAM01PT3	Metastasis	Lymph Node	Lymphatic	0.69	3.18	TETRAPLOID	IV	polyclonal
PAM01	PAM01PT4	Metastasis	Liver	Hematogenous	0.33	3.18	TETRAPLOID	IV	monoclonal
PAM02	PAM02N	Normal	Skin					IV	
PAM02	PAM02PT1	Metastasis	Liver	Hematogenous	0.19	3.59	TETRAPLOID	IV	polyclonal
PAM02	PAM02PT10	Primary	Pancreas Primary		0.30	3.60	TETRAPLOID	IV	polyclonal
PAM02	PAM02PT11	Primary	Pancreas Primary		0.58	3.52	TETRAPLOID	IV	polyclonal
PAM02	PAM02PT2	Metastasis	Liver	Hematogenous	0.37	3.55	TETRAPLOID	IV	polyclonal
PAM02	PAM02PT3	Metastasis	Liver	Hematogenous	0.34	3.61	TETRAPLOID	IV	polyclonal
PAM02	PAM02PT4	Metastasis	Liver	Hematogenous	0.45	3.57	TETRAPLOID	IV	polyclonal
PAM02	PAM02PT5	Metastasis	Liver	Hematogenous	0.42	3.57	TETRAPLOID	IV	polyclonal
PAM02	PAM02PT6	Metastasis	Liver	Hematogenous	0.22	3.60	TETRAPLOID	IV	polyclonal
PAM02	PAM02PT7	Metastasis	Liver	Hematogenous	0.55	3.57	TETRAPLOID	IV	polyclonal
PAM02	PAM02PT8	Metastasis	Liver	Hematogenous	0.41	3.51	TETRAPLOID	IV	monoclonal
PAM02	PAM02PT9	Primary	Pancreas Primary		0.40	3.61	TETRAPLOID	IV	polyclonal
PAM03	PAM03N	Normal	Skeletal Muscle					IV	
PAM03	PAM03PT1	Metastasis	Lung	Hematogenous	0.12	3.78	TETRAPLOID	IV	monoclonal
PAM03	PAM03PT10	Primary	Pancreas Primary		0.26	3.78	TETRAPLOID	IV	polyclonal
PAM03	PAM03PT11	Primary	Pancreas Primary		0.17	3.78	TETRAPLOID	IV	monoclonal
PAM03	PAM03PT2	Metastasis	Lung	Hematogenous	0.09	3.79	TETRAPLOID	IV	monoclonal
PAM03	PAM03PT3	Metastasis	Liver	Hematogenous	0.21	3.81	TETRAPLOID	IV	polyclonal

Supplemental Table 2 (continued)

PAM ID	PAM Sample ID	Sample Class	Tissue Site	Metastatic Route	Purity	Ploidy	WGD status	Stage Sample Collected	Clonal Composition
PAM03	PAM03PT4	Metastasis	Liver	Hematogenous	0.31	3.89	TETRAPLOID	IV	polyclonal
PAM03	PAM03PT5	Metastasis	Liver	Hematogenous	0.28	3.90	TETRAPLOID	IV	monoclonal
PAM03	PAM03PT6	Metastasis	Liver	Hematogenous	0.22	3.88	TETRAPLOID	IV	polyclonal
PAM03	PAM03PT7	Metastasis	Liver	Hematogenous	0.32	3.89	TETRAPLOID	IV	polyclonal
PAM03	PAM03PT8	Metastasis	Lung	Hematogenous	0.12	3.78	TETRAPLOID	IV	monoclonal
PAM03	PAM03PT9	Primary	Pancreas Primary		0.29	3.81	TETRAPLOID	IV	monoclonal
PAM04	PAM04N	Normal	Skin					IV	
PAM04	PAM04PT1	Metastasis	Liver	Hematogenous	0.27	1.89	DIPLOID	IV	polyclonal
PAM04	PAM04PT2	Metastasis	Peritoneal Cavity	Direct Seeding	0.23	1.89	DIPLOID	IV	monoclonal
PAM04	PAM04PT3	Metastasis	Peritoneal Cavity	Direct Seeding	0.24	1.88	DIPLOID	IV	polyclonal
PAM04	PAM04PT4	Metastasis	Peritoneal Cavity	Direct Seeding	0.23	1.89	DIPLOID	IV	polyclonal
PAM04	PAM04PT5	Metastasis	Peritoneal Cavity	Direct Seeding	0.12	1.89	DIPLOID	IV	monoclonal
PAM04	PAM04PT6	Metastasis	Peritoneal Cavity	Direct Seeding	0.29	1.87	DIPLOID	IV	polyclonal
PAM04	PAM04PT7	Primary	Pancreas Primary		0.12	1.89	DIPLOID	IV	polyclonal
PAM04	PAM04PT8	Primary	Pancreas Primary		0.10	1.88	DIPLOID	IV	monoclonal
PAM04	PAM04PT9	Primary	Pancreas Primary		0.34	1.89	DIPLOID	IV	polyclonal
PAM10	PAM10N	Normal	Spleen					IV	
PAM10	PAM10PT1	Metastasis	Peritoneal Cavity	Direct Seeding				IV	
PAM10	PAM10PT2	Primary	Pancreas Primary					IV	
PAM10	PAM10PT3	Primary	Pancreas Primary					IV	
PAM10	PAM10PT5	Metastasis	Liver	Hematogenous				IV	
PAM104	PAM104N	Normal	Skeletal Muscle					IV	
PAM104	PAM104PT1	Primary	Pancreas Primary		0.21	3.89	TETRAPLOID	IV	monoclonal

Supplemental Table 2 (continued)

PAM ID	PAM Sample ID	Sample Class	Tissue Site	Metastatic Route	Purity	Ploidy	WGD status	Stage Sample Collected	Clonal Composition
PAM104	PAM104PT2	Metastasis	Liver	Hematogenous				IV	
PAM112	PAM112N	Normal	Skin					IV	
PAM112	PAM112PT1	Metastasis	Lung	Hematogenous				IV	
PAM112	PAM112PT3	Primary	Pancreas Primary					IV	
PAM119	PAM119N	Normal	Skeletal Muscle					IV	
PAM119	PAM119PT1	Metastasis	Liver	Hematogenous	0.19	2.07	DIPLOID	IV	monoclonal
PAM119	PAM119PT2	Metastasis	Liver	Hematogenous	0.33	2.07	DIPLOID	IV	polyclonal
PAM119	PAM119PT3	Metastasis	Peritoneal Cavity	Direct Seeding	0.38	2.03	DIPLOID	IV	monoclonal
PAM119	PAM119PT4	Metastasis	Liver	Hematogenous	0.21	2.07	DIPLOID	IV	polyclonal
PAM119	PAM119PT5	Primary	Pancreas Primary					IV	
PAM12	PAM12N	Normal	Spleen					IV	
PAM12	PAM12PT1	Primary	Pancreas Primary		0.59	5.86	TETRAPLOID	IV	monoclonal
PAM12	PAM12PT3	Metastasis	Lymph Node	Lymphatic	0.60	5.86	TETRAPLOID	IV	monoclonal
PAM13	PAM13N	Normal	Spleen					IV	
PAM13	PAM13PT1	Primary	Pancreas Primary					IV	
PAM13	PAM13PT2	Metastasis	Liver	Hematogenous	0.94	1.75	DIPLOID	IV	polyclonal
PAM13	PAM13PT3	Metastasis	Liver	Hematogenous	0.67	2.01	DIPLOID	IV	polyclonal
PAM13	PAM13PT4	Metastasis	Liver	Hematogenous	0.88	1.58	DIPLOID	IV	polyclonal
PAM135	PAM135N	Normal	Skeletal Muscle					IV	
PAM135	PAM135PT1	Metastasis	Pericardial Sac	Unknown	0.25	2.77	DIPLOID	IV	monoclonal
PAM135	PAM135PT2	Metastasis	Lung	Hematogenous	0.27	3.45	TETRAPLOID	IV	monoclonal
PAM135	PAM135PT3	Metastasis	Liver	Hematogenous	0.35	2.87	DIPLOID	IV	polyclonal
PAM135	PAM135PT4	Metastasis	Diaphragm	Unknown	0.47	2.82	DIPLOID	IV	monoclonal

Supplemental Table 2 (continued)

PAM ID	PAM Sample ID	Sample Class	Tissue Site	Metastatic Route	Purity	Ploidy	WGD status	Stage Sample Collected	Clonal Composition
PAM14	PAM14N	Normal	Spleen					IV	
PAM14	PAM14PT1	Metastasis	Lung	Hematogenous	0.27	2.52	DIPLOID	IV	monoclonal
PAM14	PAM14PT2	Primary	Pancreas Primary		0.21	2.52	DIPLOID	IV	monoclonal
PAM14	PAM14PT3	Primary	Pancreas Primary		0.33	2.52	DIPLOID	IV	monoclonal
PAM15	PAM15N	Normal	Spleen					III	
PAM15	PAM15PT1	Primary	Pancreas Primary					III	
PAM15	PAM15PT2	Primary	Pancreas Primary					III	
PAM16	PAM16N	Normal	Pancreas					IV	
PAM16	PAM16PT1	Primary	Pancreas Primary		0.38	3.25	TETRAPLOID	IV	monoclonal
PAM16	PAM16PT2	Primary	Pancreas Primary		0.44	3.25	TETRAPLOID	IV	monoclonal
PAM16	PAM16PT3	Metastasis	Liver	Hematogenous	0.53	3.25	TETRAPLOID	IV	monoclonal
PAM16	PAM16PT4	Metastasis	Lymph Node	Lymphatic	0.54	3.25	TETRAPLOID	IV	monoclonal
PAM17	PAM17N	Normal	Pancreas					IV	
PAM17	PAM17PT1	Primary	Pancreas Primary		0.22	3.11	TETRAPLOID	IV	polyclonal
PAM17	PAM17PT2	Primary	Pancreas Primary		0.41	3.14	TETRAPLOID	IV	polyclonal
PAM17	PAM17PT3	Metastasis	Liver	Hematogenous	0.46	3.41	TETRAPLOID	IV	polyclonal
PAM17	PAM17PT4	Metastasis	Peritoneal Cavity	Direct Seeding	0.33	3.21	TETRAPLOID	IV	polyclonal
PAM17	PAM17PT5	Primary	Pancreas Primary		0.27	3.13	TETRAPLOID	IV	polyclonal
PAM18	PAM18N	Normal	Skeletal Muscle					III	
PAM18	PAM18PT1	Metastasis	Liver	Hematogenous	0.19	3.35	TETRAPLOID	III	monoclonal
PAM18	PAM18PT2	Primary	Pancreas Primary		0.31	3.35	TETRAPLOID	III	monoclonal
PAM19	PAM19N	Normal	Liver					IV	
PAM19	PAM19N	Normal	Skeletal Muscle					IV	

Supplemental Table 2 (continued)

PAM ID	PAM Sample ID	Sample Class	Tissue Site	Metastatic Route	Purity	Ploidy	WGD status	Stage Sample Collected	Clonal Composition
PAM19	PAM19PT1	Primary	Pancreas Primary					IV	
PAM19	PAM19PT10	Metastasis	Lung	Hematogenous				IV	
PAM19	PAM19PT11	Metastasis	Peritoneal Cavity	Direct Seeding				IV	
PAM19	PAM19PT12	Metastasis	Diaphragm	Unknown				IV	
PAM19	PAM19PT14	Metastasis	Liver	Hematogenous				IV	
PAM19	PAM19PT15	Metastasis	Peritoneal Cavity	Direct Seeding				IV	
PAM19	PAM19PT16	Metastasis	Peritoneal Cavity	Direct Seeding				IV	
PAM19	PAM19PT17	Metastasis	Peritoneal Cavity	Direct Seeding				IV	
PAM19	PAM19PT2	Metastasis	Lung	Hematogenous				IV	
PAM19	PAM19PT3	Metastasis	Lung	Hematogenous				IV	
PAM19	PAM19PT4	Metastasis	Lymph Node	Lymphatic				IV	
PAM19	PAM19PT5	Metastasis	Liver	Hematogenous				IV	
PAM19	PAM19PT6	Metastasis	Lung	Hematogenous				IV	
PAM19	PAM19PT7	Metastasis	Peritoneal Cavity	Direct Seeding				IV	
PAM19	PAM19PT8	Metastasis	Peritoneal Cavity	Direct Seeding				IV	
PAM19	PAM19PT9	Metastasis	Lung	Hematogenous				IV	
PAM20	PAM20N	Normal	Liver					IV	
PAM20	PAM20PT1	Primary	Pancreas Primary					IV	
PAM20	PAM20PT2	Primary	Pancreas Primary					IV	
PAM20	PAM20PT3	Metastasis	Peritoneal Cavity	Direct Seeding				IV	
PAM20	PAM20PT4	Metastasis	Peritoneal Cavity	Direct Seeding				IV	
PAM20	PAM20PT5	Metastasis	Diaphragm	Unknown				IV	
PAM20	PAM20PT6	Metastasis	Peritoneal Cavity	Direct Seeding				IV	

Supplemental Table 2 (continued)

PAM ID	PAM Sample ID	Sample Class	Tissue Site	Metastatic Route	Purity	Ploidy	WGD status	Stage Sample Collected	Clonal Composition
PAM21	PAM21N	Normal	Spleen					III	
PAM21	PAM21PT1	Primary	Pancreas Primary					III	
PAM21	PAM21PT2	Primary	Pancreas Primary					III	
PAM21	PAM21PT3	Primary	Pancreas Primary					III	
PAM21	PAM21PT5	Primary	Pancreas Primary					III	
PAM21	PAM21PT6	Primary	Pancreas Primary					III	
PAM22	PAM22N	Normal	Skeletal Muscle					IV	
PAM22	PAM22PT1	Primary	Pancreas Primary					IV	
PAM22	PAM22PT2	Primary	Pancreas Primary					IV	
PAM22	PAM22PT3	Primary	Pancreas Primary					IV	
PAM22	PAM22PT4	Primary	Pancreas Primary					IV	
PAM22	PAM22PT5	Primary	Pancreas Primary					IV	
PAM22	PAM22PT6	Primary	Pancreas Primary					IV	
PAM22	PAM22PT7	Primary	Pancreas Primary					IV	
PAM22	PAM22PT8	Primary	Pancreas Primary					IV	
PAM22	PAM22PT9	Primary	Pancreas Primary					IV	
PAM23	PAM23N	Normal	Spleen					IV	
PAM23	PAM23PT1	Primary	Pancreas Primary					IV	
PAM23	PAM23PT2	Primary	Pancreas Primary					IV	
PAM23	PAM23PT3	Primary	Pancreas Primary					IV	
PAM23	PAM23PT4	Metastasis	Peritoneal Cavity	Direct Seeding				IV	
PAM23	PAM23PT5	Metastasis	Liver	Hematogenous				IV	
PAM24	PAM24N	Normal	Spleen					IV	

Supplemental Table 2 (continued)

PAM ID	PAM Sample ID	Sample Class	Tissue Site	Metastatic Route	Purity	Ploidy	WGD status	Stage Sample Collected	Clonal Composition
PAM24	PAM24PT1	Primary	Pancreas Primary		0.20	2.10	DIPLOID	IV	polyclonal
PAM24	PAM24PT10	Metastasis	Liver	Hematogenous	0.64	2.11	DIPLOID	IV	polyclonal
PAM24	PAM24PT11	Metastasis	Liver	Hematogenous	0.55	2.09	DIPLOID	IV	polyclonal
PAM24	PAM24PT12	Metastasis	Liver	Hematogenous	0.51	2.08	DIPLOID	IV	polyclonal
PAM24	PAM24PT13	Metastasis	Liver	Hematogenous	0.43	2.09	DIPLOID	IV	polyclonal
PAM24	PAM24PT14	Metastasis	Liver	Hematogenous	0.37	2.11	DIPLOID	IV	polyclonal
PAM24	PAM24PT2	Primary	Pancreas Primary		0.13	2.12	DIPLOID	IV	monoclonal
PAM24	PAM24PT3	Primary	Pancreas Primary		0.14	2.12	DIPLOID	IV	monoclonal
PAM24	PAM24PT4	Primary	Pancreas Primary		0.21	2.09	DIPLOID	IV	polyclonal
PAM24	PAM24PT5	Primary	Pancreas Primary		0.11	2.12	DIPLOID	IV	monoclonal
PAM24	PAM24PT6	Primary	Pancreas Primary		0.22	2.10	DIPLOID	IV	polyclonal
PAM24	PAM24PT7	Primary	Pancreas Primary		0.29	2.12	DIPLOID	IV	monoclonal
PAM24	PAM24PT8	Primary	Pancreas Primary		0.36	2.10	DIPLOID	IV	polyclonal
PAM24	PAM24PT9	Metastasis	Liver	Hematogenous	0.40	2.09	DIPLOID	IV	polyclonal
PAM25	PAM25N	Normal	Spleen					III	
PAM25	PAM25PT1	Primary	Pancreas Primary		0.33	1.74	DIPLOID	III	monoclonal
PAM25	PAM25PT2	Primary	Pancreas Primary		0.31	1.74	DIPLOID	III	monoclonal
PAM25	PAM25PT3	Primary	Pancreas Primary		0.33	1.74	DIPLOID	III	monoclonal
PAM26	PAM26N	Normal	Spleen					IV	
PAM26	PAM26PT1	Primary	Pancreas Primary		0.63	3.09	TETRAPLOID	IV	polyclonal
PAM26	PAM26PT2	Primary	Pancreas Primary		0.58	3.17	TETRAPLOID	IV	polyclonal
PAM26	PAM26PT3	Primary	Pancreas Primary		0.67	3.14	TETRAPLOID	IV	polyclonal
PAM26	PAM26PT4	Primary	Pancreas Primary		0.62	3.25	TETRAPLOID	IV	polyclonal

Supplemental Table 2 (continued)

PAM ID	PAM Sample ID	Sample Class	Tissue Site	Metastatic Route	Purity	Ploidy	WGD status	Stage Sample Collected	Clonal Composition
PAM26	PAM26PT5	Primary	Pancreas Primary		0.61	3.31	TETRAPLOID	IV	polyclonal
PAM26	PAM26PT6	Metastasis	Liver	Hematogenous	0.78	3.22	TETRAPLOID	IV	polyclonal
PAM26	PAM26PT7	Metastasis	Liver	Hematogenous	0.84	3.27	TETRAPLOID	IV	polyclonal
PAM27	PAM27N	Normal	Spleen					III	
PAM27	PAM27PT1	Primary	Pancreas Primary		0.24	1.97	DIPLOID	III	monoclonal
PAM27	PAM27PT2	Primary	Pancreas Primary		0.25	1.97	DIPLOID	III	monoclonal
PAM27	PAM27PT3	Primary	Pancreas Primary		0.25	1.97	DIPLOID	III	monoclonal
PAM27	PAM27PT4	Primary	Pancreas Primary		0.26	1.97	DIPLOID	III	monoclonal
PAM27	PAM27PT5	Primary	Pancreas Primary		0.25	1.97	DIPLOID	III	monoclonal
PAM27	PAM27PT6	Primary	Pancreas Primary		0.14	1.97	DIPLOID	III	monoclonal
PAM28	PAM28N	Normal	Liver					IV	
PAM28	PAM28PT1	Primary	Pancreas Primary		0.52	3.05	TETRAPLOID	IV	polyclonal
PAM28	PAM28PT2	Primary	Pancreas Primary		0.56	2.61	DIPLOID	IV	polyclonal
PAM28	PAM28PT3	Primary	Pancreas Primary		0.48	2.67	DIPLOID	IV	polyclonal
PAM28	PAM28PT4	Metastasis	Liver	Hematogenous	0.69	1.91	DIPLOID	IV	monoclonal
PAM28	PAM28PT5	Metastasis	Liver	Hematogenous	0.59	2.02	DIPLOID	IV	polyclonal
PAM29	PAM29N	Normal	Liver					IV	
PAM29	PAM29PT1	Primary	Pancreas Primary		0.20	1.90	DIPLOID	IV	polyclonal
PAM29	PAM29PT2	Primary	Pancreas Primary		0.17	1.84	DIPLOID	IV	monoclonal
PAM29	PAM29PT3	Primary	Pancreas Primary		0.26	1.88	DIPLOID	IV	polyclonal
PAM29	PAM29PT4	Primary	Pancreas Primary		0.38	1.91	DIPLOID	IV	polyclonal
PAM29	PAM29PT5	Metastasis	Peritoneal Cavity	Direct Seeding	0.47	1.89	DIPLOID	IV	monoclonal
PAM29	PAM29PT6	Metastasis	Peritoneal Cavity	Direct Seeding	0.36	1.96	DIPLOID	IV	polyclonal

Supplemental Table 2 (continued)

PAM ID	PAM Sample ID	Sample Class	Tissue Site	Metastatic Route	Purity	Ploidy	WGD status	Stage Sample Collected	Clonal Composition
PAM29	PAM29PT7	Metastasis	Peritoneal Cavity	Direct Seeding	0.34	1.95	DIPLOID	IV	polyclonal
PAM29	PAM29PT8	Metastasis	Peritoneal Cavity	Direct Seeding	0.53	1.95	DIPLOID	IV	polyclonal
PAM31	PAM31N	Normal	Spleen					IV	
PAM31	PAM31PT1	Primary	Pancreas Primary		0.22	1.80	DIPLOID	IV	monoclonal
PAM31	PAM31PT2	Metastasis	Peritoneal Cavity	Direct Seeding	0.19	1.80	DIPLOID	IV	monoclonal
PAM31	PAM31PT3	Metastasis	Lymph Node	Lymphatic	0.51	1.80	DIPLOID	IV	monoclonal
PAM32	PAM32N	Normal	Liver					IV	
PAM32	PAM32PT1	Primary	Pancreas Primary		0.28	4.10	TETRAPLOID	IV	polyclonal
PAM32	PAM32PT2	Primary	Pancreas Primary		0.69	4.10	TETRAPLOID	IV	monoclonal
PAM32	PAM32PT3	Metastasis	Lung	Hematogenous				IV	
PAM32	PAM32PT4	Metastasis	Lung	Hematogenous	0.32	3.90	TETRAPLOID	IV	monoclonal
PAM32	PAM32PT5	Metastasis	Adrenal	Unknown	0.54	3.92	TETRAPLOID	IV	polyclonal
PAM32	PAM32PT6	Metastasis	Liver	Hematogenous				IV	
PAM33	PAM33N	Normal	Liver					IV	
PAM33	PAM33PT1	Primary	Pancreas Primary					IV	
PAM33	PAM33PT2	Primary	Pancreas Primary					IV	
PAM33	PAM33PT3	Metastasis	Liver	Hematogenous				IV	
PAM33	PAM33PT4	Metastasis	Liver	Hematogenous				IV	
PAM36	PAM36N	Normal	Breast					IV	
PAM36	PAM36PT1	Primary	Pancreas Primary					IV	
PAM36	PAM36PT2	Primary	Pancreas Primary					IV	
PAM36	PAM36PT3	Metastasis	Lung	Hematogenous				IV	
PAM37	PAM37N	Normal	Lung					IV	

Supplemental Table 2 (continued)

PAM ID	PAM Sample ID	Sample Class	Tissue Site	Metastatic Route	Purity	Ploidy	WGD status	Stage Sample Collected	Clonal Composition
PAM37	PAM37PT1	Primary	Pancreas Primary					IIB	
PAM37	PAM37PT3	Metastasis	Liver	Hematogenous				IV	
PAM37	PAM37PT4	Metastasis	Liver	Hematogenous				IV	
PAM37	PAM37PT5	Metastasis	Peritoneal Cavity	Direct Seeding				IV	
PAM37	PAM37PT6	Metastasis	Liver	Hematogenous				IV	
PAM38	PAM38N	Normal	Kidney					IV	
PAM38	PAM38PT1	Primary	Pancreas Primary					III	
PAM38	PAM38PT2	Primary	Locoregional recurrence					IV	
PAM38	PAM38PT3	Metastasis	Lung	Hematogenous				IV	
PAM38	PAM38PT4	Metastasis	Liver	Hematogenous				IV	
PAM39	PAM39N	Normal	Kidney					IV	
PAM39	PAM39PT1	Primary	Pancreas Primary		0.44	3.21	TETRAPLOID	IIA	polyclonal
PAM39	PAM39PT2	Primary	Locoregional recurrence		0.35	3.13	TETRAPLOID	IV	polyclonal
PAM39	PAM39PT3	Primary	Locoregional recurrence		0.19	3.52	TETRAPLOID	IV	polyclonal
PAM39	PAM39PT4	Metastasis	Lymph Node	Lymphatic				IV	
PAM39	PAM39PT5	Metastasis	Lymph Node	Lymphatic	0.50	2.98	DIPLOID	IV	polyclonal
PAM39	PAM39PT6	Metastasis	Liver	Hematogenous	0.64	3.66	TETRAPLOID	IV	polyclonal
PAM39	PAM39PT7	Metastasis	Diaphragm	Unknown	0.52	3.04	TETRAPLOID	IV	polyclonal
PAM39	PAM39PT8	Metastasis	Peritoneal Cavity	Direct Seeding	0.36	3.13	TETRAPLOID	IV	polyclonal
PAM39	PAM39PT9	Metastasis	Pelvis	Direct Seeding	0.37	3.10	TETRAPLOID	IV	polyclonal
PAM40	PAM40N	Normal	Kidney					IV	
PAM40	PAM40PT1	Primary	Pancreas Primary					IIB	

Supplemental Table 2 (continued)

PAM ID	PAM Sample ID	Sample Class	Tissue Site	Metastatic Route	Purity	Ploidy	WGD status	Stage Sample Collected	Clonal Composition
PAM40	PAM40PT2	Primary	Locoregional recurrence		0.29	1.98	DIPLOID	IV	polyclonal
PAM40	PAM40PT3	Primary	Locoregional recurrence		0.44	1.99	DIPLOID	IV	polyclonal
PAM40	PAM40PT4	Metastasis	Liver	Hematogenous	0.59	2.01	DIPLOID	IV	polyclonal
PAM40	PAM40PT5	Metastasis	Liver	Hematogenous	0.18	1.98	DIPLOID	IV	monoclonal
PAM40	PAM40PT6	Metastasis	Liver	Hematogenous	0.25	1.99	DIPLOID	IV	polyclonal
PAM40	PAM40PT7	Metastasis	Liver	Hematogenous	0.40	1.98	DIPLOID	IV	polyclonal
PAM40	PAM40PT8	Metastasis	Liver	Hematogenous	0.46	2.02	DIPLOID	IV	monoclonal
PAM41	PAM41N	Normal	Heart					IV	
PAM41	PAM41PT1	Primary	Pancreas Primary					IV	
PAM41	PAM41PT10	Metastasis	Liver	Hematogenous	0.74	2.01	DIPLOID	IV	polyclonal
PAM41	PAM41PT11	Metastasis	Liver	Hematogenous	0.69	1.77	DIPLOID	IV	polyclonal
PAM41	PAM41PT2	Primary	Locoregional recurrence		0.75	2.76	DIPLOID	IV	polyclonal
PAM41	PAM41PT3	Metastasis	Liver	Hematogenous	0.83	2.81	DIPLOID	IV	polyclonal
PAM41	PAM41PT4	Metastasis	Liver	Hematogenous	0.92	2.12	DIPLOID	IV	polyclonal
PAM41	PAM41PT5	Metastasis	Lung	Hematogenous	0.62	2.40	DIPLOID	IV	polyclonal
PAM41	PAM41PT6	Metastasis	Lung	Hematogenous	0.57	2.42	DIPLOID	IV	polyclonal
PAM41	PAM41PT7	Metastasis	Peritoneal Cavity	Direct Seeding	0.86	2.10	DIPLOID	IV	polyclonal
PAM41	PAM41PT8	Metastasis	Liver	Hematogenous	0.71	2.47	DIPLOID	IV	polyclonal
PAM41	PAM41PT9	Metastasis	Liver	Hematogenous	0.59	2.13	DIPLOID	IV	polyclonal
PAM42	PAM42N	Normal	Kidney					IV	
PAM42	PAM42PT1	Primary	Pancreas Primary		0.11	3.66	TETRAPLOID	IIA	monoclonal

Supplemental Table 2 (continued)

PAM ID	PAM Sample ID	Sample Class	Tissue Site	Metastatic Route	Purity	Ploidy	WGD status	Stage Sample Collected	Clonal Composition
PAM42	PAM42PT2	Primary	Locoregional recurrence		0.14	3.66	TETRAPLOID	IV	monoclonal
PAM42	PAM42PT3	Primary	Locoregional recurrence		0.20	3.66	TETRAPLOID	IV	monoclonal
PAM42	PAM42PT4	Metastasis	Lung	Hematogenous	0.30	3.66	TETRAPLOID	IV	monoclonal
PAM42	PAM42PT5	Metastasis	Lung	Hematogenous	0.28	3.66	TETRAPLOID	IV	monoclonal
PAM42	PAM42PT6	Metastasis	Pericardial Sac	Unknown				IV	
PAM43	PAM43N	Normal	Spleen					IV	
PAM43	PAM43PT1	Primary	Pancreas Primary		0.30	3.22	TETRAPLOID	IIB	polyclonal
PAM43	PAM43PT2	Primary	Locoregional recurrence		0.32	3.00	DIPLOID	IV	polyclonal
PAM43	PAM43PT3	Metastasis	Liver	Hematogenous	0.51	2.85	DIPLOID	IV	polyclonal
PAM43	PAM43PT4	Metastasis	Retroperitoneum	Direct Seeding	0.52	2.86	DIPLOID	IV	polyclonal
PAM43	PAM43PT5	Metastasis	Peritoneal Cavity	Direct Seeding	0.50	2.88	DIPLOID	IV	polyclonal
PAM43	PAM43PT6	Metastasis	Lung	Hematogenous	0.44	2.99	DIPLOID	IV	polyclonal
PAM44	PAM44N	Normal	Heart					IV	
PAM44	PAM44PT1	Primary	Pancreas Primary					IIB	
PAM44	PAM44PT2	Primary	Locoregional recurrence		0.45	2.03	DIPLOID	IV	polyclonal
PAM44	PAM44PT3	Primary	Locoregional recurrence		0.46	2.00	DIPLOID	IV	polyclonal
PAM44	PAM44PT4	Metastasis	Liver	Hematogenous	0.44	2.04	DIPLOID	IV	polyclonal
PAM44	PAM44PT5	Metastasis	Liver	Hematogenous	0.38	2.00	DIPLOID	IV	polyclonal
PAM45	PAM45N	Normal	Spleen					IV	
PAM45	PAM45PT1	Primary	Pancreas Primary		0.22	3.25	TETRAPLOID	IIB	polyclonal

Supplemental Table 2 (continued)

PAM ID	PAM Sample ID	Sample Class	Tissue Site	Metastatic Route	Purity	Ploidy	WGD status	Stage Sample Collected	Clonal Composition
PAM45	PAM45PT2	Primary	Locoregional recurrence		0.27	3.25	TETRAPLOID	IV	polyclonal
PAM45	PAM45PT3	Metastasis	Peritoneal Cavity	Direct Seeding	0.42	3.25	TETRAPLOID	IV	polyclonal
PAM45	PAM45PT4	Metastasis	Peritoneal Cavity	Direct Seeding	0.52	3.25	TETRAPLOID	IV	monoclonal
PAM45	PAM45PT5	Metastasis	Lymph Node	Lymphatic	0.20	3.25	TETRAPLOID	IV	monoclonal
PAM45	PAM45PT6	Metastasis	Lymph Node	Lymphatic	0.18	3.25	TETRAPLOID	IV	monoclonal
PAM45	PAM45PT7	Metastasis	Diaphragm	Unknown	0.29	3.25	TETRAPLOID	IV	polyclonal
PAM45	PAM45PT8	Metastasis	Pelvis	Direct Seeding	0.14	3.25	TETRAPLOID	IV	monoclonal
PAM46	PAM46N	Normal	Spleen					IV	
PAM46	PAM46PT1	Primary	Pancreas Primary					IIB	
PAM46	PAM46PT2	Metastasis	Locoregional recurrence		0.55	3.11	TETRAPLOID	IV	polyclonal
PAM46	PAM46PT3	Metastasis	Locoregional recurrence		0.33	3.08	TETRAPLOID	IV	polyclonal
PAM46	PAM46PT4	Metastasis	Locoregional recurrence		0.57	3.02	TETRAPLOID	IV	polyclonal
PAM46	PAM46PT5	Metastasis	Locoregional recurrence		0.71	3.11	TETRAPLOID	IV	polyclonal
PAM46	PAM46PT6	Metastasis	Locoregional recurrence		0.70	3.00	DIPLOID	IV	polyclonal
PAM46	PAM46PT7	Metastasis	Locoregional recurrence		0.43	3.07	TETRAPLOID	IV	polyclonal
PAM46	PAM46PT8	Metastasis	Locoregional recurrence		0.42	3.07	TETRAPLOID	IV	polyclonal
PAM46	PAM46PT9	Metastasis	Locoregional recurrence		0.53	3.05	TETRAPLOID	IV	polyclonal
PAM47	PAM47N	Normal	Pancreas					IV	
PAM47	PAM47PT1	Metastasis	Liver	Hematogenous	0.42	3.16	TETRAPLOID	IV	polyclonal

Supplemental Table 2 (continued)

PAM ID	PAM Sample ID	Sample Class	Tissue Site	Metastatic Route	Purity	Ploidy	WGD status	Stage Sample Collected	Clonal Composition
PAM47	PAM47PT2	Metastasis	Liver	Hematogenous	0.44	3.16	TETRAPLOID	IV	polyclonal
PAM47	PAM47PT3	Metastasis	Liver	Hematogenous	0.28	3.18	TETRAPLOID	IV	monoclonal
PAM47	PAM47PT4	Primary	Pancreas Primary		0.29	3.11	TETRAPLOID	IV	polyclonal
PAM47	PAM47PT5	Primary	Pancreas Primary		0.32	3.23	TETRAPLOID	IV	monoclonal
PAM47	PAM47PT6	Primary	Pancreas Primary		0.24	3.14	TETRAPLOID	IV	polyclonal
PAM47	PAM47PT7	Primary	Pancreas Primary		0.42	3.08	TETRAPLOID	IV	polyclonal
PAM48	PAM48N	Normal	Heart					IV	
PAM48	PAM48PT1	Metastasis	Liver	Hematogenous	0.67	2.98	DIPLOID	IV	polyclonal
PAM48	PAM48PT2	Metastasis	Liver	Hematogenous				IV	
PAM48	PAM48PT3	Metastasis	Liver	Hematogenous	0.54	2.75	DIPLOID	IV	polyclonal
PAM48	PAM48PT4	Metastasis	Liver	Hematogenous	0.28	3.10	TETRAPLOID	IV	polyclonal
PAM48	PAM48PT5	Metastasis	Liver	Hematogenous	0.52	2.52	DIPLOID	IV	polyclonal
PAM48	PAM48PT6	Primary	Pancreas Primary		0.27	3.12	TETRAPLOID	IV	polyclonal
PAM48	PAM48PT7	Primary	Pancreas Primary		0.20	3.03	TETRAPLOID	IV	polyclonal
PAM48	PAM48PT8	Primary	Pancreas Primary		0.58	2.63	DIPLOID	IV	polyclonal
PAM49	PAM49N	Normal	Heart					IV	
PAM49	PAM49PT1	Metastasis	Liver	Hematogenous	0.53	1.96	DIPLOID	IV	polyclonal
PAM49	PAM49PT2	Metastasis	Liver	Hematogenous	0.35	1.95	DIPLOID	IV	monoclonal
PAM49	PAM49PT3	Metastasis	Peritoneal Cavity	Direct Seeding	0.56	2.07	DIPLOID	IV	monoclonal
PAM49	PAM49PT4	Metastasis	Diaphragm	Unknown	0.35	2.03	DIPLOID	IV	polyclonal
PAM49	PAM49PT5	Primary	Pancreas Primary		0.53	2.06	DIPLOID	IV	polyclonal
PAM49	PAM49PT6	Primary	Pancreas Primary		0.38	1.95	DIPLOID	IV	polyclonal
PAM49	PAM49PT7	Primary	Pancreas Primary		0.38	1.97	DIPLOID	IV	polyclonal

Supplemental Table 2 (continued)

PAM ID	PAM Sample ID	Sample Class	Tissue Site	Metastatic Route	Purity	Ploidy	WGD status	Stage Sample Collected	Clonal Composition
PAM50	PAM50N	Normal	Skeletal Muscle					IV	
PAM50	PAM50PT1	Metastasis	Lymph Node	Lymphatic	0.07	3.10	TETRAPLOID	IV	monoclonal
PAM50	PAM50PT2	Primary	Pancreas Primary		0.12	3.10	TETRAPLOID	IV	monoclonal
PAM50	PAM50PT3	Primary	Pancreas Primary		0.09	3.10	TETRAPLOID	IV	monoclonal
PAM50	PAM50PT4	Primary	Pancreas Primary		0.06	3.10	TETRAPLOID	IV	monoclonal
PAM50	PAM50PT5	Metastasis	Peritoneal Cavity	Direct Seeding	0.12	3.10	TETRAPLOID	IV	monoclonal
PAM50	PAM50PT6	Metastasis	Peritoneal Cavity	Direct Seeding				IV	
PAM50	PAM50PT7	Metastasis	Peritoneal Cavity	Direct Seeding	0.26	3.10	TETRAPLOID	IV	monoclonal
PAM50	PAM50PT8	Metastasis	Peritoneal Cavity	Direct Seeding	0.33	3.10	TETRAPLOID	IV	monoclonal
PAM50	PAM50PT9	Metastasis	Peritoneal Cavity	Direct Seeding	0.28	3.10	TETRAPLOID	IV	monoclonal
PAM51	PAM51N	Normal	Heart					IV	
PAM51	PAM51PT1	Metastasis	Diaphragm	Unknown	0.21	1.92	DIPLOID	IV	polyclonal
PAM51	PAM51PT10	Primary	Pancreas Primary		0.54	1.88	DIPLOID	IV	polyclonal
PAM51	PAM51PT11	Primary	Pancreas Primary		0.34	1.93	DIPLOID	IV	polyclonal
PAM51	PAM51PT12	Primary	Pancreas Primary					IV	
PAM51	PAM51PT13	Primary	Pancreas Primary					IV	
PAM51	PAM51PT2	Metastasis	Peritoneal Cavity	Direct Seeding	0.34	1.86	DIPLOID	IV	polyclonal
PAM51	PAM51PT3	Metastasis	Lung	Hematogenous				IV	
PAM51	PAM51PT4	Metastasis	Pelvis	Direct Seeding	0.37	1.88	DIPLOID	IV	polyclonal
PAM51	PAM51PT5	Primary	Pancreas Primary		0.49	1.86	DIPLOID	IV	polyclonal
PAM51	PAM51PT6	Primary	Pancreas Primary		0.27	1.88	DIPLOID	IV	polyclonal
PAM51	PAM51PT7	Primary	Pancreas Primary		0.51	1.89	DIPLOID	IV	polyclonal
PAM51	PAM51PT8	Primary	Pancreas Primary		0.57	1.87	DIPLOID	IV	polyclonal

Supplemental Table 2 (continued)

PAM ID	PAM Sample ID	Sample Class	Tissue Site	Metastatic Route	Purity	Ploidy	WGD status	Stage Sample Collected	Clonal Composition
PAM51	PAM51PT9	Primary	Pancreas Primary		0.52	1.86	DIPLOID	IV	polyclonal
PAM52	PAM52N	Normal	Kidney					IV	
PAM52	PAM52PT1	Metastasis	Liver	Hematogenous	0.40	3.05	TETRAPLOID	IV	polyclonal
PAM52	PAM52PT10	Metastasis	Liver	Hematogenous	0.68	3.19	TETRAPLOID	IV	polyclonal
PAM52	PAM52PT11	Metastasis	Lung	Hematogenous	0.16	3.01	TETRAPLOID	IV	polyclonal
PAM52	PAM52PT12	Metastasis	unknown	Unknown	0.16	3.22	TETRAPLOID	IV	monoclonal
PAM52	PAM52PT13	Primary	Pancreas Primary		0.26	2.99	DIPLOID	IV	polyclonal
PAM52	PAM52PT14	Primary	Pancreas Primary		0.10	2.80	DIPLOID	IV	monoclonal
PAM52	PAM52PT15	Primary	Pancreas Primary		0.19	2.89	DIPLOID	IV	polyclonal
PAM52	PAM52PT16	Primary	Pancreas Primary		0.14	2.99	DIPLOID	IV	polyclonal
PAM52	PAM52PT17	Primary	Pancreas Primary		0.15	2.80	DIPLOID	IV	polyclonal
PAM52	PAM52PT18	Primary	Pancreas Primary		0.19	3.07	TETRAPLOID	IV	polyclonal
PAM52	PAM52PT19	Primary	Pancreas Primary		0.10	2.80	DIPLOID	IV	monoclonal
PAM52	PAM52PT2	Metastasis	Liver	Hematogenous	0.47	2.99	DIPLOID	IV	polyclonal
PAM52	PAM52PT20	Primary	Pancreas Primary		0.12	3.00	TETRAPLOID	IV	polyclonal
PAM52	PAM52PT21	Primary	Pancreas Primary		0.28	3.01	TETRAPLOID	IV	polyclonal
PAM52	PAM52PT3	Metastasis	Liver	Hematogenous	0.51	3.23	TETRAPLOID	IV	polyclonal
PAM52	PAM52PT4	Metastasis	Liver	Hematogenous	0.68	3.10	TETRAPLOID	IV	polyclonal
PAM52	PAM52PT5	Metastasis	Liver	Hematogenous	0.57	3.18	TETRAPLOID	IV	polyclonal
PAM52	PAM52PT6	Metastasis	Liver	Hematogenous	0.57	3.23	TETRAPLOID	IV	polyclonal
PAM52	PAM52PT7	Metastasis	Adrenal	Unknown	0.12	2.80	DIPLOID	IV	polyclonal
PAM52	PAM52PT8	Metastasis	Diaphragm	Unknown	0.20	2.97	DIPLOID	IV	polyclonal
PAM52	PAM52PT9	Metastasis	Peritoneal Cavity	Direct Seeding	0.13	3.20	TETRAPLOID	IV	polyclonal

Supplemental Table 2 (continued)

PAM ID	PAM Sample ID	Sample Class	Tissue Site	Metastatic Route	Purity	Ploidy	WGD status	Stage Sample Collected	Clonal Composition
PAM53	PAM53N	Normal	Heart					IV	
PAM53	PAM53PT1	Metastasis	Liver	Hematogenous	0.33	2.77	DIPLOID	IV	polyclonal
PAM53	PAM53PT2	Metastasis	Liver	Hematogenous	0.73	2.77	DIPLOID	IV	polyclonal
PAM53	PAM53PT3	Metastasis	Peritoneal Cavity	Direct Seeding	0.26	3.12	TETRAPLOID	IV	polyclonal
PAM53	PAM53PT4	Primary	Pancreas Primary		0.54	2.65	DIPLOID	IV	polyclonal
PAM53	PAM53PT5	Primary	Pancreas Primary		0.51	2.44	DIPLOID	IV	polyclonal
PAM54	PAM54N	Normal	Heart					IV	
PAM54	PAM54PT1	Metastasis	Lung	Hematogenous	0.45	2.62	DIPLOID	IV	polyclonal
PAM54	PAM54PT10	Primary	Pancreas Primary		0.60	2.63	DIPLOID	IV	polyclonal
PAM54	PAM54PT11	Primary	Pancreas Primary		0.58	2.61	DIPLOID	IV	polyclonal
PAM54	PAM54PT12	Primary	Pancreas Primary		0.61	2.61	DIPLOID	IV	polyclonal
PAM54	PAM54PT13	Primary	Pancreas Primary		0.50	2.61	DIPLOID	IV	polyclonal
PAM54	PAM54PT14	Primary	Pancreas Primary					IV	
PAM54	PAM54PT15	Primary	Pancreas Primary		0.24	2.57	DIPLOID	IV	polyclonal
PAM54	PAM54PT2	Metastasis	Liver	Hematogenous	0.57	2.62	DIPLOID	IV	polyclonal
PAM54	PAM54PT3	Metastasis	Liver	Hematogenous	0.35	2.58	DIPLOID	IV	polyclonal
PAM54	PAM54PT4	Metastasis	Liver	Hematogenous	0.31	2.57	DIPLOID	IV	polyclonal
PAM54	PAM54PT5	Metastasis	Liver	Hematogenous	0.72	2.57	DIPLOID	IV	monoclonal
PAM54	PAM54PT6	Metastasis	Peritoneal Cavity	Direct Seeding	0.59	2.57	DIPLOID	IV	polyclonal
PAM54	PAM54PT7	Primary	Pancreas Primary		0.56	2.62	DIPLOID	IV	polyclonal
PAM54	PAM54PT8	Primary	Pancreas Primary		0.41	2.59	DIPLOID	IV	polyclonal
PAM54	PAM54PT9	Primary	Pancreas Primary		0.54	2.59	DIPLOID	IV	polyclonal
PAM55	PAM55N	Normal	Heart					IV	

Supplemental Table 2 (continued)

PAM ID	PAM Sample ID	Sample Class	Tissue Site	Metastatic Route	Purity	Ploidy	WGD status	Stage Sample Collected	Clonal Composition
PAM55	PAM55PT1	Metastasis	Liver	Hematogenous	0.34	3.51	TETRAPLOID	IV	polyclonal
PAM55	PAM55PT10	Primary	Pancreas Primary		0.20	3.45	TETRAPLOID	IV	polyclonal
PAM55	PAM55PT11	Primary	Pancreas Primary		0.25	3.53	TETRAPLOID	IV	polyclonal
PAM55	PAM55PT12	Primary	Pancreas Primary					IV	
PAM55	PAM55PT2	Metastasis	Retroperitoneum	Direct Seeding	0.62	3.56	TETRAPLOID	IV	polyclonal
PAM55	PAM55PT3	Metastasis	Retroperitoneum	Direct Seeding	0.52	3.55	TETRAPLOID	IV	polyclonal
PAM55	PAM55PT4	Metastasis	Retroperitoneum	Direct Seeding	0.65	3.56	TETRAPLOID	IV	polyclonal
PAM55	PAM55PT5	Primary	Pancreas Primary		0.29	3.50	TETRAPLOID	IV	polyclonal
PAM55	PAM55PT6	Primary	Pancreas Primary		0.81	3.54	TETRAPLOID	IV	polyclonal
PAM55	PAM55PT7	Primary	Pancreas Primary		0.16	3.53	TETRAPLOID	IV	polyclonal
PAM55	PAM55PT8	Primary	Pancreas Primary		0.18	3.53	TETRAPLOID	IV	polyclonal
PAM55	PAM55PT9	Primary	Pancreas Primary		0.28	3.49	TETRAPLOID	IV	polyclonal
PAM56	PAM56N	Normal	Skeletal Muscle					IV	
PAM56	PAM56PT1	Metastasis	Lung	Hematogenous				IV	
PAM56	PAM56PT2	Metastasis	Liver	Hematogenous	0.58	2.52	DIPLOID	IV	monoclonal
PAM56	PAM56PT3	Metastasis	Liver	Hematogenous	0.51	2.73	DIPLOID	IV	polyclonal
PAM56	PAM56PT4	Metastasis	Liver	Hematogenous	0.61	2.71	DIPLOID	IV	polyclonal
PAM56	PAM56PT5	Primary	Pancreas Primary		0.52	2.74	DIPLOID	IV	polyclonal
PAM56	PAM56PT6	Primary	Pancreas Primary		0.53	2.72	DIPLOID	IV	polyclonal
PAM56	PAM56PT7	Primary	Pancreas Primary		0.59	2.60	DIPLOID	IV	polyclonal
PAM56	PAM56PT8	Primary	Pancreas Primary		0.61	2.64	DIPLOID	IV	polyclonal
PAM57	PAM57N	Normal	Skeletal Muscle					IV	
PAM57	PAM57PT1	Metastasis	Lymph Node	Lymphatic	0.44	1.78	DIPLOID	IV	polyclonal

Supplemental Table 2 (continued)

PAM ID	PAM Sample ID	Sample Class	Tissue Site	Metastatic Route	Purity	Ploidy	WGD status	Stage Sample Collected	Clonal Composition
PAM57	PAM57PT2	Metastasis	Lung	Hematogenous				IV	
PAM57	PAM57PT3	Metastasis	Lung	Hematogenous	0.17	1.81	DIPLOID	IV	monoclonal
PAM57	PAM57PT4	Metastasis	Liver	Hematogenous	0.40	1.85	DIPLOID	IV	polyclonal
PAM57	PAM57PT5	Metastasis	Liver	Hematogenous	0.31	1.80	DIPLOID	IV	polyclonal
PAM57	PAM57PT6	Metastasis	Liver	Hematogenous	0.23	1.84	DIPLOID	IV	polyclonal
PAM57	PAM57PT7	Primary	Pancreas Primary		0.21	1.86	DIPLOID	IV	polyclonal
PAM66	PAM66N	Normal	Liver					IV	
PAM66	PAM66PT1	Primary	Pancreas Primary					IV	
PAM66	PAM66PT2	Primary	Pancreas Primary		0.49	4.20	TETRAPLOID	IV	monoclonal
PAM66	PAM66PT3	Metastasis	Pelvis	Direct Seeding				IV	
PAM66	PAM66PT4	Metastasis	Peritoneal Cavity	Direct Seeding				IV	
PAM66	PAM66PT5	Primary	Pancreas Primary					IV	
PAM66	PAM66PT6	Primary	Pancreas Primary					IV	
PAM66	PAM66PT7	Primary	Pancreas Primary					IV	
PAM66	PAM66PT8	Primary	Pancreas Primary					IV	
PAM67	PAM67N	Normal	Kidney					IV	
PAM67	PAM67PT1	Metastasis	Peritoneal Cavity	Direct Seeding				IV	
PAM67	PAM67PT2	Primary	Pancreas Primary		0.26	2.91	DIPLOID	IV	polyclonal
PAM67	PAM67PT3	Metastasis	Diaphragm	Unknown				IV	
PAM67	PAM67PT4	Metastasis	Lung	Hematogenous	0.15	2.88	DIPLOID	IV	polyclonal
PAM67	PAM67PT5	Metastasis	Liver	Hematogenous				IV	
PAM67	PAM67PT6	Metastasis	Peritoneal Cavity	Direct Seeding	0.23	2.71	DIPLOID	IV	polyclonal
PAM88	PAM88N	Normal	Skeletal Muscle					IV	

Supplemental Table 2 (continued)

PAM ID	PAM Sample ID	Sample Class	Tissue Site	Metastatic Route	Purity	Ploidy	WGD status	Stage Sample Collected	Clonal Composition
PAM88	PAM88PT1	Primary	Pancreas Primary					IV	
PAM88	PAM88PT2	Primary	Pancreas Primary		0.27	3.35	TETRAPLOID	IV	polyclonal
PAM88	PAM88PT3	Primary	Pancreas Primary		0.29	3.33	TETRAPLOID	IV	polyclonal
PAM88	PAM88PT4	Metastasis	Liver	Hematogenous	0.82	3.43	TETRAPLOID	IV	polyclonal
PAM88	PAM88PT5	Metastasis	Liver	Hematogenous	0.69	3.29	TETRAPLOID	IV	polyclonal
PAM88	PAM88PT6	Metastasis	Liver	Hematogenous	0.53	3.32	TETRAPLOID	IV	polyclonal
PAM97	PAM97N	Normal	Liver					IV	
PAM97	PAM97PT1	Metastasis	Peritoneal Cavity	Direct Seeding	0.25	1.85	DIPLOID	IV	monoclonal
PAM97	PAM97PT2	Metastasis	Peritoneal Cavity	Direct Seeding				IV	
PAM97	PAM97PT3	Primary	Pancreas Primary					IV	
PAM97	PAM97PT4	Metastasis	Peritoneal Cavity	Direct Seeding	0.23	1.85	DIPLOID	IV	monoclonal
PAM97	PAM97PT5	Metastasis	Peritoneal Cavity	Direct Seeding	0.22	1.85	DIPLOID	IV	monoclonal
PAM97	PAM97PT6	Metastasis	Peritoneal Cavity	Direct Seeding				IV	
PAM98	PAM98N	Normal	Heart					IV	
PAM98	PAM98PT1	Metastasis	Lymph Node	Lymphatic	0.44	3.65	TETRAPLOID	IV	monoclonal
PAM98	PAM98PT2	Metastasis	Lymph Node	Lymphatic	0.38	3.63	TETRAPLOID	IV	polyclonal
PAM98	PAM98PT3	Metastasis	Diaphragm	Unknown	0.52	3.66	TETRAPLOID	IV	polyclonal
PAM98	PAM98PT4	Metastasis	Peritoneal Cavity	Direct Seeding	0.59	3.67	TETRAPLOID	IV	polyclonal
PAM98	PAM98PT5	Metastasis	Peritoneal Cavity	Direct Seeding	0.47	3.69	TETRAPLOID	IV	polyclonal
PAM98	PAM98PT6	Metastasis	Peritoneal Cavity	Direct Seeding	0.61	3.63	TETRAPLOID	IV	polyclonal
PAM98	PAM98PT7	Metastasis	Liver	Hematogenous	0.72	3.63	TETRAPLOID	IV	polyclonal
PAM98	PAM98PT8	Metastasis	Peritoneal Cavity	Direct Seeding	0.48	3.62	TETRAPLOID	IV	polyclonal

Patients with a ploidy value > 3 were considered tetraploid. Cells without purity, ploidy, or a WGD status indicate samples that could not be analyzed by HATCHet.